A Statistical-Process Based Approach for Modelling Beach Profile Variability

Douglas Pender

MEng

Submitted in Fulfilment of the Requirements for the Degree of

Doctor of Philosophy

School of Engineering

University of Glasgow

August 2013

ABSTRACT

As the debate into a changing global climate continues, it is important that coastal engineers and scientists have the most advanced tools to quantify any resulting variation in the coastal environment. This will aid the creation and implementation of effective shoreline management plans to mitigate these changes.

This thesis presents a new combined Statistical-Process based Approach (SPA) for modelling storm driven, cross-shore, beach profile variability at a medium-term (annual to decadal) timescale. The methodology presented involves combining the detailed statistical modelling of offshore storm data and a process based morphodynamic model (XBeach), to assess, and quantify, the medium-term morphodynamic response of cross-shore beach profiles. Up until now the use of process-based models has been curtailed at the storm event timescale. This approach allows inclusion of the post-storm recovery period, in addition to individual event impacts, thus allowing longer-term predictions. The use of a process-based model for simulating, both erosion and recovery, expands on previous work on the subject by allowing for the inclusion of antecedent beach profiles within the modelling framework.

The XBeach model and the overall SPA procedure were calibrated and validated using measured wave and beach profile data from Narrabeen Beach, NSW, Australia. XBeach was shown to give a good prediction of the post-storm profile for four varying storm events. In addition, by accounting for the hydrodynamic processes that govern accretion, and calibrating parameters accordingly, XBeach was also shown to provide a good representation of berm accretion during recovery periods. The combination of the erosion and accretion models was shown to produce extremely encouraging results at an annual timescale, by successfully following the trends in beach volume and the position of the 0m and 2m beach contours. The simulation of a longer sequence provided comparable medium-term erosion return levels.

CONTENTS

LIST OF TABLES

LIST OF FIGURES

ACKNOWLEDGEMENTS

AUTHOR DECLARATION

I declare that no portion of the work in this thesis has been submitted in support of any application for any other degree or qualification from this or any other university or institute of learning. I also declare that the work presented in this thesis is entirely my own contribution unless otherwise stated.

Douglas Pender

Glasgow, August 2013.

LIST OF ABBREVIATIONS

AHD	Australian Heights Datum
AM	Annual maxima method
BSS	Brier skill score
CFL	Courant-Friedriches-Lewey
DoC	Depth of closure
FTS	Full temporal simulation
GEV	Generalised extreme value distribution
GLM	Generalised Lagrangian mean formulation
GPD	Generalised Pareto distribution
JPM	Joint probability method
LL	Log likelihood
MC	Monte Carlo
MHL	Manly Hydraulics Laboratory
MLE	Maximum likelihood estimation
MRL	Mean residual life
NSW	New South Wales
PCR	Probabilistic coastline recession method
POT	Peaks over threshold
RMAE	Relative mean absolute error
RP	Return period
SE	Standard error
SOI	Southern Oscillation Index
SPA	Statistical-process based approach
SVM	Structural variable method
SvR	Soulsby-van Rijn sediment transport regime
vTvR	van Thiel-van Rijn transport regime
wci	wave current interaction
XB	XBeach

LIST OF SYMBOLS

A	sediment dependent parameter in equilibrium profile model
A_r	roller area
A_{sb}	bedload coefficient
A_{ss}	suspended load coefficient
A_w	wave action
c	wave celertity
C	Chézy coefficient
C_D	sediment drag coefficient
C_{eq}	sediment equilibrium concentration
cf	flow friction coefficient
c_g	wave group celerity
C_s	sediment concentration
c_w	roller speed
D	storm duration
D	wave energy dissipation
D_*	dimensionless sediment size
D_*	equilibrium wave energy dissipation
D_{50}	median sediment diameter
D_c	diffusion coefficient
E_w	short wave energy
f	wave frequency
F	wave forcing
$facAs$	factor on wave asymmetry
$facSk$	factor on wave skewness
$facua$	factor on wave skewness and asymmetry
f_m	mean wave frequency
f_p	spectral peak frequency
H	wave height

h	water depth
H_0	deep water wave height
H_b	breaking wave height
h_c	depth of closure
H_{rms}	root mean square wave height
H_s	significant wave height
$H_{s,12}$	significant wave height exceeded 12 hours per year
$H_{s,max}$	peak significant wave height of storm events
K	sediment transport rate parameter in equilibrium profile model
k_b	breaker induced turbulence
K_I	intrinsic permeability
K_P	specific permeability
k_w	wave number
L	wavelength
L_0	deep water wavelength
m	gradient of linear regression
m_{cr}	critical bed slope before avalanching
M_e	sediment mobility parameter
morfac	morphological acceleration factor
N	number of erosion events in SPA simulation
N_y	number of storm events per year
p	p-value
P	storm power index
P_b	fraction of breaking waves
q_b	bedload transport rate
Q_s	cross-shore sediment transport rate in numerical equilibrium profile model
q_s	suspended sediment transport rate
q_t	total load transport rate
q_x	cross-shore sediment transport rate
q_y	longhore sediment transport rate
S	storm event spacing
S	wave steepness

S	wave induced radiation stress
$S(f)$	spectral density
S_r	roller energy
S_w	wave energy in each directional bin
T	wave period
$T_{1/3}$	average of top 1/3 of wave periods in JONSWAP spectrum
T_m	mean wave period
T_{max}	maximum wave period in JONSWAP spectrum
T_p	spectral peak wave period
T_{RP}	Return period of erosion estimates
T_s	significant wav period
T_s	adaption time for sediment entrainment
$T_{s,12}$	significant wave period exceeded 12 hours per year
$T_{s,max}$	significant wave period corresponding to peak wave height of storm events
$T_{s,min}$	minimum significant wave period
u	flow velocity
u	threshold parameter for Generalised Pareto Distribution
u^A	cross-shore advection velocity from wave skewness and asymmetry
u_{cr}	critical flow velocity
u^E	cross-shore Eulerian flow velocity
u^L	cross-shore Lagrangian flow velocity
u_{reps}	representative velocity in XBeach
u_{rms}	wave orbital velocity
u^S	cross-shore Stokes drift velocity
$u_{stirring}$	sediment stirring velocity
v^A	longshore advection velocity from wave skewness and asymmetry
v^E	longhore Eulerian flow velocity
v^L	longhore Lagrangian flow velocity
v_{magu}	Lagrangian transport velocity in XBeach
v^S	longhore Stokes drift velocity
w	vertical groundwater flow velocity
w_s	sediment fall velocity

x	distance from shoreline in equilibrium profile model
x_b	baseline profile
x_m	measured profile
x_{ori}	x origin coordinate in XBeach
x_p	predicted profile
x_w	x world coordinate in XBeach
Y	erosion period of SPA simulation
y_{ori}	y origin coordinate in XBeach
y_w	y world coordinate in XBeach
z_0	bed roughness length
z_b	bed elevation
Z_{berm}	berm height
z_{s0}	initial water surface elevation
α	dependency parameter in logistics model
β	beach slope
β	slope of wave front
γ	JONSWAP peak enhancement factor
γ	wave breaking index
ε	porosity
ζ_u	Pr$\{X>u\}$
θ	Shields parameter
θ	wav direction
θ_{CR}	critical Shields parameter
κ	threshold parameter in 3-parameter lognormal distribution
$\lambda(t|\theta)$	storm occurrence intensity function
μ	parameter in 3-parameter lognormal distribution
ν	kinematic viscosity
ξ	surf similarity parameter
ξ	shape parameter for Generalised Pareto Distribution
ρ	fluid density
σ	scale parameter for Generalised Pareto Distribution
σ	parameter in 3-parameter lognormal distribution

σ^*	modified Generalised Pareto Distribution scale parameter
τ	bed shear stress
τ_{CR}	critical bed shear stress
τ_r	wave averaged shear stress
Ω	Dean number
ω	intrinsic wave frequency

CHAPTER 1

INTRODUCTION

1.1   Motivation

As the global population continues to rise, so does the number of people that live in coastal regions. The coastline itself is responsible for a large proportion of the economics of these regions it is therefore imperative that changes to the environmental systems within these areas are understood. For many coastal regions it is the natural beach systems that provide a source of economic benefit, by attracting people to the area through various forms of tourism. Subsequently, as the population within these areas increases, so does the socio-economic impact of any coastal erosion and flooding that occurs. Due to the significance of these systems it is important to be able to accurately quantify any longer-term changes that are likely to occur. Being able to confidently forecast medium-term beach variability therefore allows for the development and implementation of effective shoreline management plans to mitigate these changes; whether they are man-made (e.g. harbour construction) or natural (e.g. sea level rise or a changing wave climate).

In order for coastal engineers and scientists to manage the coastal zone effectively it is important that they have accurate and efficient tools available to do so. The methodology presented in this thesis expands on previous work implemented in the same field and attempts to fill a gap in the current techniques used for forecasting and quantifying medium-term beach change. This is achieved through the methodology presented being the first attempt at using a fully process-based morphodynamic model to determine profile variability at a medium-term (annual to decadal) time scale. Successful implementation of such a methodology will provide a considerably more flexible tool than previous methods, as the variability of the entire beach profile can be modelled and analysed.

1.2   Project Description

1.2.1 Statistical estimation of beach erosion

For successful development and implementation of coastal management plans, accurate quantification of beach erosion statistics is a necessity. The original method for quantifying return levels of beach erosion is the application of a 1 in N year benchmark erosion event (i.e. the largest event that occurred in N years of measurements). For quantifying beach erosion, applying a benchmark event produces limited information regarding the return period of the predictions. This is due to the return period of outputs not necessarily matching those of the forcing conditions for systems with two or more variates (Hawkes et al., 2002). For beach erosion from storm events, it was shown by Kriebel and Dean (1993) that the erosion volume is dependent on storm duration as there is a finite time required for the beach to reach a new equilibrium profile. For example, two events with a 1 in 100 year wave height will result in different levels of erosion should the durations be different. Additionally, the application of a single benchmark event does not allow for the merging of individual storm events into a single erosion event. For instance, should two storm events occur within a few days of each other then, the second event essentially picks up where the previous event finished, producing greater erosion than if separated by a number of weeks, to allow for the natural recovery of the system.

As there are a significant number of factors that control beach erosion, the use of statistical methods for estimating extreme levels is not as common as it is for other environmental parameters, such as wave heights, periods, water levels and flood magnitudes (e.g. Coles and Tawn, 1991; Tawn, 1992; Mathiesen et al., 1994; Hawkes et al., 2002; Garrity, 2006; Butler et al., 2007). Recently, Callaghan et al. (2008) assessed and combined the current methods available to produce a robust method for the statistical quantification of extreme beach erosion. Their discussion showed that there are four suitable methods that can be used. These are as follows:

    1) Fitting distributions directly to erosion measurements.
    2) Structural variable method (SVM).

    3) Joint probability method (JPM).

    4) Full temporal simulation (FTS).

Many decades of beach profile measurements are required in order to fit extreme value distributions directly to erosion measurements. This method has no flexibility and is completely site specific as it can only be applied to beaches that have continuous profile records that capture beach erosion, which are relatively rare. Additionally, it is solely based on historical data and any future changes to forcing variates (e.g. sea level rise and storm frequency) cannot be incorporated.

The SVM method uses a structural function (e.g. profile model) to transform measured wave and water levels to determine the erosion levels. The erosion volumes are then sorted into ascending order and assigned empirical probabilities. These values are then extrapolated using an extreme value distribution to predict extreme erosion volumes. As with fitting distributions directly to measurements, the temporal changes are limited to the measurement period and there is no allowance for storm frequency, a major factor governing the degree of beach erosion.

The JPM uses statistical modelling techniques to formulate joint probability density functions of all variates required by the structural function. The structural function is then combined with all combination of variates that exceed a particular threshold to determine the exceedance probability. This method, again, excludes allowances for temporal variations and the processes where several independent storms can be merged into a single event. If this were to happen, the erosion levels might be significantly more than if these events were to occur in isolation because there is very little recovery time between events.

As the erosion levels are dependent on both present storm conditions and past beach conditions, it is impossible to predict the storm duration that will result in a particular erosion level. Therefore, in order to accurately establish long-term erosion quantities, time variates (i.e. storm duration and spacing) must be incorporated into the statistical

modelling. This led to Callaghan et al. (2008) developing the FTS. Unlike the previous methods mentioned, the inclusion of a Poisson process to describe the spacing between events means the FTS accounts for event grouping and has the potential to include sea level rise and other non-stationary processes.

The FTS procedure combines the statistical modelling of an offshore storm climate with an empirical dune erosion model (Kriebel and Dean, 1993) to quantify long-term (up to 100 years) extreme beach erosion. Later, Ranasinghe et al. (2011) combined the statistical modelling framework given by Callaghan et al. (2008) with a semi-empirical dune erosion model (Larson et al., 2004) and developed a Probabilistic Coastline Recession (PCR) model, to assess the effects of sea level rise over a 110-year period. This demonstrates the robustness and flexibility of the statistical modelling procedure regarding the ability to include temporal variations in the forcing conditions. The FTS (or variations of) can therefore be considered the most comprehensive method currently available for the statistical quantification of medium to long-term beach erosion.

1.2.2 *Integrated modelling methodology*

The main limitation of the procedures proposed by Callaghan et al. (2008) and Ranasinghe et al. (2011) was shown to be the use of empirical functions for determining the storm-induced erosion and post-storm recovery of the beach. This research project, therefore, builds on these studies by developing an integrated modelling approach that combines the statistical modelling of the FTS with process-based modelling of beach variability. This integrated methodology, hereafter known as the Statistical-Process based Approach (SPA), provides a novel attempt at quantifying medium-term beach erosion and variability. This methodology will introduce a greater use of process-based models for providing statistical predictions of beach change at longer time scales. It provides an attempt to bridge the gap between, short-term, process-based modelling and long-term empirical and statistical modelling of beach erosion and variability.

Although it has been shown by Callaghan et al. (2008) and Ranasinghe et al. (2011) that long-term beach erosion statistics can be reasonably estimated using empirical and semi-empirical models; the use of a process-based model as the structural function in the SPA removes the limitations associated with the empirical models and will provide a more comprehensive estimation of storm-induced beach change. In addition, as the post-storm beach recovery is also to be modelled using the process-based model, the SPA allows for the inclusion of antecedent beach profiles, which was not possible previously. This means that the SPA methodology provides much greater flexibility than that provided by the FTS or PCR models, as the variability (e.g. contour position and volume) in the beach profile can also be assessed, in addition to the erosion. The results presented in this thesis provide a basis for an advancement of using process-based modelling to determine medium-term erosion.

The SPA can be broken down into a statistical model of the storm climate (from the FTS), allowing for the generation of a random synthetic timeseries, that is then modelled in sequence using a process-based model to quantify erosion return levels. Successful implementation of the SPA will provide a robust modelling tool able to forecast medium-term beach variability and erosion using a process-based model. This, in turn, will allow for the possibilities of forecasting medium-term beach profile change to be extended in the future, pushing the boundaries of the subject matter within the coastal engineering research community.

1.2.3 Aims

The focal point of this research is to develop the SPA integrated modelling approach such that a process-based coastal morphodynamic model can be used to successfully predict medium-term (1 to 10 year) beach erosion. The project is divided into five distinct steps in order to achieve this:

1) Identification of a suitable process-based morphodynamic model.
2) Identification of a suitable field site to develop the SPA.

3) Implementation of the statistical model within the FTS to generate a synthetic storm climate.

4) Calibration of the process-based model for simulating storm-induced erosion and post-storm recovery.

5) Quantifying medium-term (annual to decadal) beach erosion return levels.

1.3   Thesis Outline

The thesis is arranged as follows. Chapter 2 presents an overview of the coastal zone; wave dominated beach types and the hydrodynamic and morphodynamic processes in this region. Chapter 3 discusses the modelling techniques used for simulating beach morphodynamics and decides upon a suitable model for use within this research. Chapter 4 identifies Narrabeen Beach as an appropriate field site and describes its wave climate and morphology. Chapter 5 presents the theory behind the statistical modelling of the storm climate as well as the results from its implementation. A description of the process-based model used, as well as its calibration and validation at the field site is presented in Chapter 6, prior to its combination with the synthetic storm climate in Chapter 7, forming the SPA methodology. Chapter 8 draws conclusions from the research and provides a discussion of potential improvements and further recommendations.

CHAPTER 2

COASTAL PROCESSES AND THE MORPHODYNAMIC VARIABILITY OF BEACHES

This chapter provides an overview of the processes and features that influence the morphodynamics of sandy beaches. It aims to provide the necessary background information that will be expanded on in subsequent chapters of the thesis.

2.1   The Coastal Zone

The definition of the *"coastal zone"* varies depending on the literature consulted. This chapter divides the coastal zone into two main sections, the offshore zone and the littoral zone, in line with Davidson-Arnott (2010).

The offshore zone is the region where no significant, wave-induced, sediment transport takes place; with its landward boundary defined by the depth of closure (DoC). The DoC is the profile depth beyond which, waves do not produce any measureable sediment transport and change in profile shape (Hallermeier, 1981).

The littoral zone is where sediment becomes transported by wave action resulting in a changing morphology. The DoC and the limit of wave action on the beach define the seaward and landward boundaries of this zone respectively. As this research involves

modelling beach profile variability, a more detailed description of the littoral zone is provided below.

The littoral zone can be sub-divided into a number of smaller zones as shown in Fig. 2.1. Only a summary of these is provided in this thesis and for a more detailed description the reader is referred to Masselink and Hughes (2003) and Davidson-Arnott (2010) in addition to the references below.
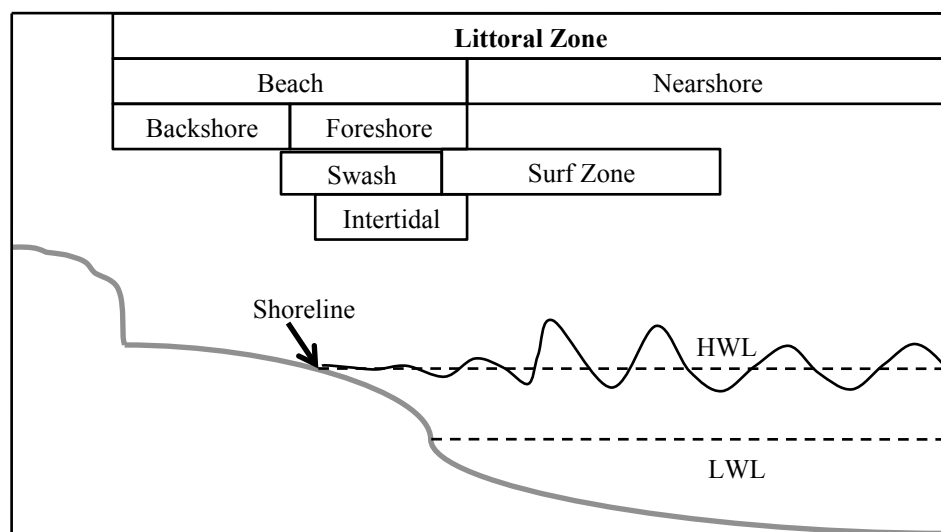
Fig. 2.1 – Schematic diagram of the littoral zone. Where HWL and LWL are the high and low water levels respectively

The nearshore zone extends from the DoC to the shoreward limit of breaking waves. Wave action and currents predominantly transport the sediment within this zone. The sediment are entrained from the bed by the wave orbital velocity and then transported in the prevalent direction of the currents within the region.

The beach gradient and incident wave conditions are responsible for controlling the limits of the surf zone. These limits extend from the offshore point of wave breaking to the beach itself. On planar beaches the surf zone has outer and inner regions. Rapid wave

transformation occurs in the outer region; with the inner region containing the broken wave bores that propagate shoreward and dissipate the remaining energy.

The swash zone is the region where dissipation of wave energy is finally completed. The limits are defined as the limits of wave uprush and backwash. The momentum of the incident waves, the beach gradient and the groundwater flow that occurs controls the swash that is present on the beach. The gravity force that acts on the water, not lost through infiltration, creates the backwash, with its velocity depending on the gradient of the beach face.

The sediment transport that takes place in the swash zone plays a large role in shaping the beach face as it is responsible for determining whether sediments remain onshore or are transported and lost offshore (Horn and Mason, 1994). The sediment transport conditions are extremely complex due to the rapidly varying non-linear flow conditions that occur. This has resulted in numerous studies regarding the measurement and modelling of swash zone sediment transport throughout the years. Details of swash zone sediment transport can be found in Fredsøe and Deigaard (1992); Turner and Masselink (1998); Butt and Russell (1999); Larson et al. (2004); Pritchard and Hogg (2005) and references therein.

The intertidal zone occurs between the levels of high and low tides. The position of the shoreline is defined instantaneously as the intercept of the mean water level along the beach; and varies along with the tidal cycle.

The beach can be defined as the region that is subaerial for extended periods of time and regularly subjected to wave action. The low tidal level and the maximum limit of wave uprush define its seaward and landward limits during normal (not extreme) storm events, respectively. The beach can be subdivided into the foreshore and backshore. The foreshore is subjected to wave action during calm (regular) sea conditions, whereas the backshore is only subjected to wave action during storm events and may consist of dune systems. The

backshore region is regularly defined as the *'beach'* for recreational purposes as it is beyond the limit of regular wave action.

2.2　Ocean tides

The tidal cycles caused from the gravitational attraction between the Earth, Moon and Sun can be significant in defining coastal morphology. Each tidal cycle is associated with a period of high water (flood tide) and low water (ebb tide). This section provides a brief overview of the characteristics of ocean tides; with a comprehensive description of their generating mechanisms discussed by Masselink and Hughes (2003); Reeve et al. (2004) and references therein.

2.2.1 Classification of tides

Tides can be classified, most basically, depending on their period. Most tides around the world exhibit a semi-diurnal cycle that and have a period of approximately 12 hours (i.e. two high and two low water levels per day). Tides can also be diurnal (one high and low water level per day) or mixed (a combination of semi-diurnal and diurnal tides).

2.2.2 Spring - Neap cycles

The position of the Earth-Sun-Moon system determines the relative height of the tidal levels. The variation in height between cycles is known as the Spring-Neap cycle. A Spring-Neap cycle occurs approximately twice a month, with Spring tides having higher water surface elevations than Neap tides. Spring tides occur when the Earth, Moon and Sun are co-linear (new moon and full moon) with individual tidal cycles having the characteristics of semi-diurnal, diurnal or mixed tides. Fig. 2.2 provides an example of a 14-day Spring-Neap cycle for a semi-diurnal tide (a) and a diurnal tide (b).
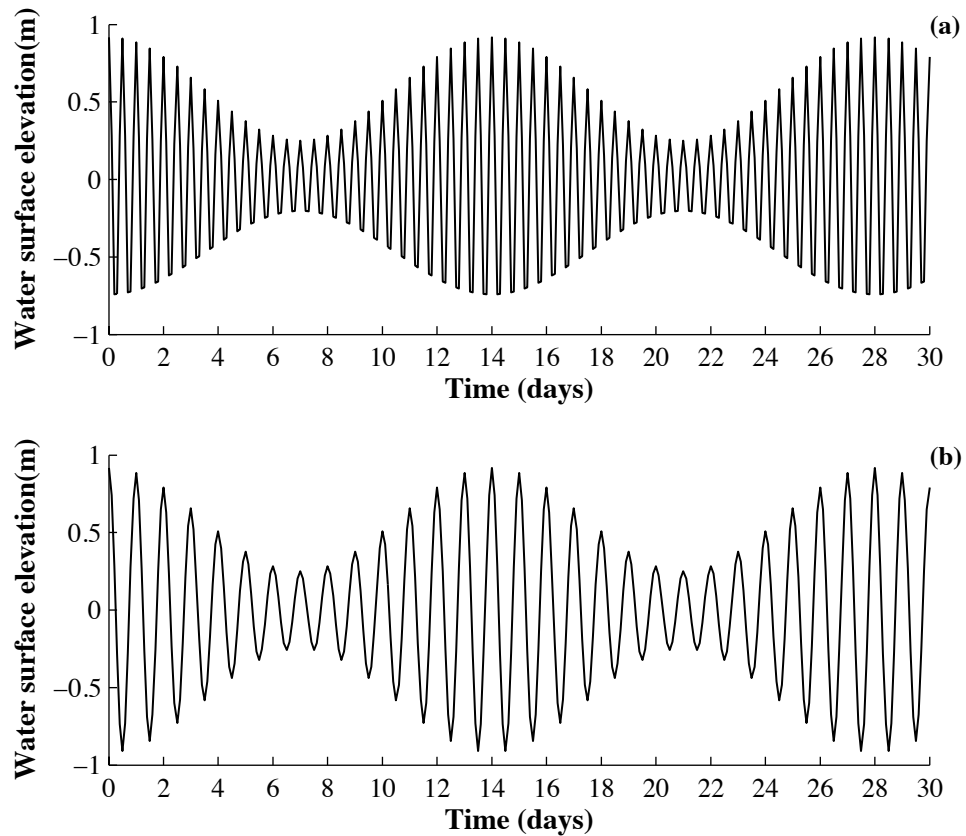
Fig. 2.2 – Schematic of Spring-Neap tidal cycles for an example (a) semi-diurnal tide and (b) diurnal tide

2.3   Nearshore Hydrodynamics

The following section describes basic hydrodynamic phenomena that occur in the nearshore region and govern beach morphodynamics. A basic understanding of linear wave theory is assumed and is therefore not discussed in any detail.

2.3.1 Ocean waves

The most common type of waves found in the ocean are those generated by wind (short waves), and typically have a period in the range of $1 - 30s$ (Reddy, 2001). The propagation of these short waves across the open ocean leads to the formation of lower frequency waves (long waves). This section discusses the short wave spectrum and transformation processes, along with a description as to how long waves are formed.

2.3.1.1 Wave spectrum

Waves viewed in the open ocean appear to be very random with various heights, directions (θ) and frequencies (f). Breaking down the ocean waves into an infinite number of wavelets (each with an individual f and θ), determining the associated energy and plotting this against f and θ gives the wave spectrum. With respect to f alone this is known as the frequency spectrum and with respect to f and θ it is known as the directional wave spectrum. The peak frequency (f_p), of any wave spectrum, can be determined as the value of f that results in the peak energy. A detailed description of ocean wave spectra is given in Goda (2010) .

JONSWAP spectrum

The JONSWAP spectrum was developed from the Joint Wave Observation Program for the North Sea (Hasselman et al. 1973) and has become one of the most widely used in coastal engineering. The density ($S(f)$) of the JONSWAP spectrum can be written in terms of wave height (H) and period (T) as follows:

$$S(f) = \beta_J H_{1/3}^2 T_p^{-4} f^{-5} \exp[-1.25(T_p f) - 4]\gamma^{\exp[-(T_p f - 1)^2 / 2\sigma^2]} \tag{2.1}$$

$$\beta_J = \frac{0.0624}{0.230 + 0.0336\gamma - 0.0185(1.9 + \gamma)^{-1}}[1.094 - 0.01915\ln\gamma] \tag{2.2}$$

$$T_p \approx T_{1/3}/[1 - 0.132(\gamma + 0.2)^{-0.559}] \tag{2.3}$$

$$\sigma = \begin{cases} 0.07 \ f \le f_p \\ 0.09 \ f > f_p \end{cases} \tag{2.4}$$

where γ is the peak enhancement factor and has a mean value of 3.3 from the North Sea measurements.

Wave dispersion and swell

An ocean wave field normally includes a spectrum of waves with a wide range of period. In deep water these different periods mean that individual waves propagate at different velocities, known as wave celerity. As the period increases so to does the celerity meaning, given enough time, longer period waves will outrun shorter period waves. This means that the wave field sorts itself into groups of similar period. This sorting phenomenon is known as wave dispersion and transforms a broad wave spectrum into a regular wave field known as swell. Swell waves are therefore a series of surface gravity waves grouped together to form a wave with a much larger period.

2.3.1.2 Wave transformation

As waves propagate from the deep ocean to the nearshore region they undergo a number of transformation processes prior to breaking. These transformations are a result of the changes in bathymetry and the angle of incidence as the wave ray approaches the seabed contours. They take place in regions where water depth is shallow enough to have an influence on the incoming waves.

Wave shoaling

As soon as the bathymetry begins to influence the incoming waves they undergo the process of shoaling. Wave shoaling is essentially the growth in wave height (H) that occurs as waves approach the shore. As waves travel from deep to shallow water, wave period (T) is the only property that remains constant. As the water depth decreases so does the associated wavelength (L) of the incoming waves, resulting in a decrease in celerity (c) and group celerity (c_g). In order for the energy flux between bed contours to remain constant, H in the shallower water must increase. This variation in H is known as wave shoaling.

Wave refraction

Should wave incidence be oblique to the seabed contours, wave refraction will occur simultaneously to shoaling, resulting in further changes to L, c and c_g. Again, these changes will result in a change in H, as the energy flux remains constant.

Fig. 2.3 shows wave transformation for an example offshore wave ray ($H = 2.0$m, $T = 10$s) that approaches parallel bed contours with an angle of 135°.
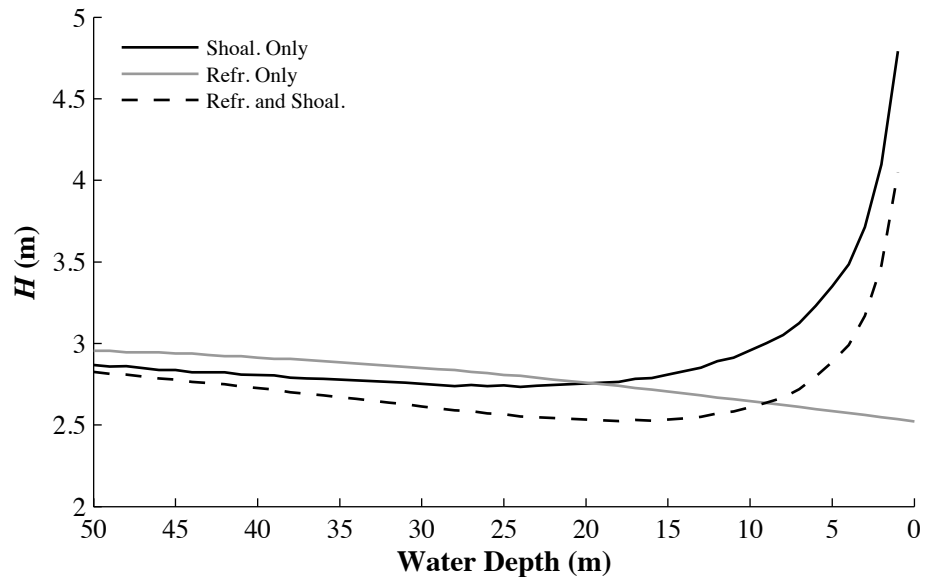
Fig. 2.3 – Example of wave shoaling and refraction

Wave diffraction

Wave diffraction is not influenced by the local water depth and occurs from the conservation of wave energy along the wave crest, rather than in the direction of propagation. When the propagation of a regular wave train is interrupted by some structure (e.g. a harbour, island, reef system) causing a shadow zone in lee of that structure, diffraction results. The diffraction of the approaching waves around the structure enables wave energy to enter these areas.

2.3.1.3 Wave breaking

As waves approach the shore the transformations discussed in the previous section occur and they grow in magnitude until they ultimately break. A breaking wave is influenced by two criteria. The first is the steepness of the wave (H/L), the second is the ratio between H and water depth (H/d), known as the breaking index (γ). The limiting values for each criteria are 1/7 and 0.78, although γ may vary between 0.4-1.2 in practice (Reeve et al., 2004). For more detailed information on wave breaking in the surf zone see Goda (2010), where a detailed analysis of the estimation of breaker height is provided.

There are principally three different types of breaker that can occur on any given beach; a spilling breaker, a plunging breaker and a surging breaker (Galvin, 1968). Breaker type can be estimated using the surf similarity parameter (or Iribarren number) (Battjes, 1974). The surf similarity parameter (ξ), shown in Eq. (2.5) and (2.6), is the ratio of the beach slope (β) to the wave steepness. The steepness and ξ can be determined from deepwater wave height (H_0) or breaking wave height (H_b) with both cases using the deepwater wavelength (L_0) to define the steepness (Fredsøe and Deigaard, 1992).

$$\xi = \frac{\tan\beta}{\sqrt{H_0 / L_0}} \tag{2.5}$$

$$\xi_b = \frac{\tan\beta}{\sqrt{H_b / L_0}} \tag{2.6}$$

The three different breaker types along with the associated ξ range are provided in Table 2.1.
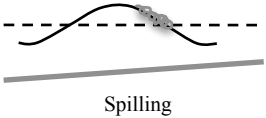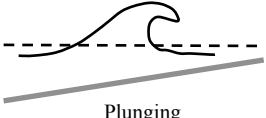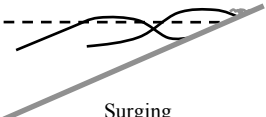
ξ_b	ξ_0	Breaker Type	Sketch
$\xi_b < 0.4$	$\xi_0 < 0.5$	Spilling	Spilling
$0.4 < \xi_b < 2.0$	$0.5 < \xi_0 < 3.3$	Plunging	Plunging
$\xi_b > 2.0$	$\xi_0 > 3.3$	Surging	Surging

Table 2.1 – Surf similarity parameter and breaker types

Spilling breakers occur on shallow sloping beaches and break when the front of the wave crest becomes unstable and spills forwards. The turbulence created by this process, known as a roller, propagates with the wave like a bore. The roller grows as H decreases rapidly across the surf zone, leading to a gradual dissipation of wave energy across the wide surf zone.

Plunging breakers tend to occur on steeper beach slopes, with breaking resulting from the wave crest steepening, becoming unstable and falling forward. This creates considerably more turbulence than a spilling breaker, meaning a more rapid dissipation of energy.

Surging breakers are found on very steep beach slopes. In these breakers it is the base of the wave front that becomes unstable when the water becomes very shallow. The steep front then rushes forward and the crest disappears, with breaking occurring onto the beach itself.

In spilling and plunging breakers, the incident wave energy is dissipated through turbulence, whereas in a surging breaker, the generation of turbulence can be limited, leading to only partial energy dissipation. The remaining energy is reflected by the beach and returns offshore as a reflected wave.

For a detailed description regarding the physics of wave breaking see Svendsen (2006) and references therein.

2.3.1.4 Infragravity waves

Infragravity waves are waves that consist of, both, wind generated waves and swell waves and have significantly higher T than the T_p of the incident wave spectrum (20-300s). These waves are bound with the short wave groups, propagate with the group velocity and are known as bound infragravity waves. When this wave group, of large H, in the incoming swell, breaks and creates a shoreward mass transport, the infragravity wave is released and continues to propagate through the surf zone. The release of the bound infragravity wave results in a free infragravity wave that is either reflected by the beach or is trapped in the surf zone as a standing wave. When this occurs a larger period (several minutes) oscillation of the water level occurs, known as surf beat. For a more detailed description of the formation and propagation of infragravity waves the reader is referred to Baldock et al. (1997, 1999); Karunarathna and Chadwick (2007) and references therein. These types of wave assist in the transport of sediment in the surf zone and the shaping of the nearshore morphology (Baldock et al., 2010).

2.3.2 Currents

2.3.2.1 Cross-shore currents

Undertow

Undertow is a cross-shore current that acts perpendicular to the shoreline and is responsible for the offshore transport of sediment during erosive events. When wave breaking occurs, there is an onshore-directed mass flux of water that is balanced, in the nearshore, by an offshore-directed undertow (Fig. 2.4). The backwash created by breaking waves feeds the undertow, with it being pulled underneath the next breaker, producing an undertow current. These currents extend seawards as far as the next breaker, with the magnitude of the breakers controlling its strength.
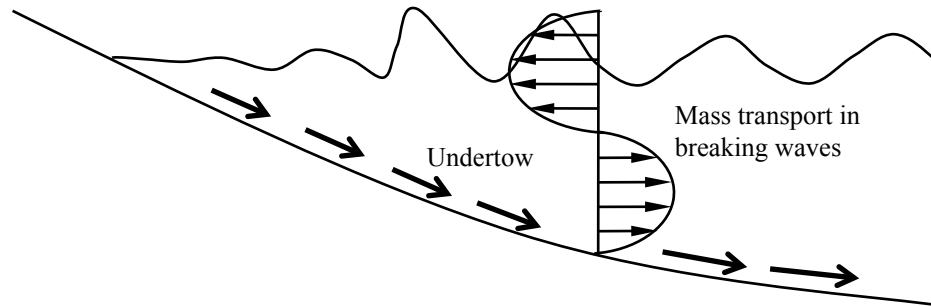
Fig. 2.4 – Formation of undertow currents

Rip currents

When a large undertow current is present on a barred coastline, weaknesses in the bar morphology may be exploited leading to the formation of rip currents. These are an integral part of the nearshore region and consist of: onshore transport of water between rip currents; longshore feeder currents that carry water into the rips; a fast flowing rip-neck that extends from the confluence of two opposing feeder current and transports water seaward; and the rip head, which is a region of lower velocities seaward of the surf zone (Masselink and Hughes, 2003). Compared to undertow currents, the velocities in rip currents are much greater meaning they can be responsible for the transport of large volumes of sediment offshore and are considerably hazardous for recreational activities.

2.3.2.2 Longshore currents

A longshore current is one that runs parallel to the shoreline and forms from oblique wave incidence. They are generated by the longshore directed radiation stresses from wave breaking that subsequently produce a longshore sediment transport gradient. Longuet-Higgins (1970) provides a detailed study about the formation of longshore currents formed from the radiation stresses from oblique wave breaking.

2.4   Sediment Transport

The transport of sediment in any moving fluid can be simplified into the following three steps:

1) Entrainment of sediment.
2) Transport of entrained sediment.
3) Settling and deposition of transported sediment.

Depending on the flow conditions, sediment transport will continue by either re-entrainment of deposited sediment or re-mobilisation of the sediment yet to settle.

Sediment can be transported as either bedload (rolling or sliding along the bed during low velocity situations) or suspended load (suspension in the water column during high velocity situations), with total load transport being the summation of both components. In high velocity situations bedload transport can develop into sheetflow, where more than one layer of sediment travels along the bed.

Wave motion, currents, or a combination of both, results in the transport of sediments within the littoral zone. The ways in which waves and currents transport sediments are inherently different leading to different equations for estimating transport rates for different forcing mechanisms. The sediment transport equations within the XBeach model, and relevant to this project, are in discussed in detail in Chapter 6. A detailed overview of the mechanics of coastal sediment transport can be found in Fredsøe and Deigaard (1992) and Soulsby (1997).

2.4.1 Threshold of motion and bedload transport

The effects of flow velocity (u) on sediment can be expressed in terms of the shear stress (τ) exerted on the bed. This relationship is given in Eq. (2.7).

$$\tau = \rho C_D u^2$$

<div align="right">(2.7)</div>

where ρ is the fluid density and C_D is the sediment drag coefficient, based on sediment size and bedforms.

The entrainment of sediment takes place when τ exceeds a critical value (τ_{CR}). This critical value can be estimated using the dimensionless Shields parameter (θ), which is the ratio of the shear force to the gravity force acting on the sediment. The critical Shields parameter (θ_{CR}) can be used to estimate τ_{CR} and determine whether entrainment and transport will occur. This is achieved using Eq. (2.8) to (2.10) (Soulsby, 1997). When τ_{CR} is exceeded sediment transport takes place, initially in the form of bedload transport.

$$\theta_{CR} = \frac{\tau_{CR}}{(\rho_s - \rho)gD}$$

<div align="right">(2.8)</div>

$$\theta_{CR} = \frac{0.3}{1 + 1.2D_*} + 0.055\left[1 - \exp(-0.02D_*)\right]$$

<div align="right">(2.9)</div>

$$D_* = \left[\frac{g(s-1)}{v^2}\right]^{-\frac{1}{3}} D$$

<div align="right">(2.10)</div>

where D is the sediment diameter and D_* is the dimensionless particle size.

2.4.2 Suspended load transport

As the flow velocity increases, sediment grains are drawn into the water column by an upward force. If this force is greater than the immersed self-weight of the sediment, then particles are transported within the water column as suspended load. When a reduction in

flow velocity decreases the upward force below the fall velocity, the sediment will begin to settle.

In addition to the transport of suspended sediments from the flow velocity, the natural diffusion of the particles aids the transport rate. The rate of diffusion depends on the concentration of sediment within the water column and the sediment characteristics.

2.4.3 Cross-shore sediment transport

Sediment transport that occurs in a cross-shore direction can have a net direction onshore (accretion) or offshore (erosion). This direction, and its magnitude, is primarily associated with the incident wave conditions. When waves break there is an onshore directed mass flux that results in the shoreward transport of sediment. After breaking the undertow and undertow currents are responsible for offshore transport. During storm events, where the incident wave height is larger, so to are the undertow currents. This produces dominant offshore-directed sediment transport resulting in beach erosion and recession. During calm weather conditions, the undertow is much smaller meaning that the sediment transported onshore by the mass flux predominantly remains on the beach. This is referred to as beach accretion.

2.4.4 Longshore sediment transport

An oblique wave incidence is the main process that governs the transport of sediment alongshore, through beach drifting and the formation of longshore currents. When waves approach a beach obliquely, the resulting swash motion occurs at the angle of wave approach. As the backwash is driven by gravity, it primarily occurs perpendicular to the shoreline. This combination results in a saw-tooth swash cycle that promotes the longshore transport of sediment in the direction of wave approach. This is known as beach drifting. A momentum transfer from the uprush to the backwash enhances the longshore transport rate as the backwash is also directed in line with the wave approach. Additionally, when oblique waves break they produce a longshore directed current (section 2.3.2.2). The

sediment that is entrained by the wave motion during breaking will then be transported alongshore by this current.

2.5   Beach Morphology

2.5.1 Beach profile shape

Sediment diameter is an important control of the slope of the beach (β). This is due to the natural angle of repose of the sediment and the effects that the sediment type has on the groundwater flow within the beach. The infiltration rate affects beach profile shape by controlling the volume of water that can return as backwash. In general, as the median grain diameter (D_{50}) increases, so does the infiltration rate. This subsequently causes a reduction in backwash and the volume of sediment that is returned offshore. The build-up of sediment on the foreshore results in the profile steepening until an equilibrium slope is formed. The gradient of the beach is therefore controlled by the D_{50} value, with smaller D_{50} resulting in shallower slopes. Gentle slopes associated with sandy beaches means there is considerable sediment exchange between the beach and the nearshore region, with the onshore mass flux in breaking waves transporting sediment onshore and the undertow (and possible rip currents) providing offshore transport mechanisms.

2.5.1.1 Equilibrium profile

The concept of the equilibrium profile assumes that there is a dynamic equilibrium between the forces that control sediment movement and distribution across the profile. It can be described as, the long-term profile that results from the incident wave conditions and sediment make up of the beach. Common features of equilibrium profiles are: they tend to concave upwards; smaller and larger sediment diameters are associated with milder and steeper slopes respectively; the beach face is approximately planar; and steep waves results in a milder slope and a tendency for bar formation (Dean, 1991). The concept of profile equilibrium and its use within modelling beach evolution is discussed in more detail in Chapter 3.

2.5.2 Cross-shore morphological features of beach profiles

2.5.2.1 Bars and troughs

The formation of bars and troughs in the littoral zone is attributed to the hydrodynamic and sediment transport gradients. Nearshore bar morphology can be widely varied in, both, the number present and the shape. It is thought that the most likely mechanism responsible for nearshore bar formation is that proposed by Roelvink and Stive (1989), who showed that bars form near the wave break point from the convergence of offshore and onshore sediment transport (Fig. 2.5).

Offshore transport

Transport convergence and bar formation
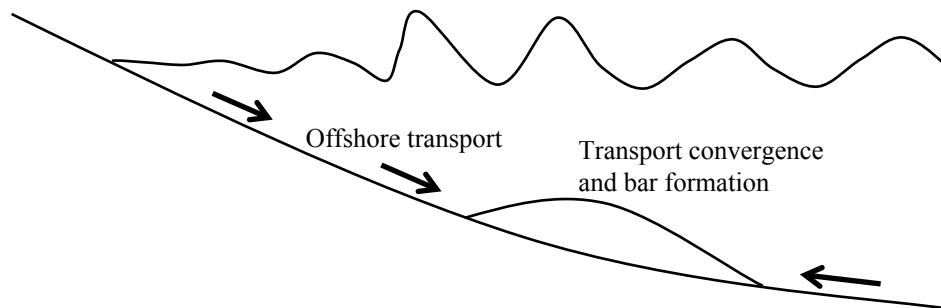
Fig. 2.5 – Schematised nearshore bar formation

Nearshore bars are highly dynamic features that migrate on and offshore when incident wave conditions change. Offshore and onshore migrations relate to higher and lower wave events respectively. The migration occurs as the alteration in the wave climate induces a change in the dominant direction of sediment flux. Upon formation, they provide a source of protection for the beach as the incoming waves break and dissipate the majority of their energy in the bar region. Beaches with a well developed bar system are therefore less susceptible to large levels of erosion. During calm wave periods, bars may merge with the beach resulting in a welded bar system.

For a more details of nearshore bar migration and modelling see Short (1992); Wijnberg (1996); Shand et al. (1999); Splinter et al. (2011); Walstra et al. (2012) and references therein.

2.5.2.2 Berms

The berm is the planar section, located landward of the beach face, that forms from an accumulation of sediment transported shoreward during calm wave conditions.

The building of a beach berm can mainly be attributed to infiltration into the beach and the spring/neap tidal cycles (Davidson-Arnott, 2010). The berm becomes overtopped when the tidal level, and subsequent swash limit, increases, resulting in sediment being deposited landward and causing build up of the crest. The height of the berm is controlled by the maximum elevation to which sediment can be transported during wave uprush. When the tide level is low, and the berm cannot be overtopped, it may build seawards rather than upwards.

Takeda and Sunamura (1982) proposed that wave height and period are directly related to berm height (Z_{berm}); and that a larger wave height and period result in a larger berm height (Eq. (2.11)).

$$Z_{berm} = 0.125 H_b{}^{5/8} (gT^2)^{3/8}$$

(2.11)

The highly dynamic nature of berms and beach faces mean that they respond rapidly to changing wave conditions, with storm events causing erosion and prolonged calm periods resulting in accretion and berm recovery.

2.5.2.3 Dunes

Coastal dunes are common features of many coastlines. They play an important role in the natural protection of coasts from erosion during extreme wave conditions. During storm events the increase in incident wave height and water level leads to erosion and the possibility of coastal flooding when a well-developed dune system does not exist. A developed dune will aid in the dissipation of wave energy through erosion, protecting the coastline from damage. The sediment eroded from the dunes will eventually be returned during calm conditions if the system is in equilibrium.

2.6   Wave Dominated Beaches

Beaches that are governed by wave action have a range of morphological features and states. These states differ considerably and are predominantly controlled by the local wave conditions and sediment characteristics.

2.6.1 Beach states

The simplest way to classify wave dominated beach states is from the D_{50} of sediment present on the beach. From Soulsby (1997) beaches can be divided into three types based on their sediment characteristics. These are sandy beaches (D_{50} = 0.1-2.0mm), gravel beaches (D_{50} = 2-250mm) and mixed beaches (D_{50} = 0.1-250mm). As this project involves modelling the variability and erosion of a sandy beach this is the only beach type discussed herein.

A more detailed and efficient classification of beach types was first proposed by Dean (1973) who used the dimensionless fall velocity of Gourlay (1968) to devise a cross-shore sediment transport model that predicted the change in the beach. This parameter has become known as the Dean parameter (Ω) and is given in Eq. (2.12).

$$\Omega = \frac{H_b}{w_s T}$$

<div align="right">(2.12)</div>

where w_s is the sediment fall velocity; H_b is the breaking wave height; and T is the period.

Wright and Short (1984) and Short (2006) extensively used Ω to categorise the morphological states of numerous Australian beach systems. These studies distinguished a basis of three possible beach states: reflective, intermediate (including four sub-states) and dissipative, which can be described by varying values of Ω. The range of Ω associated with these states is described in Table 2.2, with Fig. 2.6 providing details of these states.

Ω	**Beach State**
$\Omega < 1$	Reflective
$1 < \Omega < 6$	Intermediate
$\Omega > 6\text{-}30$	Dissipative

Table 2.2 – Dimensionless fall velocity values for beach states (Wright and Short, 1984)

$$\Omega = \frac{H_b}{w_s T}$$
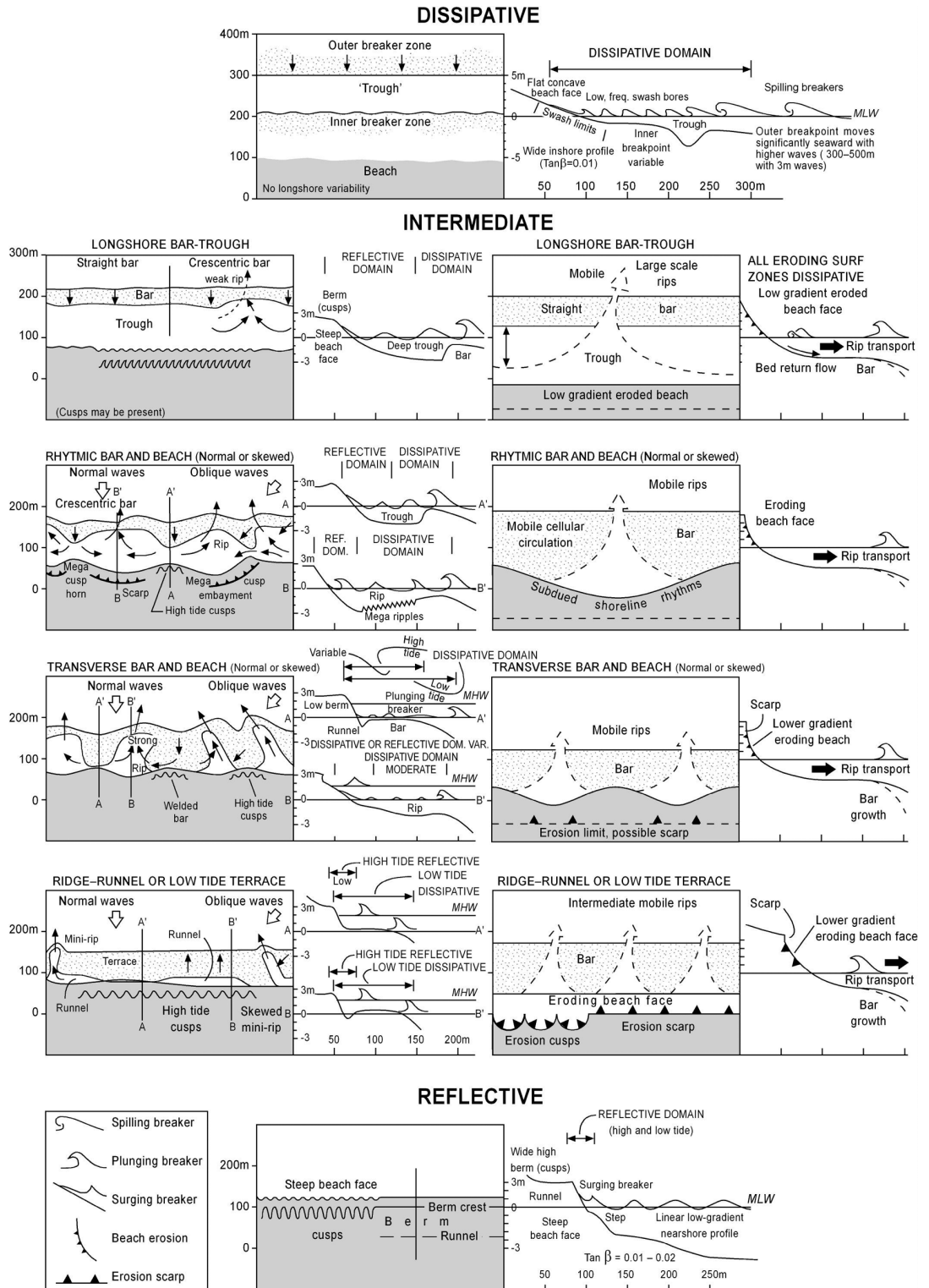
Fig. 2.6 – Definition of wave dominated beach states (Short, 2006)

2.6.1.1 Reflective beach state

A reflective state occurs on a beach with a steep gradient that allows larger waves to break close to the beach and become reflected. Breakers are predominantly surging or collapsing resulting in the formation of this steep face (Wright and Short, 1984). For sandy beaches, a reflective state can be said to be the *'fully recovered'* profile. This profile will occur from accretion after long periods of calm wave conditions and result in a complete berm that provides the highest level of natural protection to the backshore and dunes. Its formation is a result of a combination of accreted sediment and the potential welding of a nearshore bar system to the beach. A reflective beach state plays an important role in the overall long-term stability of beaches. For a beach that is frequented by high-energy storm events, the ability to return to this state during calm wave conditions is of paramount importance if long-term profile stability is to be achieved.

2.6.1.2 Intermediate beach state

Within the intermediate beach state there are four sub-states with differing morphological features. These states provide the most complex morphologies of all beach systems and are described by Wright and Short (1984) as follows.

Longshore bar-trough

This beach states include the presence of a deep trough just offshore leading to a straight or crescentic bar that extends along the length of the beach. Depending on the wave conditions, large undertow currents may exploit weaker regions, leading to increased offshore sediment transport via rip currents. As predominant wave breaking occurs at the bar it exhibits a dissipative state. The beach face exhibits a reflective state that reflects any smaller waves that break after the bar, in the trough region.

Rhythmic bar and beach

This state is the same as the longshore bar-trough formation except that the shoreline and bar are crescentic and vary in width and elevation alongshore. This state has more complex morphodynamics with constant rip channels forming and being fed by oblique wave breaking and return flows from swash events.

Transverse bar and rip current

This bar formation occurs perpendicular to the beach and is separated by deep rip channels. These rip channels are subjected to a much higher energy swash than the bar area which is responsible for producing a rhythmic shoreline pattern. Again, the wave breaking predominantly occurs on the bar, with the water flowing into the rip feeder channels and returning offshore as a strong rip current.

Ridge-runnel or Low tide terrace

These states occur in regions with lower wave heights and have a bar or terrace connected to the beach at low tide level. This means that, at high tide, smaller incident waves may not break until directly on the beach making it respond in a reflective way. During mid tide levels waves break on the bar or terrace which can lead to the formation of rip currents.

2.6.1.3 Dissipative beach state

Dissipative states are, essentially, the opposite of reflective states, with profiles having very shallow gradients and wide surf zones. These states are commonly found after storm events when the beach has eroded leaving a large shallow surf zone. This results in approaching waves breaking by spilling and dissipating their energy across this wide region, becoming very small at the beach face. In addition, when nearshore bar systems are present, the high-energy wave climate results in the offshore migration and possible flattening of the bar. This means that protection provided by the bar is now reduced and if

any high-energy wave event occurs soon after the dissipative profile has formed, the recession of the beach will increase.

2.6.1.4 Summary of beach states

From the results summarised from the study of Wright and Short (1984) (Table 2.2), it can be seen that the lowest values of Ω are therefore associated with a reflective beach state and lower incident wave heights. This has led to the reflective state being described as the '*summer*' profile, where a low energy wave climate allows for berm accretion.

As Ω increases to greater than 1, the beach state alters from fully reflective to intermediate. The intermediate beach state has the largest variation, which is evident from the categorisation of four sub-states within.

As Ω increases further the beach transitions into a dissipative state. As this increase in Ω is associated with larger wave heights the dissipative state is often categorised as the '*winter*' or '*storm*' profile. The increase in Ω within a dissipative state results in the width of the surf-zone also increasing, meaning an increase in Ω is associated with an increase in wave energy dissipated before the beach itself.

2.6.2 Beach erosion

During storm (erosive) events, the bottom sediments are mobilised within the breaker zone from a combination of the wave orbital velocity and the breaker-induced turbulence. During high-energy wave conditions the breaker-induced turbulence and return flows are large enough to cause significant offshore sediment transport. This results in shoreline recession and beach erosion. Further seaward, the sediment transport capacity of the undertow decreases and the sediment settles to form a new beach profile much wider than the pre-storm (Fig. 2.7), corresponding to a dissipative beach state. This new beach profile is in better equilibrium with storm conditions meaning that the incoming energy is

dissipated more efficiently. Based on this equilibrium principle the erosion rate therefore decreases as the storm continues.

The beach profile shape that occurs after a storm event is dependent on a number of factors. Not only are the storm event parameters (wave height, wave period, wave direction and storm duration) important but also the state of the beach prior to the storm event. The inclusion of antecedent beach states is therefore important for the development of a framework for modelling medium-term beach profile variability.
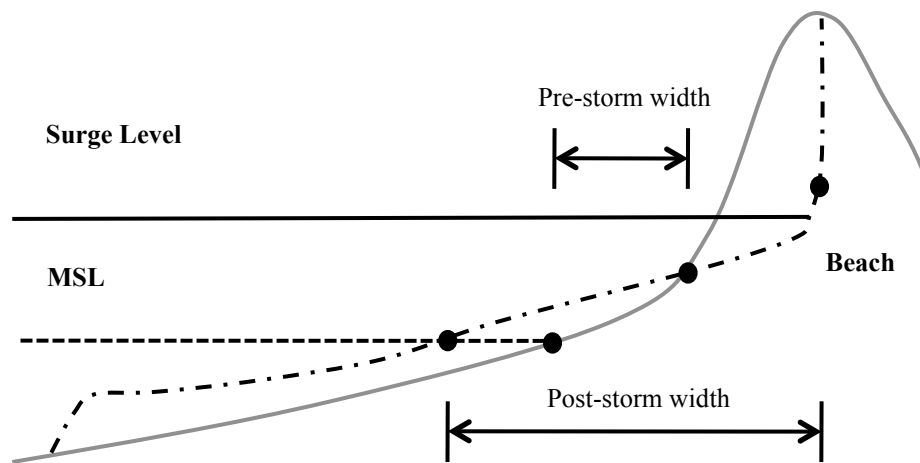
Fig. 2.7 – Schematised dune erosion during a storm event

2.6.3 Beach accretion

Beach accretion is the build up of sediment on the beach that results form onshore transport of sediment during calm incident wave conditions. Unlike storm events, these periods produce weaker return flows that are unable to transport large volumes of sediment offshore.

2.6.3.1 Wave skewness and asymmetry

For simplicity, waves are often described as a sinusoidal function of water level variation, whereas in reality they are never this shape. Sharp wave crests with flatter troughs (Stokes waves) demonstrate skewness, where higher velocities occur at the crest compared to the trough. This leads to greater sediment mobilisation under the crest and net onshore sediment transport (Grasso et al., 2011), as crest velocities are directed onshore (**Error! Reference source not found.**).

In addition to skewness, the non-linear profiles of waves are also asymmetric. Wave asymmetry is the saw-tooth formation evident in waves in the nearshore region when there is a steep front and a shallower rear. A strong asymmetric wave motion can lead to an increase in the shear stress being imparted on the bed, promoting onshore sediment transport (Walstra et al., 2007).

The experiments conducted by Grasso et al. (2011) concluded that wave skewness can lead to onshore transport when the wave asymmetry is large enough. Should the asymmetry be small, however, a large skewness will result in offshore transport due to the phase lag effects between the mobilisation and transportation of sediment. Net onshore transport of sediment can therefore only occur from a combination of asymmetry and skewness.

2.6.3.2 Surf zone sediment transport

It has been discussed previously that when waves break in the nearshore region, they generate an onshore-directed mass flux. This, combined with the skewness and asymmetry of the wave, is responsible for the onshore transport of sediment. During low energy wave conditions, this onshore mass flux is large enough that the undertow current created after breaking is insufficient to remove all of the sediment that has been transported onshore. This assists berm accretion and, if it occurs over a long enough period of time, recovery of the beach system.

2.6.3.3 Groundwater flow and swash zone transport

In addition to the wave profiles and onshore mass flux from the breaking waves, the swash zone transport and groundwater system within the beach plays an important role in the rate of accretion. Although groundwater flow also affects erosion it is not as significant due to the higher velocities and net offshore-directed sediment transport.
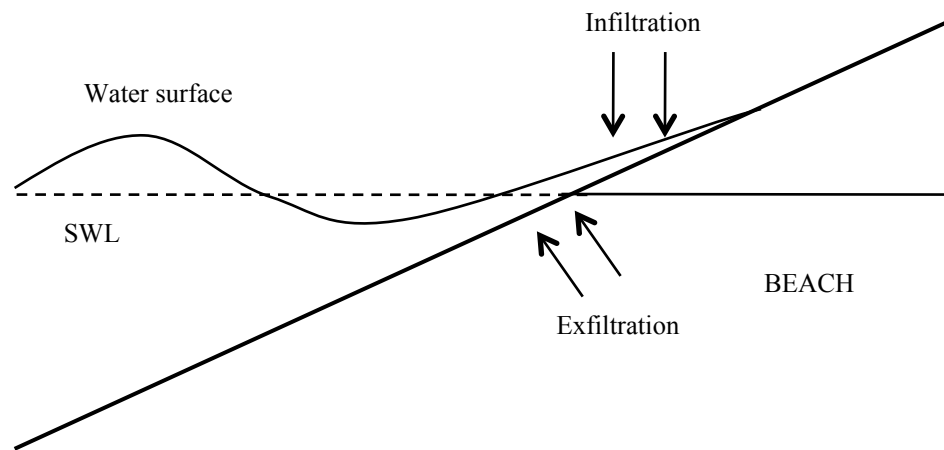
Fig. 2.8 – Schematised beach infiltration and exfiltration process

The interaction of surface flow and groundwater flow has been shown to be a key factor in controlling beach evolution. The swash zone can be divided into two regions: a lower saturated zone that promotes erosion and an upper unsaturated zone that promotes accretion (Turner, 1993; 1995). This division in the swash zone can be described as regions of infiltration and exfiltration (Fig. 2.8). Infiltration is the process in which water from the swash lens flows into the beach, with exfiltration being an outflow of water from the beach into the swash lens.

Numerous studies investigating the importance of infiltration and exfiltration on sediment transport in the swash zone have been conducted (Turner and Nielsen, 1997; Turner and Masselink,1998; Masselink and Li, 2001; Horn, 2002, 2006).

For beach accretion to occur, infiltration of water into the beach has to be dominant over exfiltration from the beach, with the unsaturated zone reducing the backwash. It has been discussed previously that the backwash created by incident waves is responsible for the feeding and magnitude of the undertow currents. During low energy wave conditions the magnitude of backwash and, subsequently, the undertow are lower. Therefore any further reduction in backwash magnitude from infiltration will reduce the volume of sediment that is transported offshore in the undertow and aid beach accretion and berm creation shoreward of the swash zone.

In/exfiltration to/from the beach depends on a number of parameters with the most important being, the groundwater level, the permeability of the beach material and the degree of saturation of the beach. Although the effects of infiltration are greater on gravel beaches, due to the larger sediment diameter and porosity, it is still an important mechanism for aiding accretion on some sandy beaches.

2.7   Chapter Summary

This chapter has provided an overview of the processes and morphodynamics that occur at sandy beaches. It has described the common hydrodynamics in the nearshore region and what affect these have on the sediment transport and morphodynamics of the beach. Many of the topics discussed will be expanded on in later chapters when discussing the behaviour of Narrabeen Beach and the modelling of beach morphodynamics.

CHAPTER 3

MODELLING CROSS-SHORE BEACH MORPHODYNAMICS

The modelling of cross-shore beach profile morphodynamics is a subject that has seen considerable advancement over the past few decades; in line with the increase in knowledge regarding the processes; and the advancement in computing capabilities. This has led to the development of numerous models capable of simulating cross-shore evolution, for most beach types. The use of these models provides quantitative prediction of beach change, allowing for sustainable solutions to complex coastal problems to be implemented. For coastlines where dune systems provide natural flood protection (i.e. Gulf of Mexico and the Dutch coast), the ability to model the erosion of these systems during extreme storm events is of paramount importance.

This chapter presents an overview of the commonly used techniques for modelling beach profile change and beach erosion. The types of models available are divided into analytical and process-based; with the development of model types, up to the current uses of XBeach discussed in detail.

3.1   Analytical Models

For the purposes of this thesis, analytical models of beach profile evolution are divided into three different types. These are, descriptive models, equilibrium profile models and empirical models. The development and use of these types of models is discussed within this section.

3.1.1 Descriptive models

The first step towards establishing a model able of predicting the way profiles evolve was through observation of profile behaviour over a range of time scales and the use of the Dean parameter (Dean, 1973) to predict the changes in beach state. It has been discussed previously (Chapter 2) that, although this model has proved useful at indicating the transitions between morphological states, its quantitative capability is extremely limited.

3.1.2 Equilibrium profile models

Equilibrium profile models have been used in a wide range of studies throughout coastal engineering to investigate beach profile change. The concept of the equilibrium profile was first investigated by Bruun (1954), who proposed the simple relationship given in Eq. (3.1), for determining water depth (h) at a distance (x) from the shoreline, using a sediment dependent parameter (A). This relationship was confirmed by Dean (1977), with A being related to the sediment fall velocity (w_s) using Eq. (3.2) by Dean (1987), as a result of fitting a linear relationship to experimental data obtained by Moore (1982). More recently, Kriebel et al. (1991) modified the relationship by accounting for the energy dissipation in breaking waves and settling sediment. This modified relationship is given in Eq. (3.3).

$$h = Ax^{2/3} \tag{3.1}$$

$$A = 0.067 w_s^{0.44} \tag{3.2}$$

$$A = 2.25(w_s^{2}/g)^{1/3} \tag{3.3}$$

The first significant use of an equilibrium profile model was by Bruun (1962) who proposed a rule that allows for the prediction of beach erosion due to sea level rise. This model is known as the *Bruun Rule* and works on the principal that sea level rise will cause the profile to become out of equilibrium, as the depth of water at a given distance from the shoreline has increased. For equilibrium to be restored to the profile, the water depth must

therefore decrease. With the absence of any external sediment input, this reduction in depth can only be achieved from the sediment eroded from the dune, due to shoreline retreat from the rising sea level, being distributed across the profile.

As the available computational power increased in line with the development of this concept, numerical schemes were included within these models. Kriebel and Dean (1985) proposed a model that expresses a cross-shore sediment transport rate (Q_s) as the difference between the actual and equilibrium levels of wave energy dissipation (D and D_* respectively) across the profile. This simple relationship is provided in Eq. (3.4) where K is a sediment transport rate parameter.

$$Q_S = K\left(D - D_*\right)$$

(3.4)

To provide a time dependent solution of profile evolution, the conservation of sediment within the profile was included. This solution is given in Eq. (3.5).

$$\frac{\partial x}{\partial t} = -\frac{\partial Q_S}{\partial h}$$

(3.5)

This simple relationship can be used to determine the time-dependent evolution of a cross-shore beach profile, assuming that sediment is conserved within the depth of closure. Although inherently limited by the lack of physical processes, the model was shown to produce good predictions for some idealised dune erosion cases (Kriebel and Dean, 1985).

Vellinga (1986) conducted a series of experiments that formed the basis behind a model developed to estimate dune erosion due to storm impacts. The model is based on profile equilibrium and is represented as a function of storm surge, wave height and sediment settling velocity. It was verified against a range of hydrodynamic conditions and profile shapes, using a series of experiments, and field data. Although application of the model

exhibited a degree of success at estimating dune erosion, it was shown to only be applicable where the coast is relatively straight and the beach can be schematised in 1D.

Modelling using the equilibrium profile concept was further developed by Dean (1991) who accounted for additional physical processes. This lead to Kriebel and Dean (1993) developing a solution that determines the time dependent response of beach profiles to extreme storm impacts. From their study, it was shown that the magnitude of erosion depended on the maximum response, if the profile forms a new equilibrium; and an erosion time scale that defines the time that this new equilibrium takes to form.

A full description of the equilibrium profile model concept and implementation is out with the scope of this thesis. Further examples of its application can be seen in Bruun (1988); Dean et al. (1993); Larson et al. (1999); van Goor et al. (2003) and Coelho and Veloso-Gomes (2004) in addition to the literature discussed above.

Although equilibrium models have been widely used for a number of years, their application and development is not without criticism. Pilkey et al. (1993) led this criticism by showing that this simplistic model breaks down in real world applications, as all of the assumptions required to implement the model are invalid for most cases. It was concluded that, although the concept of the equilibrium profile exists in nature, the model assumptions are too great to accurately represent the behaviour that exists in reality. The main assumptions that proved too restricting are, sediment being conserved within the DoC and the wave orbital velocities being solely responsible for the transport of sediment across the profile. Although some of these issues had been addressed by Kriebel and Dean (1993), the limitations of employing an equilibrium profile model are still in abundance.

Over the last decade there have been numerous further discussions into the validity of applying the equilibrium profile concept (e.g. Cooper and Pilkey, 2004; Pilkey and Cooper, 2004; Ranasinghe and Stive, 2009; Stive et al., 2009; Ranasinghe et al., 2011). These discussions are mainly concerned with the modelling of sea level rise using the

Bruun Rule, which, although not the most precise method, still provides a quick estimation that can be compared to the advanced techniques currently being developed.

Although equilibrium profile models have been heavily criticised, due to their simplicity to implement there is still use for such models for providing quick initial estimates. Many of the original critiques (e.g. Pilkey et al., 1993) were quick to highlight the limitations of the technique without proposing any solutions. The implementation of numerical techniques within these models (Kriebel, 1986; Kriebel and Dean, 1985; Larson and Kraus, 1989) has lead to the development of the process-based models that are widely used today.

3.1.3 Empirical models

The development of the equilibrium profile concept within numerical techniques was further enhanced by the inclusion of empirical relationships that describe a range of morphodynamic behaviour. This led to the development of the beach profile model SBEACH (Larson and Kraus, 1989). SBEACH combines the use of the equilibrium profile concept with empirical relationships relating sediment transport to hydrodynamic conditions. Unlike the previous attempts at numerical modelling using an equilibrium profile concept (e.g. Kriebel and Dean, 1985; Kriebel, 1986), SBEACH is a complete profile model rather than a dune erosion model. In SBEACH the cross-shore profile is divided into a number of sections based on incident wave conditions. These sections are then assigned different empirical relationships to govern the sediment transport and morphodynamics occurring within them. Although not without its limitations, SBEACH provided one of the first numerical solutions that enabled the prediction of the morphological variability of the entire nearshore beach profile.

Later Powell (1990) expanded the advancing empirical profile models by creating a similar model (SHINGLE) capable of simulating the short-term response of shingle beaches. Like the previous model discussed, SHINGLE is also an empirical model with morphodynamic relationships determined from laboratory tests.

Again, in a similar approach to SBEACH, Stive and de Vriend (1995) proposed a simple panel model that divides the profile into; a fast changing upper region, a slower changing lower region and a transitional zone between the two. The main basis of this model was to apply rules based on the conservation of mass between regions; and determine sediment supply and demand of these regions using empirical relationships. When tested against the observed behaviour of the Central Holland Coast, using approximately one century (1896 to 1975) of hindcast wave data and a rate of sea level rise, the model was shown to estimate profile variability at a similar order of magnitude estimate to that observed. Although this model was reasonably successful, Stive and de Vriend (1995) highlighted that fact the coefficients used in the empirical relationships may well be responsible for *"hiding"* some of the mechanisms not incorporated in the model. At a similar time, Cowell et al. (1995) developed a model for quantifying large-scale coastal behaviour. This model is similar to that of Stive and de Vriend (1995) as it parameterises dynamic processes and applies local rules to the beach profile that governs its response when sediment mass balance is included.

The development of many of the empirical models (e.g. Cowell et al., 1995 and Stive and de Vriend, 1995) were focussing on long-term profile change. Therefore, to more effectively represent the short-term erosion of dunes and beaches by empirical means, a technique known as *"wave impact theory"* was derived. This technique was first proposed by Fisher and Overton (1984) and then extended by Nishi and Kraus (1996). It uses empirical relationships to determine the recession that occurs from individual swash bores that impact the beach. Larson et al. (2004) further developed this technique and proposed a model that combines wave impact theory with the sediment volume conservation equation to provide a model that could estimate dune recession and erosion during storm events.

The main limitation of these models is the calibration of the empirical coefficients. These coefficients cover so many processes that they cannot be widely applied to different coastlines. However, due to their simplicity and limited computational requirements, there is the possibility to combine such models with longshore models of sediment transport to attempt to simulate longer-term beach evolution.

3.2 Process-based Models

The use of process-based models within coastal engineering has become much more prevalent in recent years. This has lead to the development of numerous such models that have been shown to be successful at simulating some form of cross-shore beach profile evolution. This type of model explicitly accounts for the different morphodynamic processes that govern profile evolution. As these models provide a more complete description of the physics behind the morphodynamics, they are considered more accurate and widely applicable than the previously discussed analytical modelling techniques. However, along with this degree of accuracy and applicability are a number of disadvantages. The most significant of which are; insufficient descriptions of non-linear process interactions, the accumulation of errors that occur when simulating longer time scales; and the large computational time required.

3.2.1 Description and structure

Process-based models provide a more comprehensive description of the physics that govern beach morphodynamics by including a mathematical description of these processes. These models rely on the physical processes alone and attempt to provide detailed descriptions of the hydrodynamics, flow velocities, sediment transport rates and corresponding changes in morphology. Although these models attempt to completely represent the physics behind the processes, they still make use of empirically derived sediment transport equations to determine the transport rates and subsequent changes in bathymetry.

For simplicity, process-based models can be split into two modules, the hydrodynamic module and the sediment transport module. The hydrodynamic module describes the interaction of the incoming waves, tidal conditions, wave-induced set-up, flow velocities and currents. The sediment transport module uses the hydrodynamic outputs and determines the associated sediment transport gradients. The change in sediment distribution across the profile enables the morphology to be updated and the process looped allowing for the simulation to continue (Fig. 3.1).
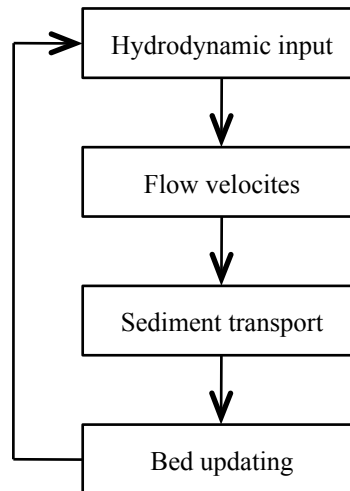
Fig. 3.1 – Simplified process-based model structure

These types of models define the domain as a structured grid system, with the grid spacing commonly varying throughout this domain. This variation is typically user defined (rather than adaptive) and allows for the regions where larger variation in parameters (i.e. the nearshore region and beach) to be defined using a finer spacing than further offshore.

The strength of these models is that they do not rely on an equilibrium assumption, which is dependent on local conditions and is often determined from measured data, and they include detailed descriptions of physical processes. However, due to the empirical relationships used for sediment transport calculations, the use of such models requires caution when applying them to simulate beach change over large time scales.

3.2.2 Modelling beach profile evolution

The first comprehensive description of process-based modelling of beach profiles is provided by Roelvink and Broker (1993) who give a detailed description of the theory and development of these models, in addition to the assessment of some of the original models developed (e.g. Watanabe and Dibajnia, 1988; Roelvink and Stive, 1989; Nairn and Southgate, 1993; Southgate and Nairn, 1993). From this study, the usefulness of using a

process-based technique for modelling the short-term evolution of coastal profiles became evident. It was shown that, the current models operated best in the central part of the surf zone where waves are breaking and bar systems develop. Additionally, although some of the necessary physical processes had not been incorporated at this stage, the ability to simulate beach accretion using such models was well recognised.

From the study of Roelvink and Broker (1993) it became clear that the errors produced within the morphological steps were added up throughout the simulations, meaning their applicability is limited. Due to the lack of knowledge regarding many of the physical processes at this stage in model development, many of these were not accounted for in the early model attempts discussed.

As with the increase in accuracy and applicability of analytical models, process-based models have seen continual development in line with the knowledge of coastal processes and the increase in computational power and techniques. Since the original assessment by Roelvink and Broker (1993) the accuracy, robustness and use of process-based models has developed steadily. These developments lead to van Rijn et al. (2003) conducting a similar study, that compared the ability of five process-based models at predicting beach profile response at a time-scale of storms and seasons. The models tested were UNIBEST-TC of Delft Hydraulics (Reniers et al., 1995), COSMOS of HR Wallingford (Nairn and Southgate, 1993; Southgate and Nairn, 1993), CROSMOR of the University of Utrecht (van Rijn and Wijnberg, 1996), BEACH1/3D of the University of Liverpool (O'Connor et al., 1998; O'Connor and Nicholson, 1999) and CIIRC of the University of Catalunya (Sierra et al., 1997; Sierra, 1999).

At this stage in the development of process-based models van Rijn et al. (2003) concluded that, a *"reasonable"* prediction of wave heights and undertow currents across the profiles could be simulated by the models. However, these results were only achieved after calibration of key empirical parameters, highlighting the level of caution that is required when using these types of models. As well as the distribution of wave heights and undertow, the models were shown to *"reasonably"* reproduce the behaviour of offshore

and nearshore bar systems at short-term, storm, time scales. This shows that the models can pick up on the offshore migration of bars that occurs during high-energy wave conditions. Although, some models could capture this movement, the models poorly represented the behaviour and variability of the beach itself during storm events.

In addition to the study at a storm time-scale, the models were tested on the ability to reproduce morphological behaviour at a seasonal time scale. These tests indicated that, at a seasonal time scale, only the behaviour of the outer bar could be simulated to any degree of accuracy. At this time scale it was shown that these models are limited in their prediction of nearshore bar and beach behaviour. It was discussed previously by Roelvink and Broker (1993) that using process-based models at long timescales would result in an inaccurate prediction due to an accumulation of errors within the processes. The poor results obtained at the seasonal timescale by van Rijn et al. (2003) highlights this. However, as the velocities are considerably lower in the offshore bar region, this may have led to the error accumulation being less significant, meaning offshore bar system behaviour could be effectively simulated by some models.

From the study of van Rijn et al. (2003) it can be concluded that, although a number of models can reproduce the behaviour of various morphological features, a single model cannot predict the behaviour of the entire beach profile effectively, at storm or seasonal time scales.

3.2.3 Beach profile and dune erosion modelling

During extreme storm events Sallenger (2000) and Sallenger et al. (2003) showed that dunes are subjected to the following four regimes:

1) Swash regime: When the swash is confined to the beach foreshore, seaward of the dune or berm crest.

2) Collision regime: When the wave run-up collides with the dune resulting in erosion.

3) Overwash regime: When the erosion of the dune lowers the crest level causing overtopping from incoming waves.

4) Inundation regime: When the overtopping can no longer be considered overwash and the entire dune becomes submerged.

To model the morphodynamic changes that occur during dune erosion more successfully, many of the original process-based profile models were developed further to account for the regimes outlined above. An example of this is the extension of the CROSMOR model (van Rijn and Wijnberg, 1996) to CROSMOR2007 (van Rijn, 2009). This model focuses on the collision regime that occurs during extreme storms and was shown to successfully replicate experimental tests of dune erosion. Although this proved to be a successful development in process-based modelling it was limited in the fact that it only focuses on the collision regime. For this reason the CROSSMOR2007 model cannot accurately represent dune overwash or inundation and therefore, does not provide a complete estimate to all stages of beach erosion induced by extreme storms.

In 2009 Roelvink et al. (2009) proposed the XBeach model for simulating eXtreme Beach behaviour. XBeach was developed to effectively simulate the four dune erosion regimes outlined previously, while also extending the capabilities to include longshore (2DH) morphodynamics. Although XBeach is a relatively new model, the principles and structure behind it were taken from existing models, such as that of Reniers et al. (2004), and expanded upon. XBeach has now become one of the most widely used process-based models, for simulating storm-induced beach erosion.

The original XBeach model has been extensively validated against numerous flume (1D) and field (2DH) studies. The most comprehensive set of flume results is discussed by Roelvink et al. (2009), with its application for modelling erosion of sandy beaches discussed by Roelvink et al. (2009); Bolle et al. (2010); Lindemer et al. (2010) and McCall et al. (2010).

The successful validation and use of XBeach for modelling sandy beaches has lead to its extension into the modelling of gravel beaches. This was led by Jamal et al. (2010) who showed that modification of the flow velocities and the inclusion of infiltration, resulted in the ability to reproduce berm formation evident in flume tests of gravel beaches. In addition, field tests de Alegria-Arzaburu et al. (2010) and Williams et al. (2012) showed that the erosive and accretive profiles occurring on gravel barriers can be simulated effectively.

During the experimental tests and field studies outlined above, all have focused on the short-term (storm) time scale. So far the use of XBeach has been curtailed at this time scale, making the calibration discussed in this thesis providing a first attempt at using XBeach to simulate longer-term (monthly) beach recovery simulations.

The use of XBeach as a modelling tool has become much more prevalent in recent years and as such it is in continual development. A test case of assessing the ability of XBeach at simulating erosion around sea walls and revetments (van Geer et al., 2012) showed that XBeach generally coped well with the observed erosion. However, it was shown that the erosion above the structures was underestimated, as XBeach did not include any mechanism for short wave run-up. To remedy this van Thiel de Vries (2012) included short wave run-up into the model so as to better represent the erosion above revetments.

More generally, the entire XBeach model has been extended to allow application to curvilinear grids (Roelvink et al., 2012) by including a finite volume scheme. The tests from this study showed that the model provided better skill scores using a curvilinear grid than individual 1D simulations.

In addition to the extension of the model for sandy beach scenarios, there have been advancements in the modelling of gravel beach morphodynamics using XBeach. The success of the original modifications of Jamal et al. (2010) led to a further study investigating morphological changes of a gravel beach during tidal cycles (Jamal et al.,

2012). This study shows that the original modifications to the model means it can also provide approximations of profile change when a tidal fluctuation occurs. In addition to the modifications of Jamal et al. (2010, 2012), the work of McCall et al. (2012) shows a further example of the extension of XBeach, into the modelling of gravel beaches, by including a quasi-3D process-based groundwater flow module into the model. This inclusion provides a much more detailed description of the run-up and overwash that occurs during erosion of gravel beaches.

3.2.4 Beach accretion

Although modelling beach accretion was first mentioned by Roelvink and Broker (1993), up until recently the majority of modelling cross-shore beach evolution has focused on erosive conditions. Although, the study of van Rijn et al. (2003) simulated accretive (calm) hydrodynamic conditions at the seasonal time scale, the focus of the simulations was across the entire profile with no specific attention paid to berm build up or recovery of the beach itself.

van Rijn et al. (2011) carried out a number of tests on the advanced CROSMOR, UNIBEST-TC and DELFT3D (Lesser et al., 2004) models to assess their ability at simulating accretion. However, as the tests began with a planar sandy beach profile, during accretionary wave conditions, the profile suffered erosion with the eroded material deposited offshore. These results provided no indication of the models' capabilities at simulating berm build up during beach recovery.

3.3   Longer-term Modelling

Modelling longer term coastal evolution has been discussed for a number of years (e.g. de Vriend, Capobianco, et al., 1993; de Vriend et al., 1993; Stive and de Vriend, 1995; Hanson et al., 2003) with the earlier discussions focusing on the use of empirical or behaviour-orientated numerical models and the 2D evolution of beaches.

In terms of longer-term, cross-shore, beach profile change using a process-based model, there are limited studies. van Rijn et al. (2003) showed some success in the use of such models at simulating certain profile behaviour at the seasonal timescale. This seasonal timescale was divided into three six-month periods (two summer and one winter), with skill scores for each model at predicting changes in the outer and inner bar systems and the beach. The results showed that only the UNIBEST-TC and CROSMOR models provided sensible results, as the other models were primarily storm impact models. The results from these tests showed that the models could simulate the response of an outer bar system (after sufficient parameter calibration) with relative accuracy. That being said, the simulation of the beach and inner bar changes were unsuccessful, even with parameter tuning.

The seasonal event timescale was again investigated by van Rijn et al. (2011) using DELFT3D to assess the impacts of beach nourishment over a 140-day period, even though no direct comparison to any measured data was provided. Although this showed that the nourishment would erode at a rate approximately equal to that observed; the erosion regime used within DELFT3D is insufficient to provide an accurate representation of beach change during storm events. Additionally, the wave climate for the first 100 days was low (1m) meaning that large-scale erosion of the beach did not occur.

3.4   Choice of XBeach

To ensure that the SPA is implemented effectively, it is important that a suitable process-based model be identified for use within the methodology. The main requirement of the model is that it has to be able to effectively simulate beach erosion. In order to do this it is imperative that its formulation allows for the modelling of sediment transport and morphodynamics in the swash region. As many of the older process-based models, discussed previously, do not allow for this, they are unsuitable for use within the SPA. In addition, the more recent morphodynamic model, DELFT3D, is also primarily a nearshore model and cannot effectively simulate the change of the beach itself. The development of CROSSMOR2007 by van Rijn (2009) does however allow for effective simulation of beach erosion and would be therefore be a suitable candidate for use. That being said, it

was decided that XBeach is the most suitable process-based model for the following reasons.

Firstly, XBeach provides a 2DH description of the short wave groups; with nearshore water levels derived from short wave motions. This allows the swash zone to be included in the model and detailed simulation of beach erosion in this region is therefore achievable. Additionally, the robustness of the model has been extensively tested through validation at different field sites. Also, for longer-term simulations the computational efficiency is important and the fact that XBeach can be run on multiple processors means that this can be optimised in the SPA methodology. Finally, XBeach is an open-source model with an active user and support community, meaning that there is scope to alter and change components of the source code if this is required. All of these reasons have led to XBeach being selected as the most appropriate process-based model for use within the integrated methodology of the SPA.

The use of XBeach leads to a number of requirements for the SPA methodology to be implemented effectively. As with any process-based model there is a certain level of calibration required to achieve accurate simulations, meaning that suitable field data are required to calibrate the model effectively. It has been discussed previously that the SPA will use the process-based model to simulate erosion and accretion, to allow for the inclusion of antecedent beach profiles into the framework. As XBeach has been developed as a dune erosion model, the simulation of accretion will require an additional parameter calibration. This will lead to the requirement for the switching between two model setups to attempt to simulate continual profile variability. This switching mechanism means that there is an additional requirement for the identification of erosion and accretion periods at the selected field site.

3.5   Chapter Summary

This chapter has demonstrated the considerable advancement in the techniques used for modelling, cross-shore, beach profile evolution. It has been discussed how the current

process-based models available provide robust modelling tools that have been extensively calibrated through flume and field test cases. However, most of these test cases have focused on the concept of beach and dune erosion with little attention being paid to accretion and the recovery of beaches. The calibration of XBeach presented in Chapter 6 therefore provides a first attempt at using a process-based model for estimating the recovery of a sandy beach.

Additionally, most of the longer-term modelling discussed predominantly involved the simulation of profile change during low energy wave climates. Accurate modelling and quantification of the evolution of the beach itself at these time scales is a considerably more difficult prospect due to the changes in morphology that occur almost on a wave-by-wave time scale. These difficulties are significantly enhanced when attempting this at an extremely dynamic location with a highly energetic wave and storm climate. From this it is evident that, the use of XBeach within the SPA provides the first significant attempt to use a process-based model for estimating medium-term erosion and variability.

CHAPTER 4

NARRABEEN BEACH

To implement and validate the SPA methodology proposed in this thesis, a field site that has an extensive record of offshore wave and beach profile data is required. There are a number of sites throughout the world (e.g. Duck, North Carolina and the Dutch coast) that would be suitable for developing the methodology presented here. However, as the aim is to expand on the previous work of Callaghan et al. (2008), it was decided that this project should also use Narrabeen Beach as a field site as it will allow for future comparisons between these methods to be drawn. At Narrabeen Beach an extensive set of beach profiles and wave climate measurements that span several decades exists. This provides adequate data for the calibration of XBeach and makes it suitable for the statistical modelling of the storm climate and the validation of the SPA methodology. In addition, due to the extensive studies that have been conducted on erosion events (e.g Lord and Kulmar, 2000; Kulmar et al., 2005; Harley et al. 2009) there is common agreement on the division of erosion and accretion wave conditions, a prerequisite for the use of XBeach in the SPA modelling framework.

This chapter provides an overview of Narrabeen Beach, focusing on the wave and storm climate of the region and its morphological variability. A brief analysis of the available wave and beach profile data is conducted to provide an understanding of the data used within the SPA methodology.

4.1   Location and Characteristics

Narrabeen Beach is located approximately 20 km north of Sydney (34S 42' 49.84", 151E 18' 5.32") and is a 3.6 km embayed beach (Fig. 4.1). The beach can be described as predominantly having an intermediate state with a transverse bar and rip system (Short,

1984), that experiences semi-diurnal, microtidal conditions (spring tide range $\approx$ 1.25 m). The region is subjected to a highly variable, moderate to high-energy wave climate, with frequent storm events impacting the beach throughout the year.

The sediment are quartz and carbonate sands with a median diameter (D_{50}) ranging from 0.25 to 0.50 mm (Short, 1985) resulting in a relatively steep beach face (Fig. 4.2). The sediment distribution across the beach face varies, with the coarser sediments found in the trough features, that are extensively rippled from waves and currents (Short, 1984).
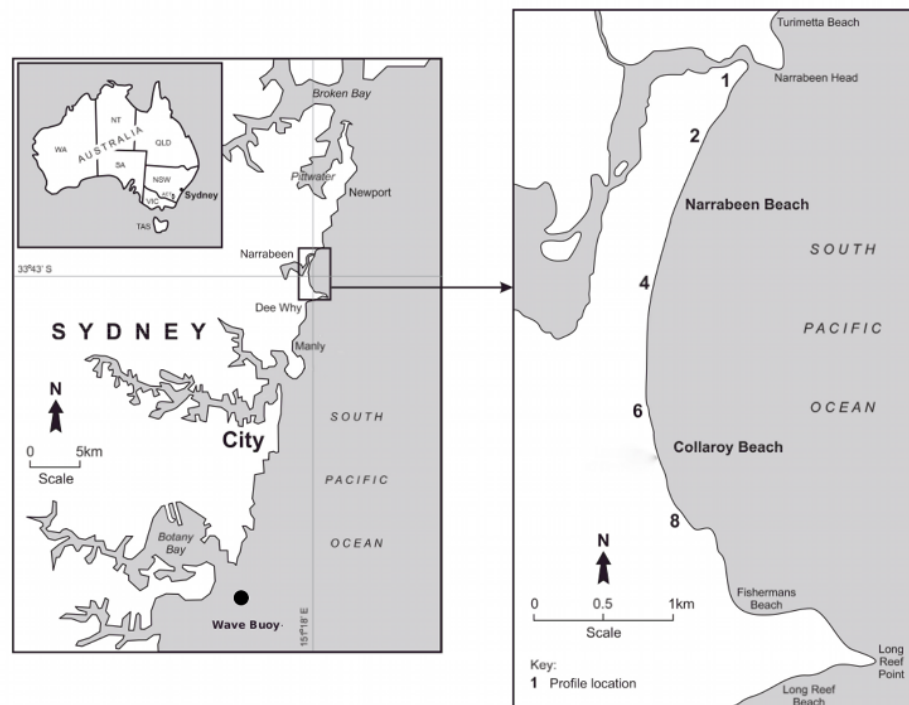
Fig. 4.1 – Location of Narrabeen Beach, measured profiles and Waverider buoy (modified after Harley et al., 2011)

Fig. 4.2 – Beach face and sediment characteristics at Narrabeen Beach

4.2　Wave Climate

The wave approach at Narrabeen Beach is from easterly, southeasterly or northeasterly directions. Due to the generating sources, the region is subjected to a persistent, high-energy wave climate with a large degree of variability. This section provides a summary of the characteristics of the wave climate based on the studies of Short and Trenaman (1992), Lord and Kulmar (2000) and Harley et al. (2010).

4.2.1 Meteorological controls

The wave climate of the Sydney region is controlled by five meteorological systems: tropical cyclones; east-coast cyclones; mid-latitude cyclones; zonal anti-cyclonic highs and local sea breezes. Tropical cyclones generated in the Coral Sea, to the northeast, travel southwards towards the NSW coast. These are infrequent, occur in mid to late summer (December to April) and produce a high-energy wave component during a period when relatively low wave heights and periods are usually most prevalent (Short and Trenaman, 1992). East-coast cyclones are generated along the NSW coast in the Tasman Sea, rather than travelling from the tropical region to the north. Compared to the tropical cyclones, these have much shorter durations but are twice as frequent. They are responsible for producing the largest waves experienced on the coast, contributing to the high variability of annual wave heights (Short and Trenaman, 1992). Mid-latitude cyclones are the systems that provide the most frequent wave conditions in the Sydney region (approximately 200

days/year). Again, these are generated in the Tasman Sea and result in predominant wave incidence from the southeast (Short and Trenaman, 1992). Anti-cyclonic pressure systems are generated by calm easterly winds and are responsible for a low to moderate energy waves. Due to the calm nature of this system it is uncommon for storm events to be generated. This weather system is particularly prevalent during the summer period and generates local sea breezes that result in several days per month of northeast wave incidence (Short and Trenaman, 1992).

4.2.2 Wave height, period and direction

Short and Trenaman (1992) showed that Sydney has a moderate to high swell and wind wave climate (significant wave height H_s = 1-2m, 63%) with few periods of low waves (<1m, 10%) and significant periods of high waves (2-3m, 22%; 3-5m, 5%).

By analysing 20 years of directional wave data measured off the Sydney coast between 1971 and 1991, Short and Trenaman (1992) showed that, waves from the northeast predominantly occur during the summer months and have a relatively low average H_s (1.25m) and T_s (7-8s); and rarely exceed 3.0m and 10s respectively. Wave incidence from easterly and southeasterly directions occurs throughout the year, peaking during March and November, for easterly waves, and May and November, for southeasterly waves. The average H_s for waves approaching from the east is 1.5m (T_s = 9s), with waves from the southeast having a much larger variability in H_s and T_s. These southeasterly waves have a larger maximum H_s (4m), with their associated period also being greater.

Waves that arrive at Sydney from the northeast account for 17% of the annual contribution and are associated with summer conditions attributed to the tropical cyclones that form in the Coral Sea during this period. Wave approach from the east accounts for 42% of the annual occurrence and has more variability in their annual and monthly trend. Waves from the southeast occur 41% of the year and increase in frequency from February to August before exhibiting a decline from August to January. This monthly modal direction described by Short and Trenaman (1992) simplifies to the breakdown provided in Table 4.1.

Direction	Dominant Months
Northeast	Apr-Sep, Dec
East	Jan-Mar, Oct-Nov
Southeast	All (summer max and winter min)

Table 4.1 – Summary of predominant wave direction in Sydney region

Combining all wave directions, Short and Trenaman (1992) concluded that there are two distinct patterns regarding wave direction in the Sydney region. These can be described as winter and summer seasons. Winter (April-September) is dominated by a broader spectrum of height and period; with longer period waves having a wide range of heights. Whereas, in summer (October-March) moderate waves (1.5–2.0m) with 7-8s periods dominate.

The overall annual mean H_s during the recording period was 1.59m, with the variability being greatest between February and July and least between October and January. The annual mean T_s was 7.98s with the monthly variation increasing from December (7.32s) to a peak in June (8.65s), before decreasing back to the December minimum.

4.3 Morphodynamic Variability of Narrabeen Beach

4.3.1 Beach state and morphology

Due to the high energy of the wave climate and the frequent occurrence of storm events, the beaches in the Sydney region are some of the most dynamic on the planet. This is due to the inner continental shelf being steep and thus, allowing for most of the wave energy to reach the shore, producing highly variable morphology (Short and Wright, 1981).

From the beach states discussed in Chapter 2, Narrabeen Beach is characterised as predominantly having an intermediate state. However, due to the high energy wave climate found in the region, Wright and Short (1984) showed that Narrabeen Beach exhibits a wide range of Dean parameter (Ω), that covers almost all of the beach states defined in Chapter

2. Due to the variable wave climate, a change between states was shown to occur as frequently as once per week (Wright et al., 1985).

Although the state of Narrabeen Beach changes frequently, the occurrence of transverse bar and rip channels is regular. The rip channels were shown to form during the intermediate beach state, accompanied by moderate to high wave heights. The rip currents are categorised into three types: erosion, mega and accretion (Short, 1985). Erosion rips are associated with rising waves and accompany general beach erosion during storm events. They are responsible for removing sediment from the beach and transporting it seaward of the surf zone, thus altering the beach state from intermediate to dissipative. Mega rips are large scale (> 1km) and are erosion rips controlled by the bathymetry. They occur in locations where the beach cannot develop a dissipative state. Accretion rips occur during stable, low-energy wave conditions, that usually follow erosive conditions (Short, 1979). During these periods the rip currents are still responsible for the offshore transport of sediment but this now occurs at a lower rate than the onshore transport, resulting in overall accretion.

From the beach profile surveys, carried out at Narrabeen Beach, it is possible to identify the three states that occur. By using measurements at profile 4 (Fig. 4.1), Short and Wright (1981) identified the three states in measurements made on 25th November 1977 (reflective), 12th February 1978 (intermediate) and 8th June 1978 (dissipative).

The result shown by Short and Wright (1981) has been replicated in Fig. 4.3. This shows the transition of Narrabeen Beach through the three beach states. On 25th November 1977 the beach was seen to have a fully reflective state with a steep face and high berm crest, resulting from accretion during a period of low energy wave conditions. The intermediate beach state measured on 12th February 1978 shows the characteristics described previously, with a rip channel and nearshore bar forming. It is evident that these features are due to moderate to high incident wave energy as sediment has been eroded from the shoreface and transported offshore, leading to bar formation in line with the theory of Roelvink and Stive (1989) discussed in Chapter 2. A dissipative beach state has been

measured during the winter period (8th June 1978) and shows evidence of high-energy waves (storms events) that cause major beach erosion. The erosion rips have transported sediment further offshore causing bar migration and leaving a wide shallow surf zone.
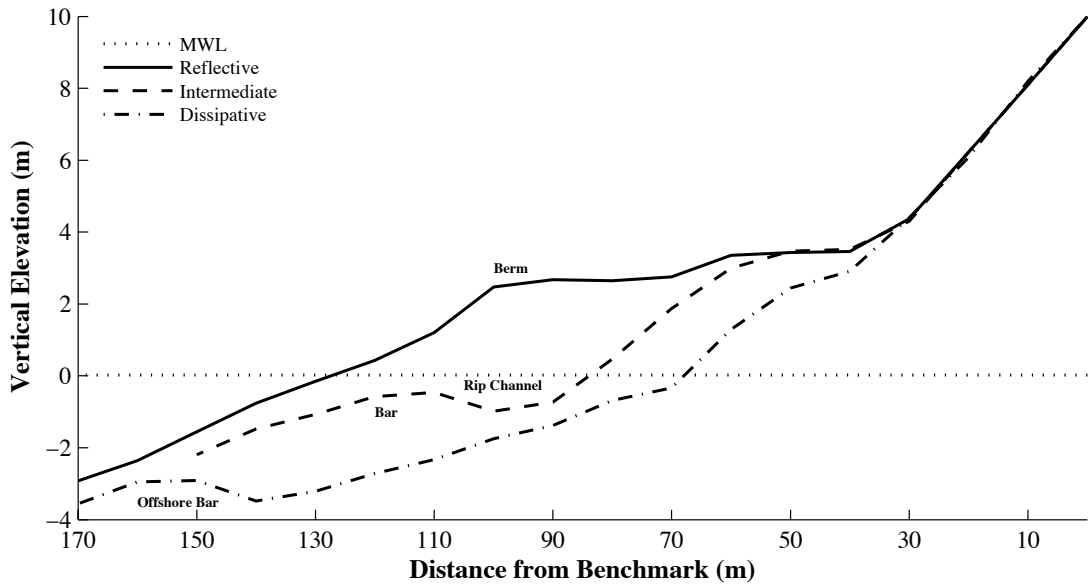
Fig. 4.3 - Variation in beach states exhibited at Narrabeen Beach from Short and Wright (1981)

4.3.2 *Beach rotation*

After the initial studies into the states and cross-shore variability of Narrabeen Beach, the longshore variability was assessed (Short et al., 1995; Short et al., 2000). These studies indicated evidence of a medium-term process known as beach rotation. Beach rotation causes periodic erosion/accretion cycles at Narrabeen Beach, with these varying between the northern and southern ends of the beach depending on predominant wave incidence. A pattern of northern end erosion and southern end accretion is evident from August 1990 to October 1994 (Fig. 4.4). It was suggested by Short et al. (1995) that there is a correlation with this rotation and the El Niño/La Niña Southern Oscillation Index (SOI), and its effects on the wave climate of the Pacific Ocean region. The SOI is a measurement of the atmospheric component of El Niño/La Niña events and the changes in sea surface temperature. El Niño events are associated with a negative SOI and an increase of sea surface temperatures, whereas La Niña is the opposite (positive SOI and lowering of sea

surface temperatures). From the wave generating systems discussed in section 4.2.1, Phinn and Hastings (1995) showed that tropical cyclones and east-coast cyclones have less of an influence on the Sydney wave climate during El Niño events. From these studies, a hypothesis was formed that wave incidence can shift south during El Niño events and north during La Niña events. This hypothesis lead Short et al. (2000) to propose that the El Niño events result in northward longshore transport leading to erosion at the southern end and accretion at the northern end of Narrabeen Beach. Thus, La Niña events should have the opposite affect on the beach (southward transport, northern end erosion and southern end accretion).

Ranasinghe et al. (2004) conducted a further study using profile measurements made along Narrabeen Beach and attempted to provide a definitive correlation between the SOI in order to gain a better understanding of the mechanisms that govern this rotation. Their study confirmed the proposition of Short et al. (2000) that El Niño events cause northern end accretion and southern end erosion, resulting in a net clockwise rotation. It was shown that, although the predominant wave direction remains southeast during both events, wave approach becomes more northerly/southerly with increasing/decreasing (La Niña/El Niño) SOI causing the rotation of Narrabeen Beach.

Short and Trembanis (2004) investigated the affects of the SOI on the change in beach width and rotation of Narrabeen Beach using the same profiles. This study established a large variation in beach width and natural shoreline movement in what can generally be considered a stable beach system. The net change in beach width, during these cycles, was quantified by Ranasinghe et al. (2004) for profiles 1, 4 and 8 during the 1986 – 1989 El Niño / La Niña period and is summarised in Table 4.2.

These results demonstrate the observed rotation with the maximum net changes in width occurring at the northern and southern ends of the beach (profiles 1 and 8) and the centre (profile 4) being least susceptible. Although profile 4 was shown to have the lowest net change in width there was still a large degree of variation in width (+13m and -12m) evident during some periods (Ranasinghe et al., 2004).

(a)   (b)
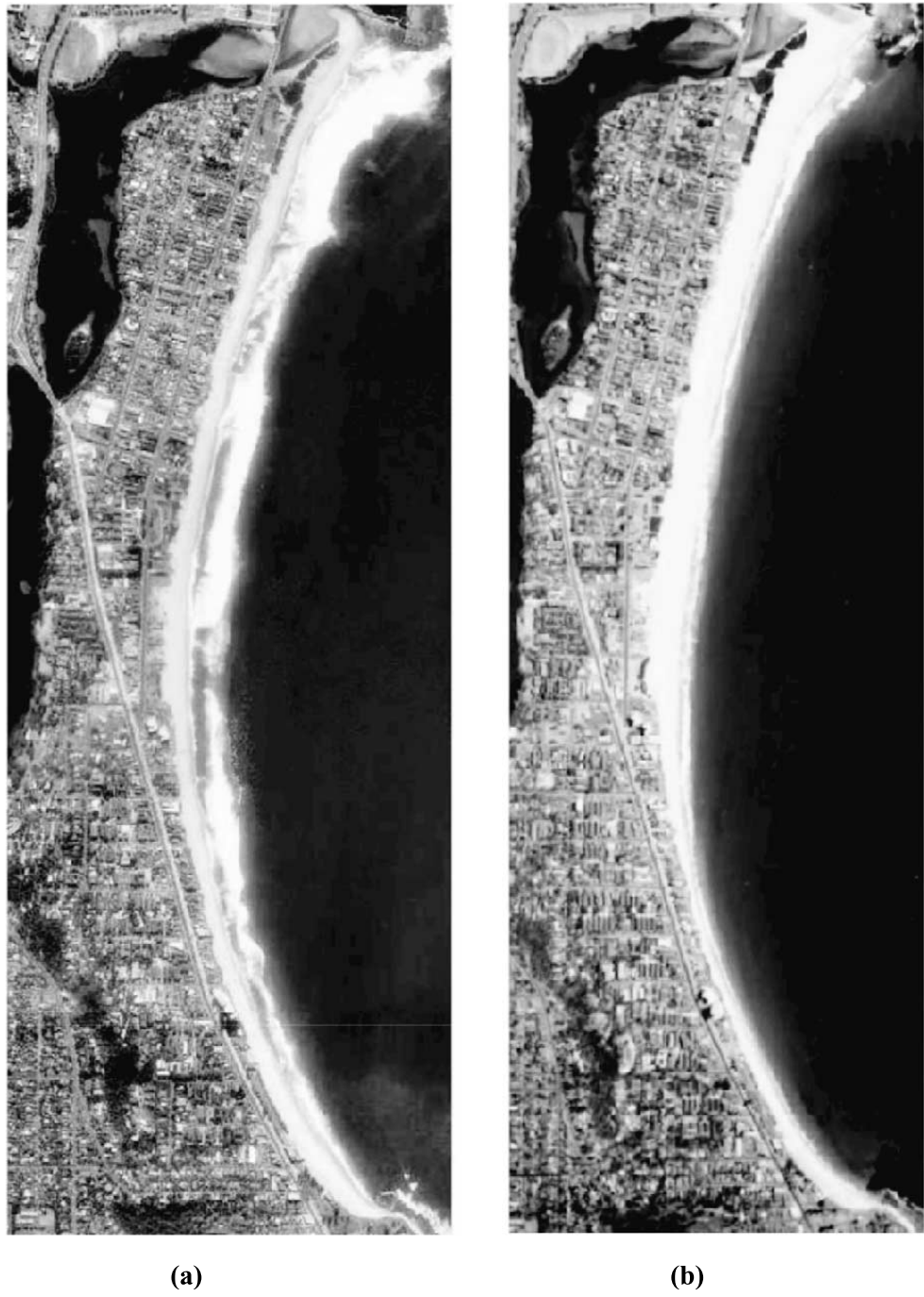
Fig. 4.4 – Beach rotation exhibited at Narrabeen Beach from August 1990 to October 1994. The erosion at the south and accretion at the north is clearly evident (Ranasinghe et al., 2004)

	Beach Profile		
	1 (North)	**4 (Centre)**	**8 (South)**
Net accretion (+)/erosion (-) during El Niño (m)	+14	+1	-10
Net accretion (+)/erosion (-) during La Niña (m)	-12	-2	+15

Table 4.2 – Net erosion and accretion at Narrabeen Beach during 1986-1989 El Niño / La Niña cycles (Ranasinghe et al., 2004)

The monitoring of the variability of Narrabeen Beach has continued, more recently, through the use of video imaging techniques along with profile measurements (e.g. Turner and Anderson, 2007; Harley and Turner, 2008; Harley et al., 2011).

4.4   Measured Wave Climate Data

4.4.1 Data Preparation

The wave data available have been measured between 1971 and 2006, offshore of Botany Bay (Fig. 4.1) by the NSW Maritime Services Board and are non-directional data collected from a Waverider buoy. Today, Manly Hydraulics Laboratory (MHL) is responsible for wave data collection within NSW, with it now being collected from a directional Waverider buoy located offshore of Long Reef Point (Fig. 4.1). Detailed information regarding wave measurements can be found in Kulmar et al. (2005).

The original data were recorded from 8th April 1971 to 22nd May 2006 and include measurements of date, time, H_s and T_s. The frequency of the recordings varies throughout the dataset, ranging from six-hourly intervals at the start, to ten-minute intervals towards the end. Along with the irregular sampling frequency there are a number of gaps in the data. To make the modelling procedure efficient it was decided that the original data be transformed into a set with a regular sampling interval. This was achieved through interpolation, where appropriate, and the addition of null values (*NaNs*) where large gaps occurred. This allows for the grouping of storm events to be automated and also provides the means to simply apply the methodology to other field sites in the future. The raw dataset was therefore transformed into a timeseries with a regular 20-minute sampling

interval spanning from the 1st January 1981 to 31st December 2005 (*ca.* 25 years). Although reducing the number of data used within the statistical model will result in less accurate extreme value predictions, a time series of 25 years is considered appropriate for the purposes of this project. Fig. 4.5 provides a plot of the daily mean H_s from 1981 to 2005.
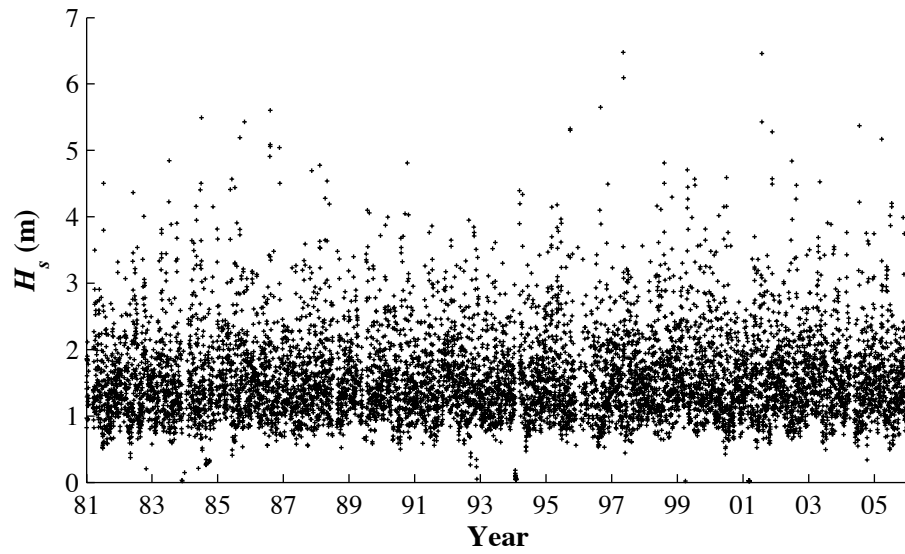
Fig. 4.5 – Daily mean H_s from 1981 to 2005

4.4.2 Data analysis

4.4.2.1 H_s and T_s

Initial analysis of the wave data indicated that there are possible outlier values. Taking into consideration that wind generated ocean waves typically have a period of 1 to 30s (Reddy, 2001), waves with T_s >30 were defined as outliers and removed from the data set. In order to maintain the regular 20-minute sampling frequency, the outliers are replaced with *NaNs*. Fig. 4.6 shows the distribution of the measured H_s and T_s data after the removal of these outliers. In Fig. 4.7 respective histograms are shown.
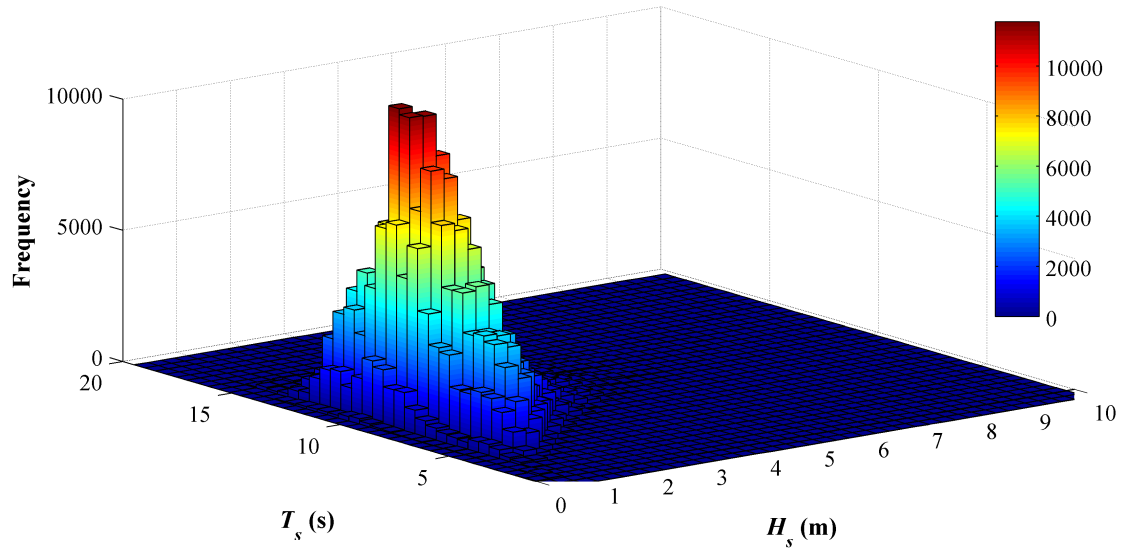
Fig. 4.6 – Distribution of measured T_s vs. H_s from 1981 to 2005
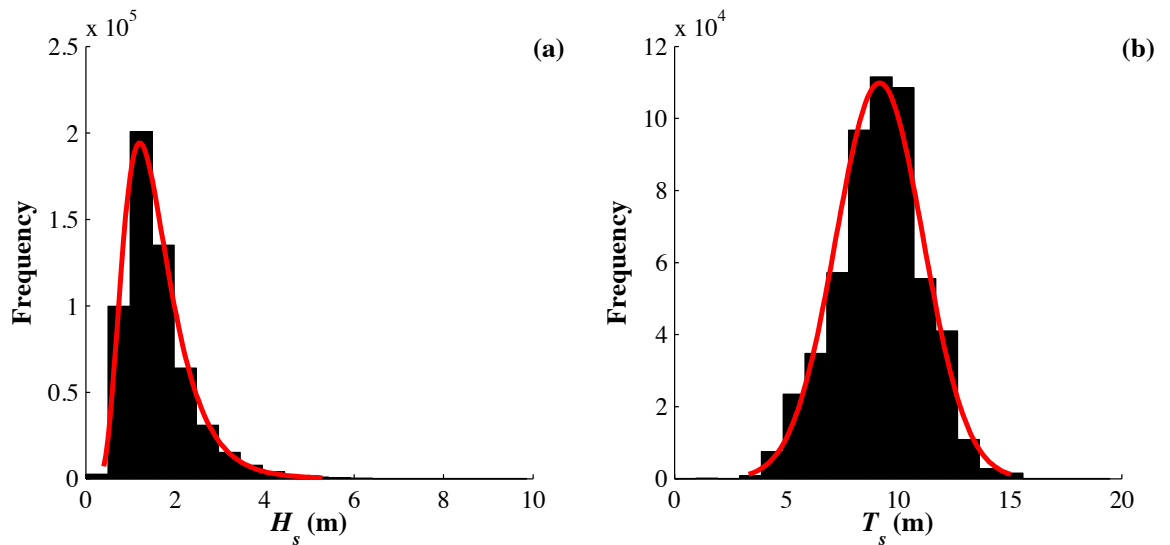
Fig. 4.7 – Histograms of (a) H_s compared to a lognormal distribution with μ = 0.374m and σ = 0.431m; and (b) T_s compared to a normal distribution with μ = 9.17s and σ = 1.95s

The measured H_s data shows that the vast majority of them are clustered near the mean (1.60m), with the maximum value (9.86m) being considerably larger and emphasising the high degree of variability in the wave climate discussed by Short and Trenaman (1992) and summarised in section 4.2.2. Significant wave period closely follows a normal distribution,

with a mean value of 9.17s and a standard deviation of 1.95s. Table 4.3 provides a brief overview of the main statistical properties of the measured H_s and T_s data.

	H_s	T_s
N	657,432	657,432
Minimum	0.01 m	1.01 s
Maximum	9.86 s	19.47 s
Mean	1.60 m	9.17 s
Median	1.43 m	9.34 s
1st quartile	1.09 m	7.98 s
3rd quartile	1.91 m	10.36 s
Variance	0.55 m	3.82 s
Standard deviation	0.74 m	1.95 s

Table 4.3 – Properties of measured wave data from 1981 - 2005

4.5   Occurrence of Storm Events

4.5.1 Identification of independent storm events

The statistical modelling framework, used in the SPA, requires data of independent storm events to be abstracted from the measured wave time series. Based on previous studies of the Sydney storm climate (Lord and Kulmar, 2000; Kulmar et al., 2005) a storm event is considered to occur when H_s exceeds 3.0m (Fig. 4.8). Storm events were abstracted from the dataset by grouping data using an $H_s \geq 3.0$m threshold. Previous modelling studies at Narrabeen Beach (Callaghan et al., 2008; Harley et al., 2009; Ranasinghe et al., 2011) have defined storm events using this threshold level, with Harley et al. (2009) finding that using the 3.0m threshold value successfully captured the observed erosion.

A high wave event is considered as a single storm if H_s stays above 3.0 for a minimum duration of one hour and it is separated from the previous or the next event by a 24-hour period (Mark Kulmar – MHL, personal communication). This means that if H_s decrease below 3.0m, should it rise above 3.0m within a 24-hour period it is considered a single

event rather than multiple events that are less than 24 hours apart. This procedure established that 539 storm events occurred between 1981 and 2005.
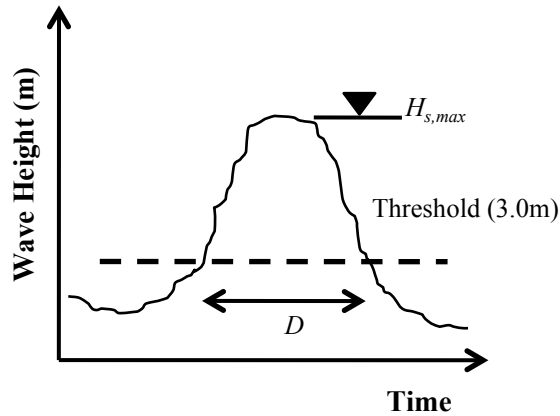
Fig. 4.8 – Definition of an independent storm event

For the individual storm events isolated, peak significant wave height ($H_{s,max}$), the corresponding period ($T_{s,max}$), storm duration (D) and spacing (S) are determined. Fig. 4.9 shows the distribution of D vs. $H_{s,max}$ and $T_{s,max}$ vs. $H_{s,max}$ with Table 4.4 providing basic statistical properties of these parameters. The chronological distribution of the storm events is provided in Fig. 4.10 with a mean spacing between events of approximately 15 days.

	$H_{s,max}$	$T_{s,max}$	D
Minimum	3.04 m	7.0 s	1.33 hours
Maximum	9.86 m	15.7 s	151.00 hours
Mean	4.08m m	10.0 s	25.64 hours
Median	3.81 m	9.9 s	18.33 hours
1st quartile	3.38 m	9.0 s	7.00 hours
3rd quartile	4.52 m	11.1 s	33.67 hours
Variance	0.881 m^2	2.3 s^2	641.25 hours^2
Standard deviation	0.938 m	1.5 s	25.323 hours

Table 4.4 – Properties of independent storm event variables
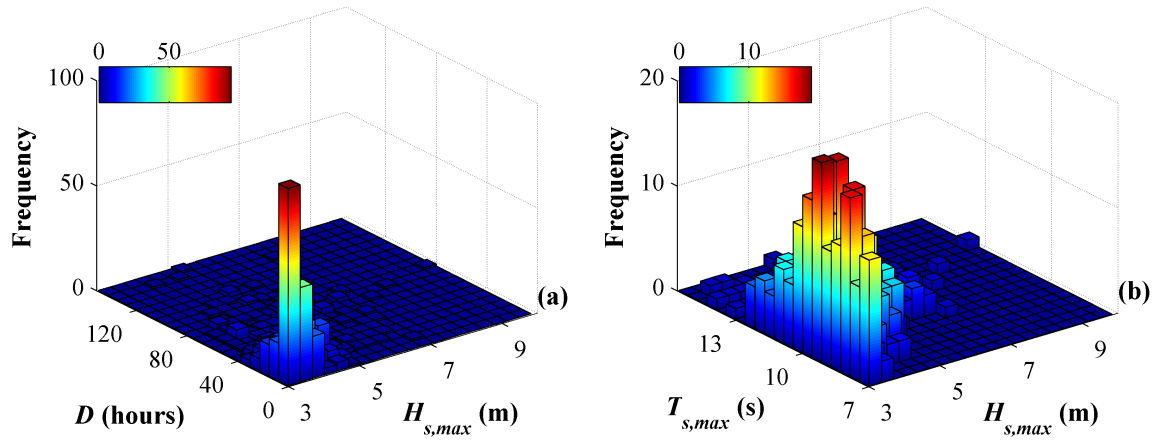
Fig. 4.9 – Storm events that occurred during 1981 to 2005. (a) *D* vs. *H*$_{s,max}$ and (b) *T*$_{s,max}$ vs. *H*$_{s,max}$
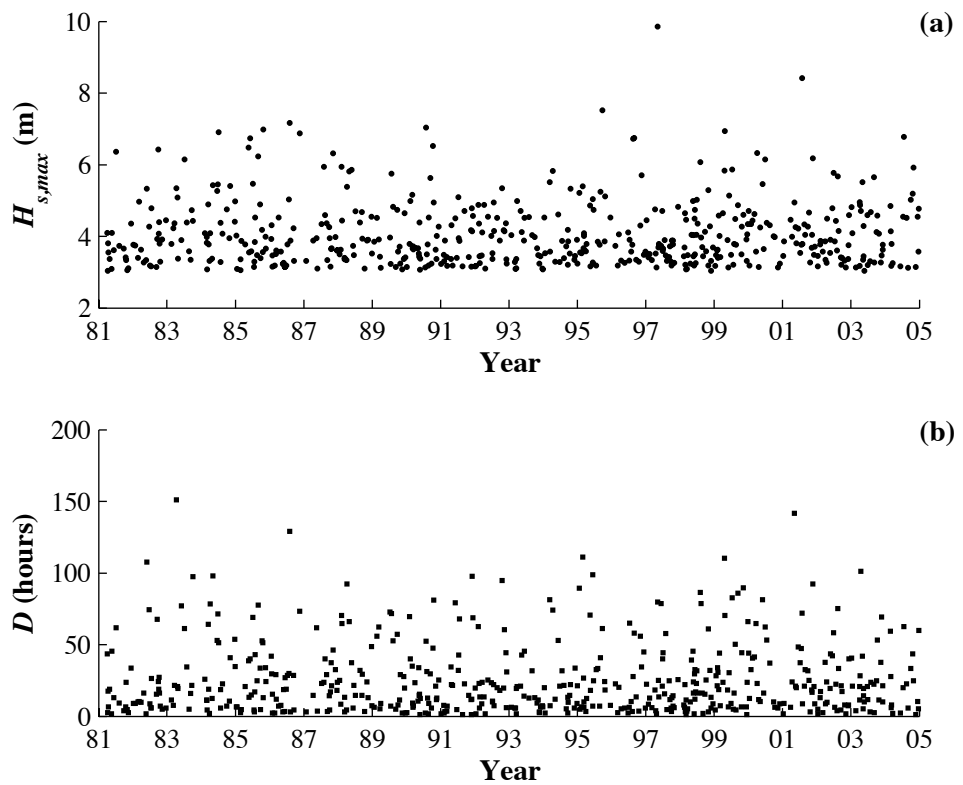
Fig. 4.10 – Occurrence of determined independent storm events from 1981 to 2005. (a) *H*$_{s,max}$ and (b) *D*.

4.5.2 Annual and seasonal trends

Fig. 4.11(a) shows the annual occurrence of storm events from 1981 to 2005 along with a linear regression of the data. The average number of storm events per year during this period is 21.56, with a maximum of 33 occurring in 1998 and a minimum of 16 occurring in 1981 and 2005. The linear regression shows that the number of events per year is relatively constant although there is evidence of a marginal increase as the gradient of the linear fit, $m = 0.146$. Although there is evidence of a slight increase, there are not enough data to firmly establish a long-term trend in annual storm event occurrence. This is confirmed by a low R^2 value (0.056) and the gradient not being significantly different from zero ($p = 0.255$). Assuming a constant annual average of 21.56 within the SPA methodology can therefore be deemed acceptable.

It can also be seen in Fig. 4.11(b) that there is slight variation in mean $H_{s,max}$ throughout the period with less than 1m between the maximum and minimum annual average. Again, the regression indicates a slight increase in $H_{s,max}$ across the measurement period. However, this is amplified by the scale of the y-axis, with $m = 0.006$, $R^2 = 0.046$ and $p = 0.301$ confirming no significant increase in the data. Comparing mean $H_{s,max}$ and D (Fig. 4.11(b) and (c)) a correlation can be seen between the two parameters. In 1993 both were at their minimum values, and in 1983, when D was at a maximum, the corresponding $H_{s,max}$ is also higher than the average. This provides evidence that $H_{s,max}$ and D are dependent. The gradient of the linear regression of D, $m = 0.013$, indicates no significant variation throughout the measurement period. This is confirmed by $R^2 < 0.001$ and $p = 0.942$,

To attempt to establish any potential seasonal trends in the storm event time series, the monthly occurrence of mean $H_{s,max}$ and D were plotted (Fig. 4.12). Short and Trenaman (1992) summarised results from historical storm data (1920-1944 and 1957-1980) to show that there is a distinct peak during the winter (June-July). This peak is not as prominent in Fig. 4.12(a) due to the high frequency of storm events that occurred in March, although the average month that events occurred in, from this data, was deemed to be between June and July.
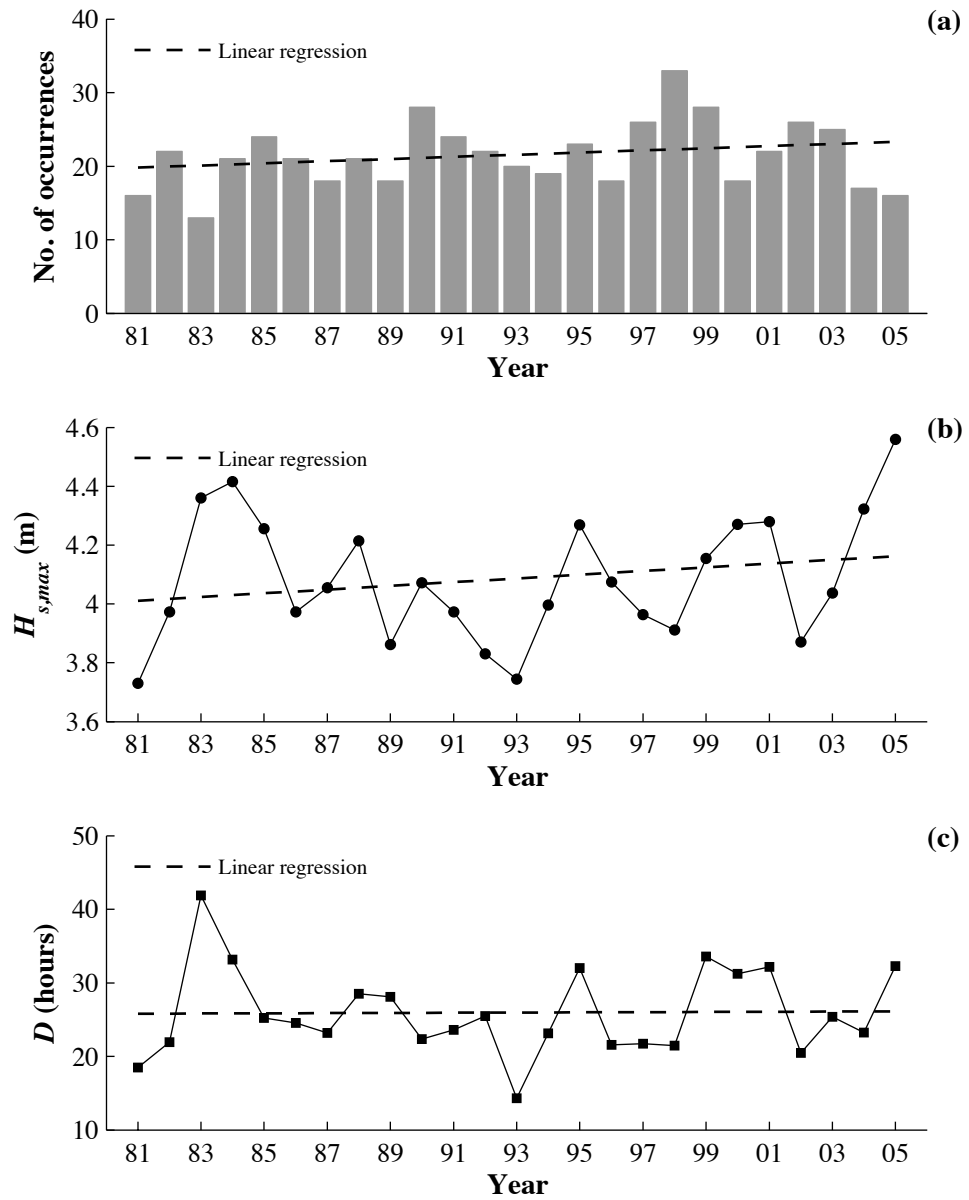
Fig. 4.11 – Annual trend in independent storm events. (a) Annual occurrence, (b) mean $H_{s,max}$ and (c) mean D.
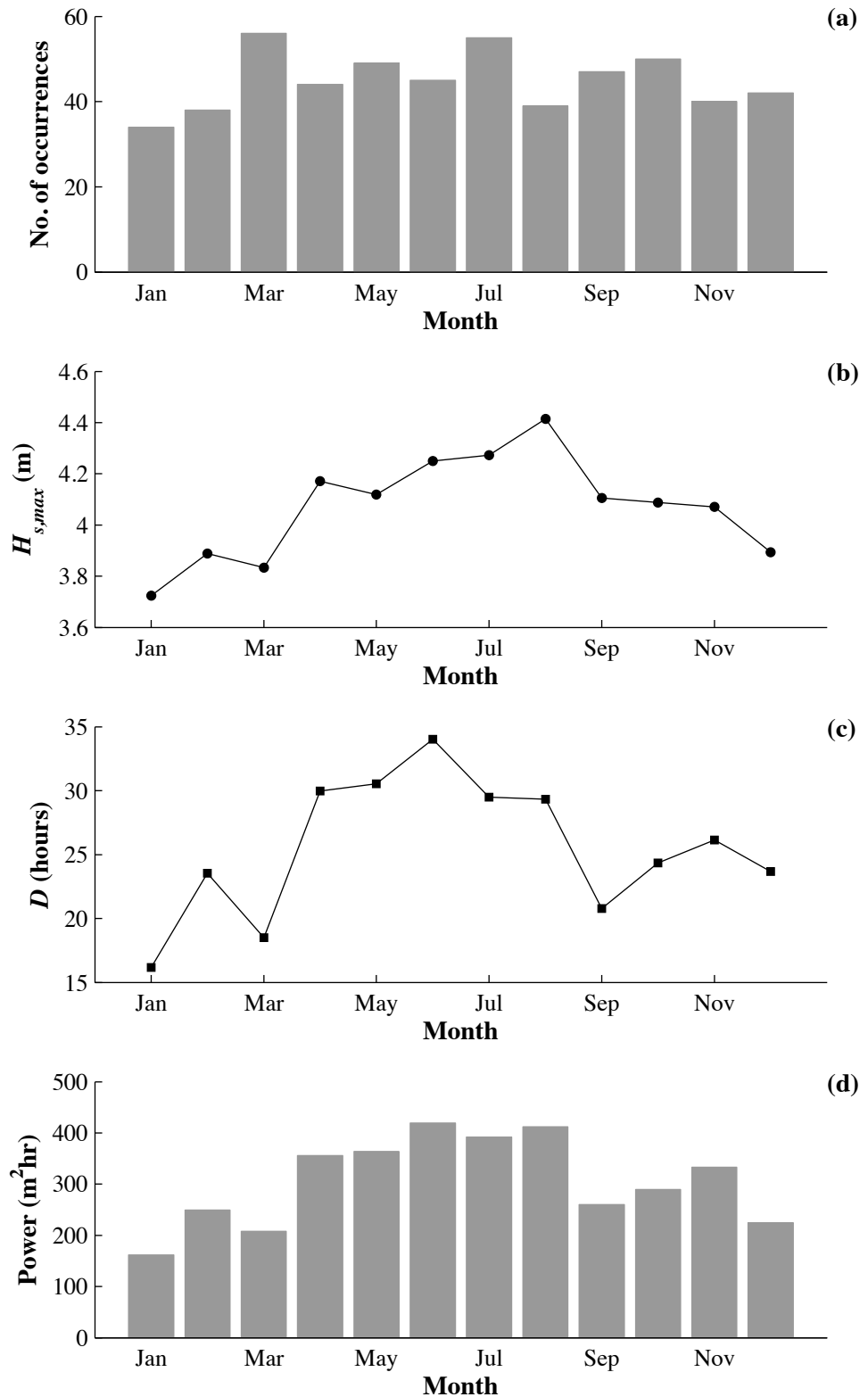
Fig. 4.12 – Seasonal trend in independent storm events. (a) Occurrence, (b) mean $H_{s,max}$, (c) mean D and (d) mean P

The monthly trends in $H_{s,max}$ and D (Fig. 4.12(b) and (c)) provide a clearer representation of a seasonal trend in the storm climate. From these figures it is evident that there is a clear peak during the winter months, which is confirmed by Short and Trenaman (1992). Additionally these plots partially explain the large number of events that are observed during March. In March, both, $H_{s,max}$ and D decrease meaning that there is a large number of lower magnitude events. The mean monthly storm power index (P) of Dolan and Davis (1994) is given by Eq. (4.1). Plotting P (Fig. 4.12(d)), further highlights the fact that there is a clear seasonal trend in the magnitude of storm events in the Narrabeen region.

$$P = H_s^{\ 2}D$$

<div align="right">(4.1)</div>

4.6   Measured Beach Profile Data

The morphodynamic variability of Narrabeen Beach has been regularly and extensively monitored during the last few decades, with profiles being surveyed at 5 locations (Fig. 4.1) along the beach at approximately monthly intervals from 1972 to present by the Coastal Studies Unit, University of Sydney (Short and Trembanis, 2004).

As profiles 1, 2, 6 and 8 are located at the northern and southern ends of the beach respectively, they are much more susceptible to the rotation that occurs (section 4.3.2). The analysis by Short and Trembanis (2004) showed that profile 4 acts as the fulcrum during beach rotation. This means that, it is least influenced by longshore processes and therefore, most suitable for use within the SPA methodology for modelling the medium-term variability of Narrabeen Beach. This was confirmed by Ranasinghe et al. (2004), who showed that profile 4 exhibited the smallest net variation in width during La Niña/El Niño events (Table 4.2). For these reasons, beach profile surveys at profile 4 are used in this research.

Measurements for all profiles begin at a constant benchmark beyond the limit of wave attack. For profile 4 this benchmark is +10m above Australian Heights Datum (AHD). To

keep a consistency between the wave data and profile survey data, profiles measured between 1981 and 2005 are used.

To analyse the variability of profile 4 during this period the mean, maximum and minimum bed levels, along with the variance in each measurement were determined (Fig. 4.13). These plots highlight the large degree of cross-shore variability that occurs at profile 4. The largest variance in the profile occurs around the shoreline and swash zone, which is unsurprising as this region undergoes rapid morphological change (Wright et al., 1985). It also highlights a peak in the variance where the nearshore bar is evident. This emphasises what was discussed previously regarding the bar migration and morphological changes that occur during erosive and accretive periods, when the beach state changes.
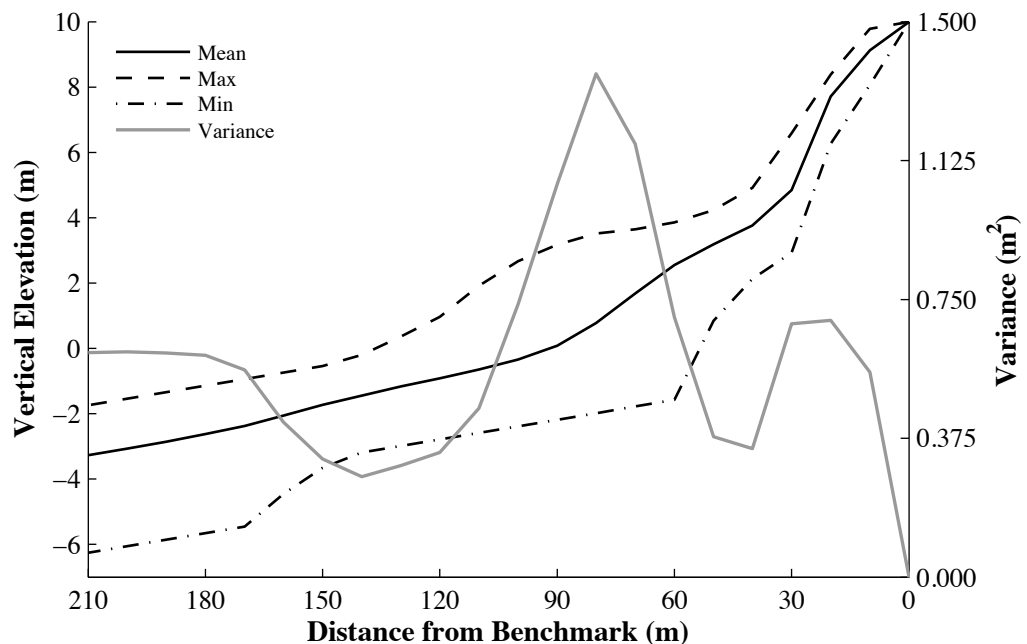
Fig. 4.13 – Variability in profile 4 measurements from 1981 to 2005

To further assess the variability of profile 4 the subaerial (above MSL) volume per metre run of beach was determined (Fig. 4.14). From the linear regression analysis it is evident that although there is poor linear correlation ($R^2 = 0.099$), the overall trend shows a decrease in subaerial beach volume. This is confirmed with the regression slope $m = -0.006$

and $p = 3.048 \times 10^{-7}$, meaning the null hypothesis of $m = 0$ is rejected. Although the most volumetrically stable profile (Ranasinghe et al. 2004) is being used for the analysis, it is clear that there is still a high level of variability in the volume of the beach at this location. This may also be attributed to El Niño / La Niña events but this is difficult to identify in this simple analysis due to the lag effects in beach response identified by Ranasinghe et al. (2004). Although this analysis provides an insight into the volumetric variability of profile 4, more data would be required to firmly establish a long-term trend in the beach volume.
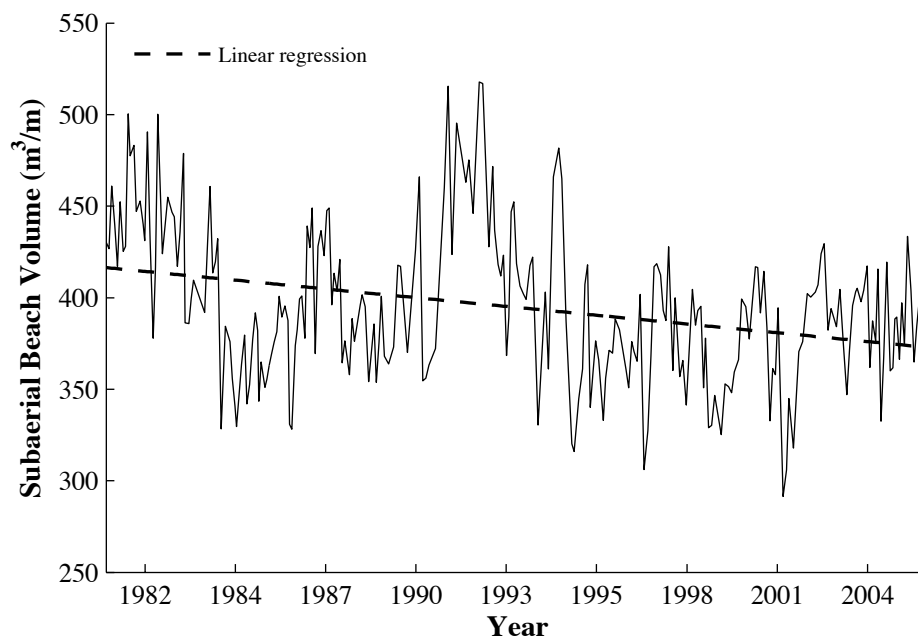
Fig. 4.14 – Variation in subaerial beach volume at profile 4 during 1981 to 2005

Throughout this period, profile 4 had a mean volume of $400\text{m}^3/\text{m}$, with corresponding maximum and minimum values of $519\text{m}^3/\text{m}$ and $292\text{m}^3/\text{m}$. This emphasises the extent to which the frequent storm events affect beach volume, with the overall maximum change in volume being $227\text{m}^3/\text{m}$.

To assess what affect the storm climate has on the erosion that occurs at profile 4, a simple analysis was conducted in an attempt to correlate storm power index (P) with beach erosion. The beach erosion is defined as the volume change, above the 2m beach contour

(Fig. 4.15), which is common for analysis in the NSW region (Hoffman and Hibbert, 1987; Callaghan et al., 2008; Ranasinghe, Callaghan, et al., 2011). In order to make the data more manageable, the erosion volumes were grouped into blocks of 6-month durations and averaged over the block. *P* is taken as the average *P* throughout the block. The plots in Fig. 4.16 (a) and (b) show the mean *P* and beach erosion per block, respectively.
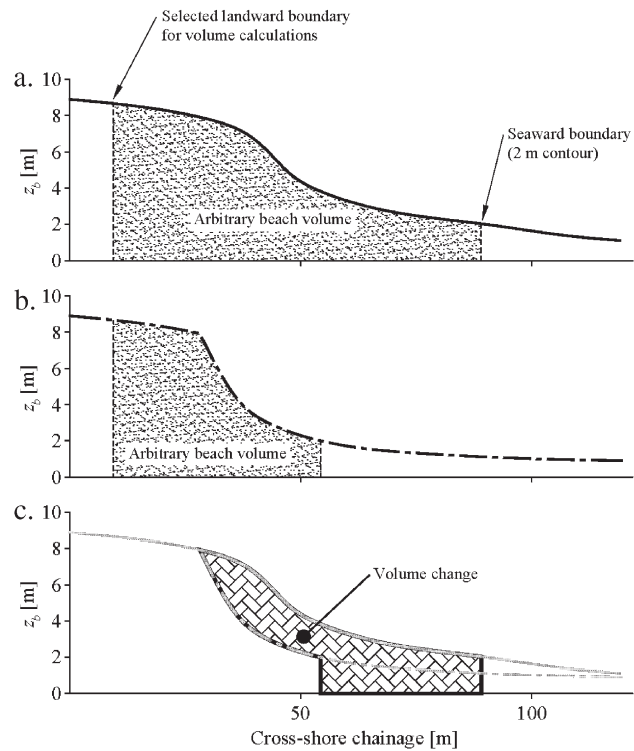
Fig. 4.15 – Definition of beach erosion, bounded by the 2m contour, from Hoffman and Hibbert (1987) and Callaghan et al. (2008)

In an attempt to provide a more definitive correlation between *P* and erosion, the values (*X*) were normalised (*X*$_{norm}$) and a moving average of these were then determined and plotted. The normalisation means that the units are removed from each data set to allow for a comparison. Normalisation of data means that the values are scaled so as they fit in a range of 0 to 1 (unity based normalisation). This can be achieved for any parameter using Eq. (4.2).

$$X_{\mathrm{norm}} = \frac{X_i - X_{min}}{X_{max} - X_{min}}$$

(4.2)
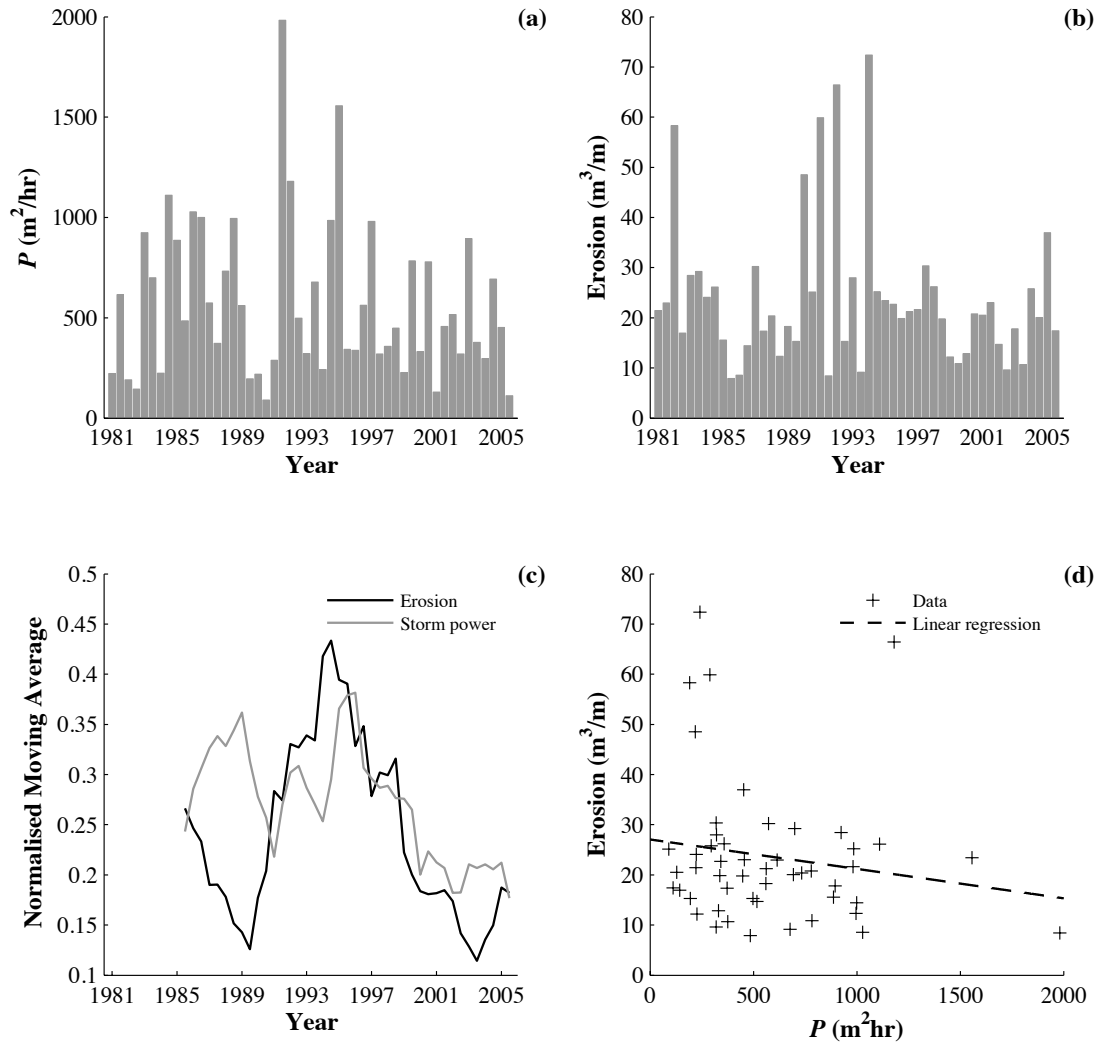
Fig. 4.16 – Narrabeen Beach erosion and storm power index. (a) mean *P*, (b) mean erosion, (c) *P* and erosion comparison and (d), erosion vs. *P*.

Due to the large number of data the simple moving average (SMA) of these normalised values were determined and plotted (Fig. 4.16c). The SMA procedure involves dividing the data into an arbitrary block and moving this block across the data and computing the average values. It is evident from the plot that although, there may be a correlation between *P* and erosion volume towards the end of the data set, the first part of the data set indicates a large divergence. To further attempt to establish a relationship, the correlation

coefficient (R^2) between P and erosion volume was determined to check if there is a linear trend between them (Fig. 4.16d). From the data the R^2 was determined to be -0.16 indicating that no substantial linear correlation is evident in the data.

It would be expected that there is a clear correlation between P and beach erosion, which has not been deduced from the measured data. The following reasons are proposed for the lack of correlation.

1) The profile data are not representative of beach erosion.
2) All storm events measured offshore of Botany Bay may not induce erosion at Narrabeen Beach.
3) The directions of the incident storm waves have not been accounted for.
4) There are longshore processes present that affect the beach erosion and accretion.

It has been previously discussed that Narrabeen Beach profiles predominantly exhibit intermediate state. That, combined with the fact the beach states alter frequently, means that the profile measurements (made at monthly intervals) may not accurately represent the actual erosion due to storm events impacting the beach.

Additionally, it may be the case that defined storm events do not necessarily result in significant beach erosion. As the Waverider buoy is located a number of kilometres offshore, there is a possibility that storm events measured at this location may not result in expected erosion. This is the reason behind the concept of "*effective storms*" in the erosion analysis conducted by Callaghan et al. (2008). An effective storm was one that was deemed to have a significant erosive impact on the beach. As a result of changes in direction of the storm path or the direction of the waves themselves some offshore events were observed to not produce as much erosion as expected (Dr D Callaghan, personal communication). As the wave data are non-directional, and there is no information regarding the storm paths, it is not possible to comment on this any further.

It has also been shown how the longshore variability of Narrabeen Beach is controlled by the SOI, with frequent cycles of beach rotation occurring. Although the studies into these phenomena have indicated that profile 4 is the least susceptible to the SOI it may still have some effect at controlling levels of erosion during certain periods as variation in beach width is evident along the entire beach (Ranasinghe et al., 2004).

4.7   Chapter Summary

This chapter has provided a description of the wave and storm climate of the Sydney region and the effects that it has on the variability of Narrabeen Beach (the chosen field site for the implementation of the SPA). It has discussed how the wave climate is highly energetic, variable and is driven from five different meteorological systems. This highly energetic wave climate has shown to result in frequent storm events with an annual average occurrence of 21.56 events. The annual storm data indicate a possible increasing trend in the annual average storm occurrence and $H_{s,max}$, while annual average D remains approximately constant. However, providing a definitive conclusion on long-term trends of variability in the storm climate would require more data. The monthly data indicate a clear peak in event magnitude with the power index during the winter months (Apr-Sep) being noticeably higher than those in the summer (Oct-Mar).

Independent storm events have shown to occur frequently with an average spacing of 15 days. These frequent storm events produces high degree of variability in the beach morphology, where profile 4 varies between reflective, intermediate and dissipative beach states, as discussed in section 4.3.1. Wright et al. (1985) showed that the state of Narrabeen Beach changes as frequently as once per week, which is understandable given the frequency of occurrence of storm events.

The beach is subjected to cyclic rotation and oscillation from the El Niño/La Niña phenomena meaning it suffers subsequent erosion/accretion cycles at its northern/southern ends. Profile 4 was shown to act as the fulcrum of this rotation meaning it is the most suitable for validating medium-term modelling SPA methodology. Although profile 4 is

the most stable in the longer-term (Ranasinghe et al. 2004), the subaerial beach volume is still highly variable with a maximum potential volumetric change of $227m^3/m$.

It has been shown that, from the data available, a definite trend between P and erosion volume cannot be established. In order to firmly establish a trend between P and erosion volume, beach profile surveys that correctly replicate pre and post storm profiles would be necessary.

The storm and beach profile data presented and discussed in this chapter are used in the implementation and validation of the SPA methodology.

CHAPTER 5

STATISTICAL MODELLING OF THE NARRABEEN STORM CLIMATE

This chapter describes the statistical framework implemented to model the storm climate of the Sydney/Narrabeen region. As outlined in Chapter 1, the statistical modelling follows the procedure within the Full Temporal Simulation (FTS) approach of Callaghan et al. (2008) for modelling long-term beach erosion. The procedure was implemented using the *R* statistical modelling software package (http://www.r-project.org/).

The FTS procedure includes an estimation of beach erosion using an empirical beach profile model integrated with a statistical simulation model of storm climate. As the SPA methodology uses XBeach to simulate beach profile response, the statistical modelling and erosion modelling are treated as two separate procedures. This chapter describes the modified FTS procedure that uses the measured wave climate (discussed in Chapter 4) to produce a synthetic storm climate to be modelled with XBeach to determine beach profile variability over medium-term timescales.

The methodology of the FTS has been simplified to complement the data being used and to increase the efficiency of the parameter fitting. These modifications are discussed in detail within the chapter and Appendix A. Following this procedure allows for the generation of a synthetic storm climate, which provides the input conditions for the XBeach simulations in the SPA methodology.

5.1   Statistical Modelling of Environmental Extremes

5.1.1 Extreme value theory

Within natural science and engineering disciplines, the prediction of extreme values is of the highest importance as sustainable solutions, able to withstand unknown future conditions, are required. Extreme value theory is the driving force behind these estimations and is an integral part of many coastal engineering projects. For the extreme value modelling of environmental parameters, the most basic approach is to apply a benchmark event; which is the largest within a series of historical measurements. Following on from this approach, the use of historical data combined with a probability density function (pdf) can provide parameter estimates of return periods for extreme events.

5.1.2 Modelling extreme events

5.1.2.1 Univariate events

The statistical modelling of single parameter (univariate) systems has been thoroughly documented and widely used by engineers and scientists for a number of years. Fundamentally, this approach involves fitting the measured data to an extreme value pdf and determining the variate levels at the return periods of interest. Applying this method to coastal engineering Mathiesen et al. (1994) provided a breakdown of the recommended practice for extreme wave analysis based on a univariate (wave height) case. The procedure is described in the following steps:

1) Select data for analysis.
2) Fit an extreme value distribution to the observed data.
3) Compute (extreme) return values from the fitted distribution.
4) Compute confidence intervals.

This procedure provides predictions of extreme wave heights, along with the confidence intervals for determining the accuracy and associated errors of the predictions. The estimation of extreme values is a user-integrated process that may

require amendments along the way based on the experience and judgement of the modeller. For this reason, complete automation of any extreme value modelling framework is highly improbable, as the behaviour of the data have to be analysed and understood prior to the fitting and estimation processes.

Mathiesen et al. (1994) also showed that the fitting of an extreme value distribution to a dataset might not provide accurate predictions at extreme levels. These inaccuracies are due to the tail (extreme events) of the data being sparse and behaving differently, thus requiring a more detailed modelling approach to establish accurate parameter estimates. This led to the use of the annual maxima (AM) method, where maximum annual values are abstracted from the data and modelled using an extreme value distribution. Although the AM method may be more efficient than fitting a dataset of regular observations, the use of AM data is inefficient as some extremes may be omitted if they are not the largest in a given year. To provide a good fit to extreme data and avoid omitting values, a threshold model can be used: giving rise to the Peaks-Over-Threshold (POT) modelling concept.

The POT modelling concept uses a method where a threshold value, that divides the data into subsets whose behaviours differ in some way, is set. Setting a threshold results in only the extreme (tail) data being modelled, unlike the block maxima approach where all data are said to be extreme. An example of this method can be found in Cañellas et al. (2007) who discuss the application of a POT model for estimating extreme wave heights.

5.1.2.2 Multivariate events

It has been discussed previously that, when modelling systems with more than one random variate (multivariate modelling), the return period of the outcomes are not necessarily equal to the return period determined for the forcing parameters (Hawkes, 2000). Including more than one random variate in the statistical modelling of storm events provides a more complete representation of the forcing conditions and, in turn, a more accurate quantification of the occurrence probabilities of the erosion levels. The main reason for multivariate modelling is that there is a greater interest in the combination of variates than

there is in the individual variate. This is extremely relevant in the modelling of climatic and oceanographic events and has been covered extensively in various literature (e.g. Tawn, 1988a, 1990, 1992; Coles and Tawn, 1991; Coles et al., 1999; Hawkes et al., 2002; Luceño et al., 2006; Liu et al., 2010).

5.1.2.3 Extreme value distributions

Historically, extreme value modelling has three different distribution families: Gumbel, Fréchet and Weibull. These distributions provide different tail behaviours at the extreme limits resulting in a decision having to be made as to which distribution is the most suitable for the data in question.

The Generalised Extreme Value (GEV) distribution is a probability distribution developed to combine the Gumbel, Fréchet and Weibull families. The shape parameter (ξ) of the GEV governs the tail behaviour of the distribution where, $\xi \to 0$, $\xi > 0$ and $\xi < 0$ represent the Gumbel, Fréchet and Weibull distributions respectively.

The Generalised Pareto Distribution (GPD) is a threshold model developed in order to fit the tail of a wide range of data. This model is discussed in detail in Appendix A.

5.2   Statistical Modelling Implementation

This section discusses the implementation of the statistical modelling framework used in this research. The method requires data of the peak significant wave height of the storm ($H_{s,max}$), storm duration (D), peak wave period ($T_{s,max}$) and spacing between single storm events (S). These details have been abstracted from the wave data timeseries as described in Chapter 4. A description of the modelling methodology is given below with a detailed guide of the steps provided in Appendix A.

1) Identify meteorologically independent storm events.

2) Fit the GPD to $H_{s,max}$ and D.

3) Fit the dependency (logistics) distribution between $H_{s,max}$ and D.

4) Fit the 3-parameter lognormal distribution to $T_{s,max}$.

5) Fit a non-homogeneous Poisson process to S.

6) Simulate the storm climate using the fitted distributions including storm spacing.

The final outcome of this procedure is a random timeseries of storm events that can be input into XBeach to determine beach erosion and variability.

5.2.1 Fitting of extreme value and dependency distributions to $H_{s,max}$ and D

To generate estimates of $H_{s,max}$ and D of storm events, the Generalised Pareto Distribution (GPD) and the logistics dependency model are fitted to the data, following the methods of Hawkes et al. (2002) and (Coles, 2001). The fitting of the GPD and logistics models is carried out using the *fbvpot* function in the **evd** package (Stephensen and Ferro, 2008) which provides a maximum likelihood estimation (MLE) of the parameters for the marginal distributions of $H_{s,max}$ and D and the dependency between them (α), following the procedure of Coles (2001).

5.2.1.1 Threshold estimation

Prior to the fitting of the distribution to the storm data, suitable thresholds for the GPD have to be determined. For this, the procedure of threshold estimation outlined by Coles (2001) was followed. According to this, the selection of an appropriate threshold level is important as, too low a value will lead to a bias, whereas, too high a threshold will result in few exceedences and subsequently lead to low confidence in the estimations. For this reason Coles (2001) states that, so long as a reasonable fit to the data is provided, as low a threshold as possible should be chosen. The two methods indicated for this purpose are exploratory techniques, carried out prior to the model estimation, or an assessment of the

stability of parameter estimates, based on the fitting of models across a range of different thresholds (e.g. Dupuis, 1998; Tancredi et al., 2006; Thompson et al., 2009).

The method recommended by Coles (2001) involves creating and examining a mean residual life (MRL) plot of the data. A MRL plot is a plot of the mean of the excesses to any given threshold (u) with any approximately linear section of the plot providing a good range for the threshold; and any value in this range fitting the GPD adequately. A MRL plot is a plot of the mean of the excesses to any given threshold (u) Further examination by plotting parameter estimates at various thresholds is recommended to ensure an acceptable threshold has been chosen. If the GPD is a reasonable distribution for a threshold u_0, then excesses at a higher threshold should also follow a GPD. If this is true then the shape parameters of the two distributions are identical. The scale parameter (σ) varies with the threshold level unless the shape parameter (ξ) = 0. This can be overcome by modifying σ as shown by Eq. (5.1).

$$\sigma^* = \sigma_u - \xi_u \qquad\qquad\qquad \textbf{(5.1)}$$

σ^* is the modified scale parameter and is relatively constant with respect to the threshold. This means that estimates of, both, σ^* and ξ should be constant above u_0, if u_0 is a valid threshold for excesses to follow the GPD. Plots that show how σ^* and ξ vary with respect to u will therefore provide a further basis for threshold estimation.

5.2.1.2 Threshold selection

$H_{s,max}$ threshold selection

Fig. 5.1 shows the MRL plot for $H_{s,max}$ values of the Narrabeen storm data, ranging from minimum to maximum values.
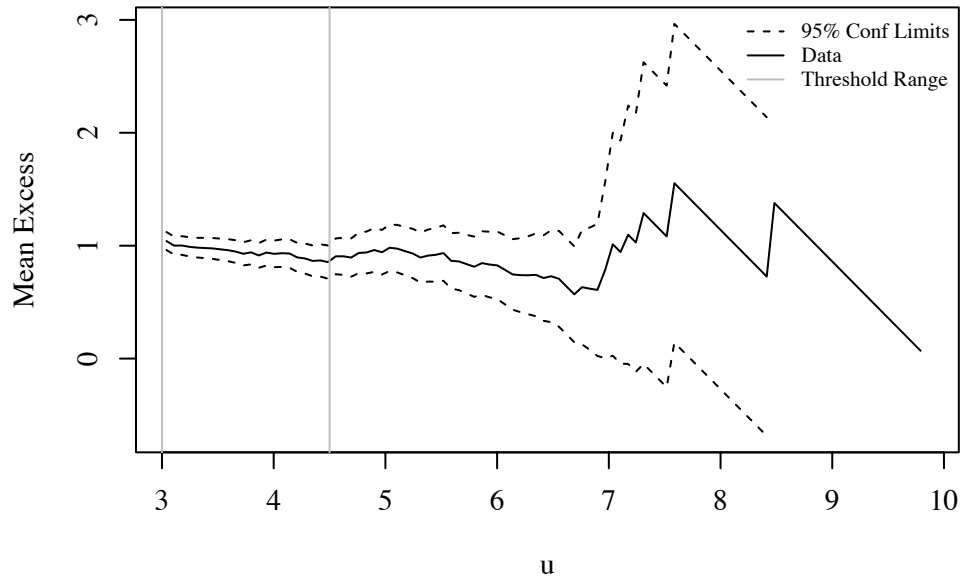
Fig. 5.1 – MRL plot for $H_{s,max}$ with thresholds ranging from 3m to 10m

From Fig. 5.1 it can be said that a linear section of the plot continues from the start point (u = 3.0m) up to approximately u = 4.5m, after which the plot deviates from the linear trend indicating that there are not enough exceedences to establish an accurate threshold. Therefore, any value within the 3.0m to 4.5m range should provide a suitable threshold for modelling with the GPD. To further assess the acceptable threshold, levels of σ^* and ξ against u were plotted (Fig. 5.2), as discussed in the previous section. The plots can be seen to show the same trend as the MRL plot for the same threshold range, with the higher values showing a change in pattern. As the variation in the values after the 3.0m to 4.5m range is small compared to the associated errors, this range is deemed reasonable for threshold selection (Coles, 2001).
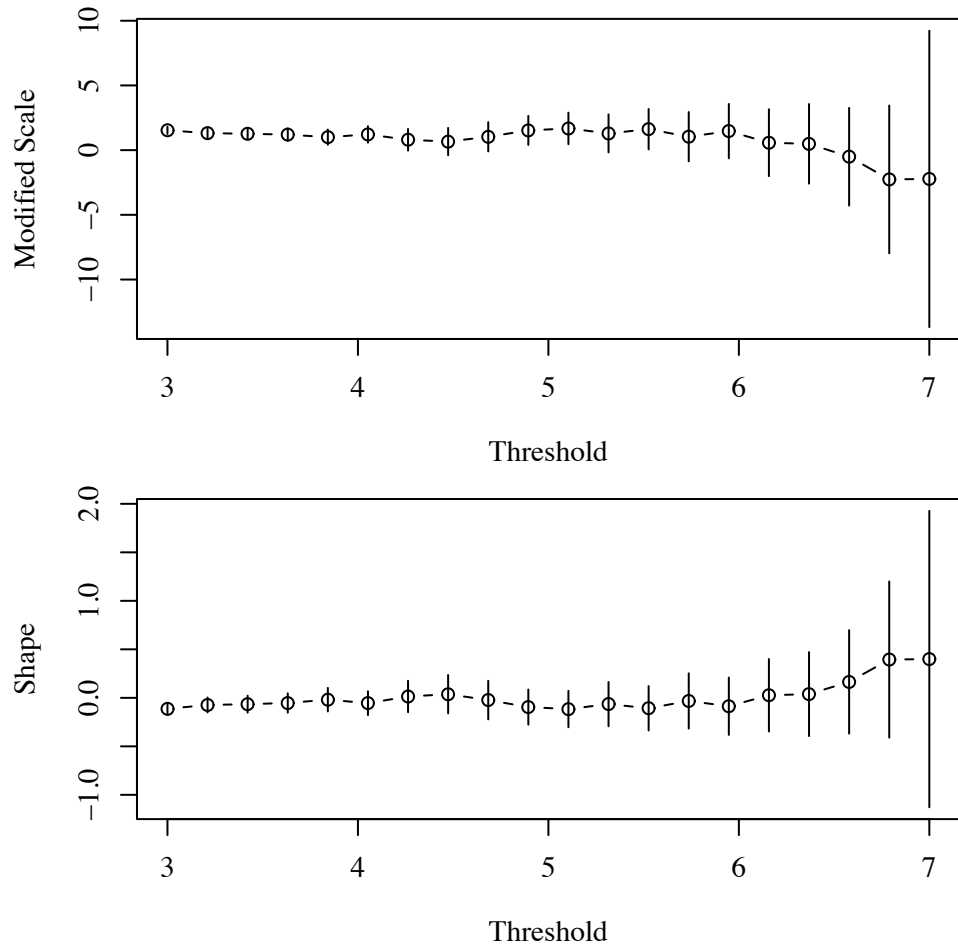
Fig. 5.2 – Plot of modified shape and scale parameter estimates for $H_{s,max}$ thresholds ranging from 3m to 10m

As a storm event is defined when $H_s > 3.0$m, the threshold value for H_{smax} should be larger than 3.0m to avoid all data points being fitted to the GPD. Finalising the threshold selection was achieved by fitting data to the GPD using values of 3.5m, 4.0m and 4.5m and assessing the differences. Diagnostic plots for the 3.5m, 4.0m and 4.5m threshold fittings are provided in Fig. 5.3 to Fig. 5.5 respectively.
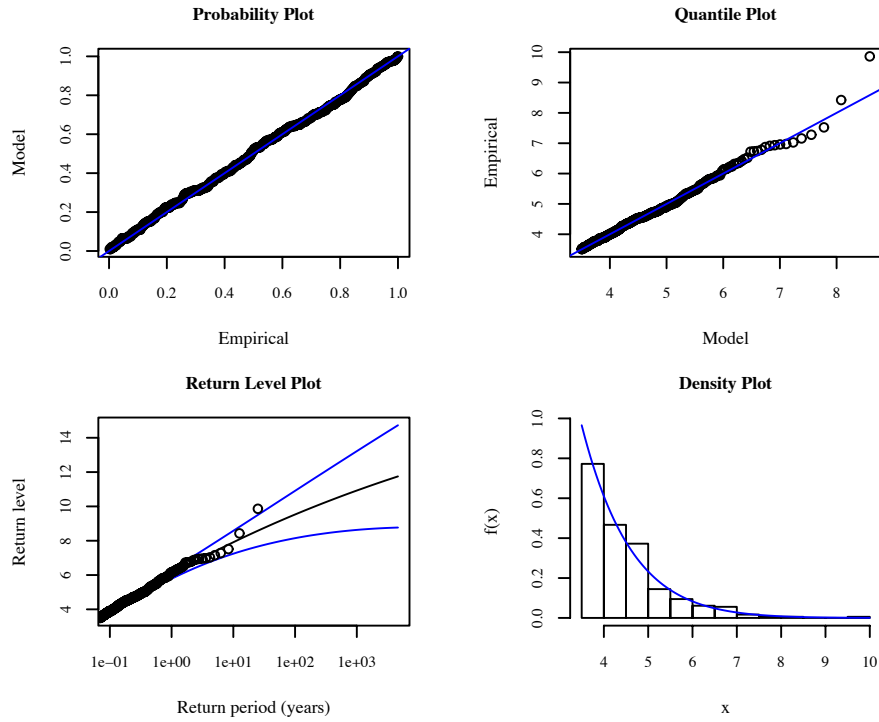
Fig. 5.3 – Diagnostic plots for $H_{s,max}$ threshold of 3.5m
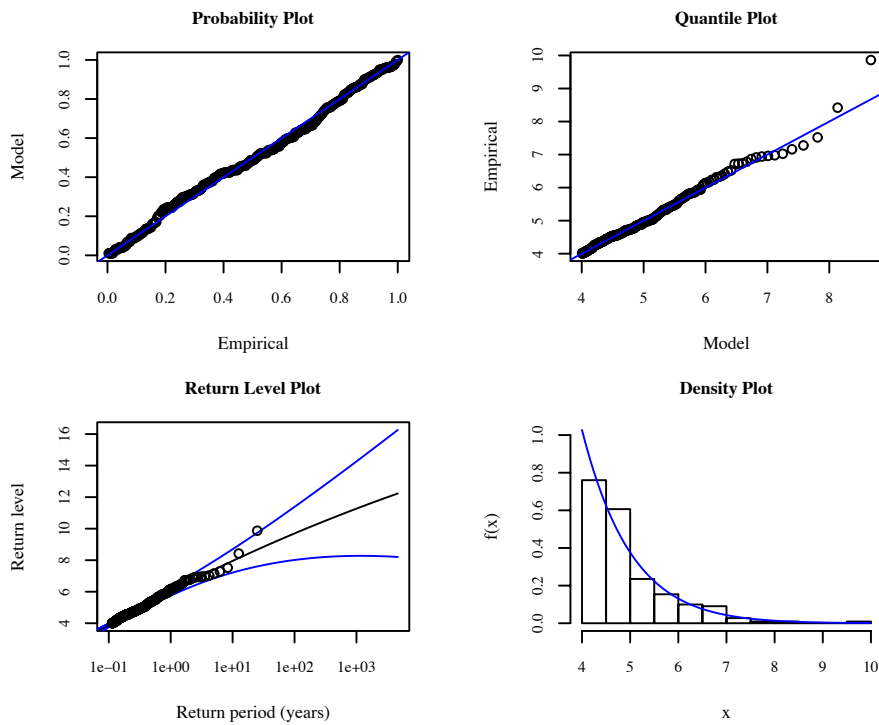
Fig. 5.4 – Diagnostic plots for $H_{s,max}$ threshold of 4.0m
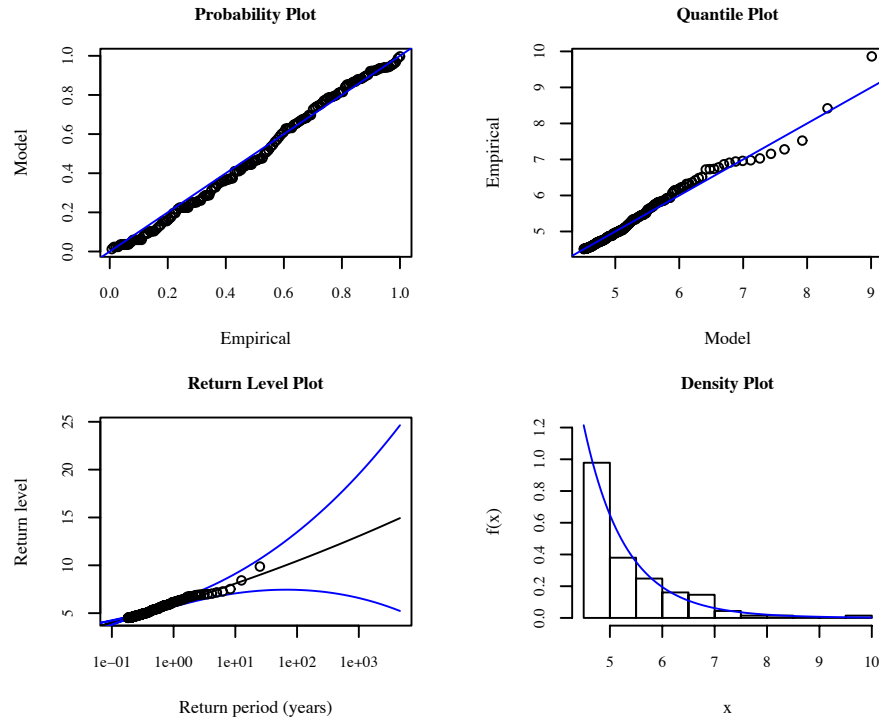
Fig. 5.5 – Diagnostic plots for $H_{s,max}$ threshold of 4.5m

The quantile plots in Fig. 5.3 to Fig. 5.5 show that, the lower the threshold, the better the fit to the GPD, with the 4.5m threshold showing the largest deviation in the tail region. Additionally, if the return level plots are analysed, the 95% confidence interval is largest for the 4.5m threshold. These can both be explained as, the higher the threshold, the lesser the number of exceedences (number of data points), which results in greater uncertainty. This greater uncertainty is the reason for the confidence intervals being greatest in the 4.5m plot. However, larger confidence intervals mean that all data fit within these limits for the 4.5m threshold, which is not the case for both the 3.5m and 4.0m threshold levels. Although this is true, it is felt that there is no benefit in having all empirical values lying within the 95% confidence limit if this limit is considerably larger. The final consideration for choosing the threshold was that, as the data are used to generate a synthetic storm climate, a lower value might be more appropriate. The Monte Carlo procedure outlined in Appendix A shows that the empirical distributions are used to simulate events below the threshold. As the synthetic storm climate time series will be considerably longer than the measured data, a higher threshold will require more sampling from the empirical distribution and may result in a poorer representation of events below the threshold. The

statistics of the empirical data (Chapter 4) show that the median of $H_{s,max}$ is 3.81m. This means that the data between the median and the max (9.86m) is much sparser than from the median to the min (3.04m). When the empirical distribution has to be used for the Monte Carlo simulation of $H_{s,max}$, a higher threshold may result in unnecessary spacing below the threshold level. For these reasons it was decided that a 4.5m threshold is inappropriate.

The 3.5m threshold accounts for approximately 70% of the data being modelled. Therefore, this value was also considered as too low and the most appropriate threshold was taken as 4.0m. A level of 4.0m, not only has a more suitable quantile plot than the 4.5m threshold, but also results in less sampling from the empirical data being required during the Monte Carlo simulation. This will provide better representation of events under the threshold during the MC simulation.

D threshold selection

As with $H_{s,max}$, the threshold for D was selected by inspecting a MRL which ranged from the minimum to maximum values of D (Fig. 5.6). It is evident that a linear section of the plot extends from approximately $u = 35$ to 65 hours. Unlike the $H_{s,max}$ data the starting threshold value is much greater that the minimum storm duration (1.33 hours) leading to 35 hours being selected for the threshold level in order to maximise exceedances. This in line with Coles (2001) who said that as low a threshold as possible should be chosen, provided a appropriate fit is provided. The diagnostic plots for fitting the GPD to the D data is provided in Fig. 5.7.

The quantile plot in Fig. 5.7 shows there is already some deviation at the tail of the distribution with some of the measured values lying on the upper 95% confidence limit. This justifies the selection of 35 hours for the threshold as anything greater would result in larger deviations towards the tail in the quantile plot as less data are being used for the fitting.
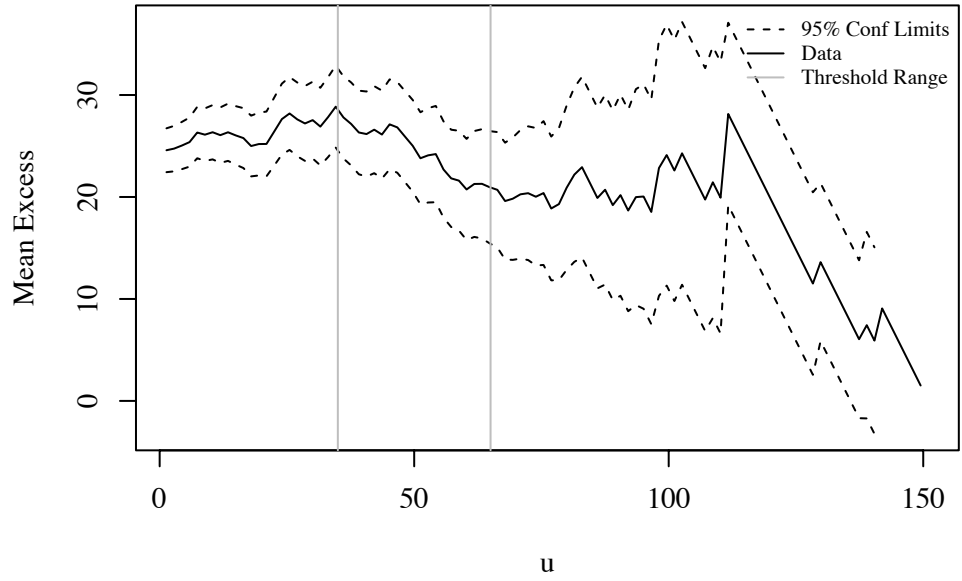
Fig. 5.6 – MRL plot for *D* with thresholds ranging from 0 to 150 hours
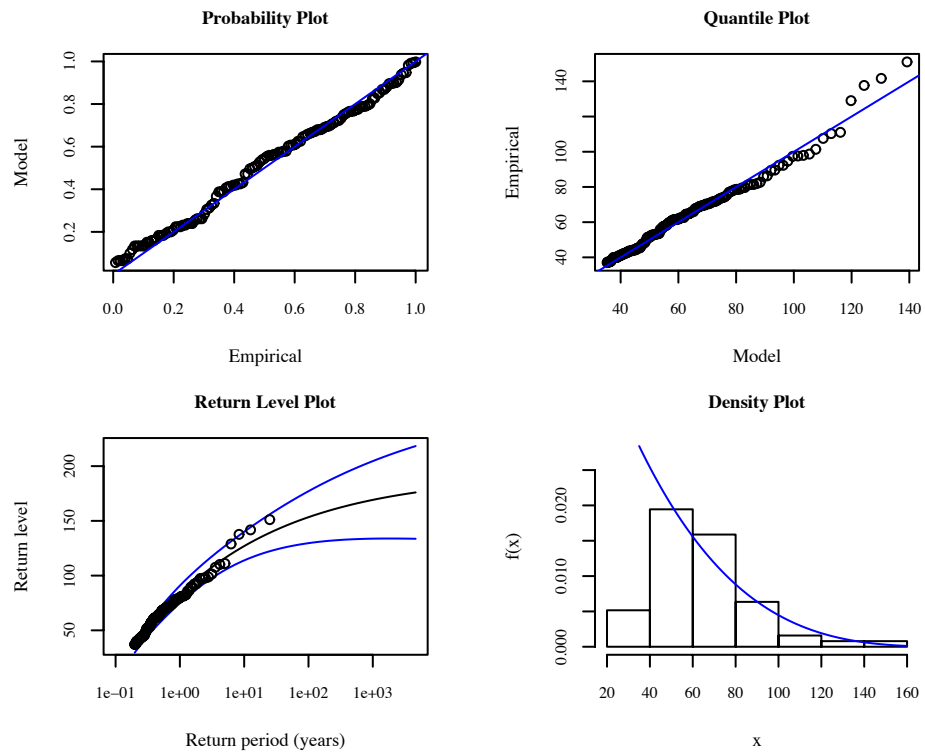
Fig. 5.7 – Diagnostic plots for *D* threshold of 35 hours

5.2.1.3 Fitting of GPD and logistics distributions

Once the threshold levels were finalised, the GPD and logistics distributions were fitted to the data. The probability of exceedance for the GPD and logistics models are given in Eq. (5.2) and Eq. (5.5), with full details of the fitting procedure provided in Appendix A.

$$\Pr\{X > x \mid X > u\} = \left[1 + \xi\left[1 + \left(\frac{x-u}{\sigma}\right)\right]\right]^{\frac{-1}{\xi}} \tag{5.2}$$

$$\Pr\{X \geq x, Y \geq y\} = 1 - e^{-x^{-1}} - e^{-y^{-1}} + e^{-(xy)^{-1}\left(x^{-\alpha^{-1}} + y^{-\alpha^{-1}}\right)^{\alpha}} \tag{5.3}$$

where x and y are Fréchet variates.

The fitting of these data resulted in the MLE of the scale (σ) and shape (ξ), for the marginal distributions, and the dependency between the parameters (α) shown in Table. 5.1, along with the standard errors (SE). These estimates are comparable with those of Callaghan et al, (2008) for the same data. The large SE in the ξ estimate for $H_{s,max}$ and D justifies the use of the GPD as the selection of a single extreme value distribution (Fréchet, Gumbel or Weibull) would have fixed the tail behaviour and underestimated the uncertainty in the fit.

	u	σ (SE)	ξ (SE)	α (SE)
$H_{s,max}$	4.0 m	0.910 (0.086)	0.082 (0.072)	0.624 (0.035)
D	35 hours	34.326 (4.109)	-0.112 (0.094)	0.624 (0.035)

Table. 5.1 – Parameter estimates for fitting $H_{s,max}$ to marginal GPD distributions and logistics model

The α parameter in the logistics model can range from 0 to 1, representing completely dependent and independent variables respectively. As the upper limit of the 95% confidence interval (0.692) is less than 1, this indicates that there is a dependency between

$H_{s,max}$ and D of storm events occurring in the Sydney/Narrabeen region. This confirms the dependency proposed in Chapter 4 by examining the measured data.

5.2.2 Fitting of a conditional distribution to $T_{s,max}$

Modelling $T_{s,max}$ uses a 3-parameter lognormal distribution and follows the same procedure outlined by Callaghan et al. (2008) and described in Appendix A. The procedure in this project differs by using pairs of $H_{s,max}$ and the corresponding period ($T_{s,max}$) rather than pairs of H_s and T_s. This modification was decided upon as it is thought that the inclusion of pairs of H_s and T_s below the storm threshold was unnecessary and may in fact introduce a greater degree of uncertainty in the estimations. Information regarding the use and fitting of the 3-parameter log-normal distribution can be found in Hill (1963); Sangal and Biswas (1970); Calitz (1973); Cohen and Whitten (1980); Muir and El-Shaarawi (1986); Hirose (1997) and Cohen (2011).

The pdf for the 3-parmeter log-normal distribution is given in Eq. (5.4) with, κ being a threshold parameter used to ensure exceedance over a certain limiting value. The parameters are related to $H_{s,max}$ using Eq. (5.5) to ensure that the steepness criteria at Narrabeen Beach is not violated. This leads to the expectation given in Eq. (5.6) meaning that the parameters (a, b, c, d, f and g) required estimating. Again, full details of the procedure are provided in Appendix A.

$$\Pr\{T_{s,max} = x\} = \left\{(x - \kappa)\sigma\sqrt{2\pi}\right\}^{-1} e^{-\frac{1}{2}\left(\frac{\ln(x-\kappa)-\mu}{\sigma}\right)^2} \qquad (5.4)$$

$$(\kappa, \mu, \sigma) = \left(aH_{s,max}{}^b, \ \ln cH_{s,max}{}^d, \ \sqrt{\ln fH_{s,max}{}^g}\right) \qquad (5.5)$$

$$E(T_s) = aH_{s,max}{}^b + cfH_{s,max}{}^{d+g} \qquad (5.6)$$

There are many optimisation functions and algorithms available in **R** and for this procedure the **optimx** (Nash, 2012) package was chosen, as it is more robust than the standard **optim** package. The *optimx* function provides various methods that can be used for optimisation and orders the results of most efficient should, a number of methods converge to a solution. For the fitting, using a Non-Linear Minimisation algorithm (NLM) gave the best fit to the measured data. The NLM is an algorithm developed for the minimization of nonlinear functions as proposed by Dennis and Schnabel (1983) and Schnabel et al. (1985). More information on the various optimisation methods can be found in **optimx** user manual (Nash, 2012) and references therein.
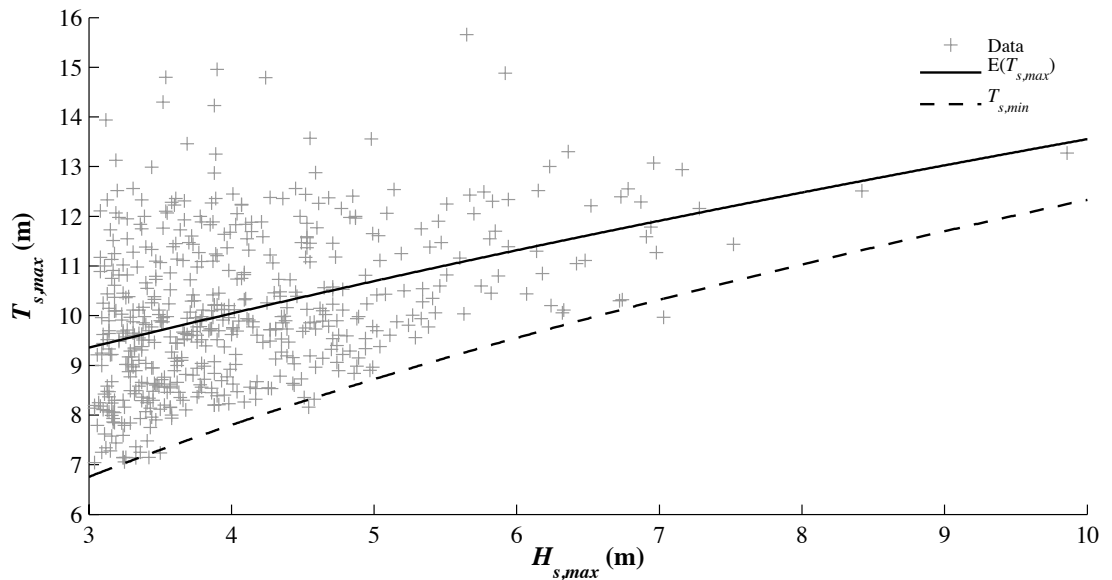
Fig. 5.8 – Fitting of 3 parameter log-normal distribution to T_s

Fig. 5.8 shows the scatter plot of $T_{s,max}$ against $H_{s,max}$ with the corresponding expectation $(E(T_s))$ from the estimated parameters. Examination of this shows that the $E(T_s)$ provides a good fit to the data from the estimates. It also highlights that the minimum threshold level of $3.9H_s^{0.5}$ is acceptable for the data as the majority exceed this limit. Table 5.2 shows the parameter estimates from the optimisation procedure.

Parameter	*a*	*b*	*c*	*d*	*f*	*g*
Value	2.77	0.57	4.72	-0.17	1.11	-0.03

Table 5.2 – MLE of parameters for fitting the 3 parameter log-normal distribution to $T_{s,max}$

5.2.3 Fit non-homogeneous Poisson process to storm spacing

As discussed previously, the spacing between events is critical, as more erosion will occur if the beach has not had sufficient time to recover prior to the next event. In order to produce a realistic random storm climate, an accurate representation of the seasonal change is required. The seasonal variation in storm frequency is modelled using a non-homogeneous Poisson process. A non-homogeneous Poisson process is one in which the rate of the process is a function of time, with their use common for forecasting climatic patterns (e.g. Restrepo-Posada and Eagleson, 1982; Parisi and Lund, 2000; Lu and Garrido, 2005).

In order to estimate the seasonal frequency, three intensity functions were fitted to the data. These are functions of constant, once-annual and twice-annual seasonal variation and are provided in Eq. (5.7), with the fitting procedure discussed in detail in Appendix A. As with the fitting of $T_{s,max}$, the fitting of the intensity functions to S also uses the **optimx** package. Table 5.3 provides the parameter estimations for the intensity functions, with Fig. 5.9 showing the fit of these estimations in comparison to the measured data. Again these are comparable with those of Callaghan et al. (2008) for the same data.

$$\lambda(t \mid \theta) = \theta_0, \quad \text{constant}$$

$$\lambda(t \mid \theta) = \theta_0 + \theta_1 \sin(wt) + \theta_2 \cos(wt), \quad \text{annual}$$

$$\lambda(t \mid \theta) = \theta_0 + \theta_1 \sin(wt) + \theta_2 \cos(wt)\theta_3 \sin(2wt) + \theta_4 \cos(2wt), \quad \text{twice annual}$$

(5.7)

To compare the estimations with the measured data the parameters have to be adjusted to take account of the average annual storm duration. As the measurements of storm occurrence are from the start-to-start of events and the intensity function is a measurement

of the spacing, the estimates must be scaled to account for storm duration in order to compare the functions to the measured occurrence data. Multiplying the parameter estimates by 1-av(D) scales back the spacing to start-to-start measurements by adjusting the estimates. The average storm duration (av(D)) is the average annual duration, which is the total storm duration over the 25-year measurement period divided by 25 years. These were determined to be approximately 553 hours (0.063 years) of storm conditions per year giving a scaling factor of 0.94.

In addition to the scaling of the parameters, the measurement time period has to be accounted for so that the intensity function has the correct shape. Although the measurements of H_s and T_s have been reduced into a dataset spanning from 1st January 1981 to 31st December 2005, the first storm event takes place on 3rd April 1981 (92 days after the beginning of the year). Therefore, the intensity functions have to be appropriately shifted to account for this. The shifting of the intensity functions leads them being determined over a time period ranging from -92 to 273 days instead of 0 to 365 days.

	θ_0 (scaled)	θ_1 (scaled)	θ_2 (scaled)	θ_3 (scaled)	θ_4 (scaled)
Constant	23.33 (21.93	NA	NA	NA	NA
Once-annual	23.33 (21.93)	1.88 (1.77)	0.47 (0.44)	NA	NA
Twice-annual	23.33 (21.93	1.74 (1.64)	-0.26 (-0.24)	0.21 (0.20)	0.68 (0.64)

Table 5.3 – MLE of parameters for fitting intensity functions to the spacing between storm events
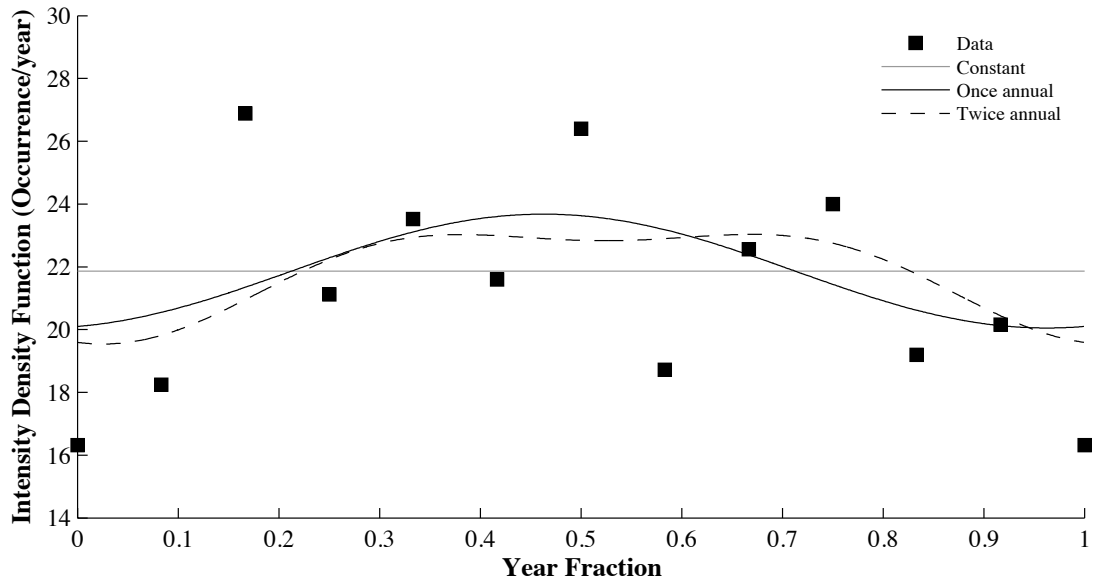
Fig. 5.9 – Fitting of intensity functions to the spacing between storm events

Due to the high intensity of measure events in March, the fit is somewhat flattened resulting in low evidence of correlation on initial inspection. However, it can be seen that the once and twice-annual intensity functions have picked up the winter peak that is evident in the seasonal trend of the data. The constant intensity does not showing any correlation as expected.

Upon visual inspection of the data, both, the once and twice-annual intensity functions, represent the measured data equally efficiently. As the twice-annual occurrence intensity function does not provide a significantly more efficient fit to the measured data, it was decided that the once-annual occurrence intensity function should be used. The principle of parsimony states that, unless there is a significantly strong reason, the number of model parameters should be minimised (Coles, 2001). As the twice-annual model has two more parameters than the once-annual, the twice-annual model was rejected.

5.2.4 Monte Carlo simulation of synthetic storm climate

5.2.4.1 Gibbs sampling to generate $H_{s,max}$ and D pairs

The generation of random $H_{s,max}$ and D pairs was carried out using a Gibbs sampling technique. This procedure was implemented by creating two different Gibbs samplers. The first one is used to ensure the random realisations converge to a Markov Chain with the second then taking over and generating the random Fréchet pairs of $H_{s,max}$ and D. In order to ensure convergence the first 10,000 random realisations are wasted (Callaghan et al., 2008).

Once the Gibbs sampler has wasted the first 10,000 cycles, the final number of $H_{s,max}$ and D Fréchet variates are determined using the same procedure, beginning with the last values of the wasted cycles. The length of the synthetic climate generated is dependent on its use. For example, if the maximum erosion return level of interest is 20 years then, the minimum length of synthetic climate that allows for an accurate estimation of this return level is required. The generation of a climate longer than required will result in unnecessary computational time. According to Hawkes (2000) the maximum return period of interest should be defined by the user with the corresponding Monte Carlo simulation length being; the number of events per year (N_y) multiplied by the return period (RP) and then by 10 (Record length = N_y x RP x 10).

As the synthetic wave climate is to be used in order to assess medium-term beach erosion it was decided that an accurate return level for more than a 10-year return period is not required. Following Hawkes (2000) the required record length is 2,156 events for an accurate 10-year return level, based on 21.56 events per year. A record of this length corresponds to approximately 100 years worth of storm events, based on the annual average number of events remaining constant.

Fig. 5.10 shows the distribution of random $H_{s,max}$, $T_{s,max}$ and D variables along with a good correlation to the measured data. This is confirmed with the comparison of the probability

distributions for the data (Fig. 5.11) and the mean values from each dataset being comparable (Table 5.4).

	Measured	**Random**
Mean ($H_{s,max}$)	4.08 m	4.11 m
Mean (D)	25.64 hours	26.49 hours
Mean ($T_{s,max}$)	10.1 s	10.1 s

Table 5.4 – Comparison of mean values from measured and synthetic storm climates
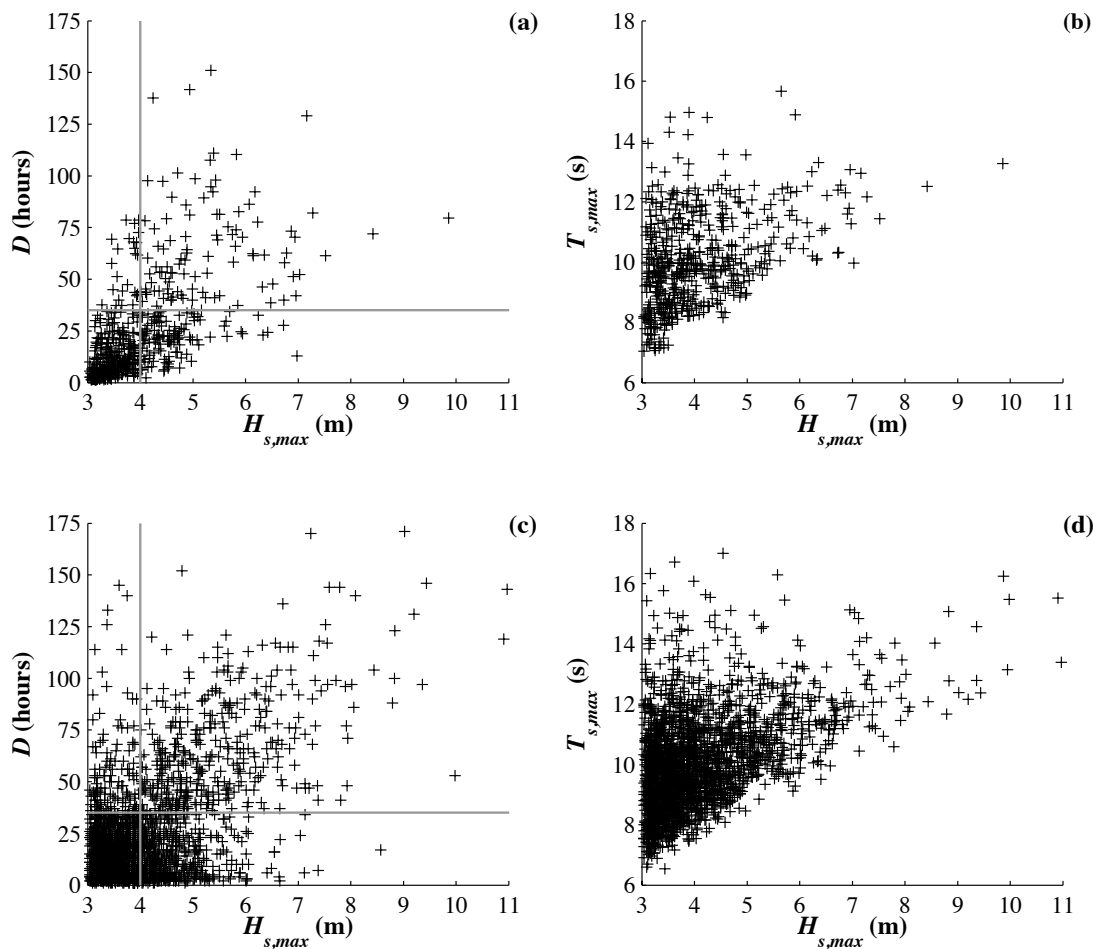
Fig. 5.10 – Comparison between measured (a) D vs. $H_{s,max}$ and (b) $T_{s,max}$ vs. $H_{s,max}$ with 100 years (2,156 events) of random storm events (c) D vs. $H_{s,max}$ (c) and (d) $T_{s,max}$ vs. $H_{s,max}$
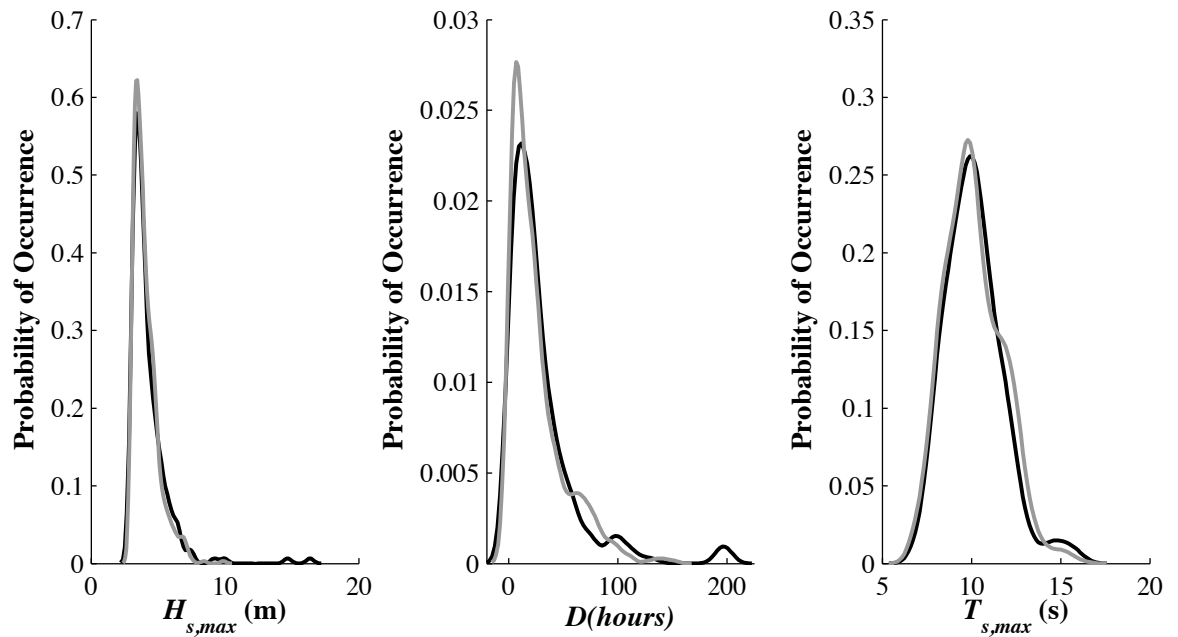
Fig. 5.11 – Comparison of probability distributions of measured (black line) and random (grey line) storm events.

5.3   Chapter Summary

This chapter has demonstrated the implementation of a statistical model used for simulating the offshore storm climate of the Sydney/Narrabeen region. The model implemented here is a modified version of the FTS of Callaghan et al. (2008). These modifications complement the data being used and increase the efficiency of the parameter fitting. It has been shown that the synthetic storm climate generated from the model is in good agreement with that measured. The 100-year storm timeseries generated provides the input conditions for the XBeach modelling within the SPA methodology. This will allow for 100 years of beach evolution to be modelled and the medium-term (annual to decadal) erosion levels to be quantified.

CHAPTER 6

XBEACH MODELLING

This chapter provides a brief description of the XBeach model along with its calibration for simulating the storm-induced erosion and post-storm recovery that occurred at Narrabeen Beach. This is achieved through a number of sensitivity tests on model parameters that control erosion and accretion. The results from this chapter provide the model setups that will be used within the SPA to assess the medium-term erosion and variability of Narrabeen Beach. The accuracy of each individual simulation is assessed using, both, a Brier Skill Score and the volumetric error between the simulated and measured profiles. Upon completion of the individual model calibrations, an annual storm climate is simulated and compared with the measured profile data to establish the validity of reducing the wave climate into simplified erosion and accretion periods for modelling within the SPA.

6.1   The XBeach Model

6.1.1 Description and structure

XBeach is an open source, process-based, numerical model, developed jointly by UNESCO | IHE, Deltares, Delft University of Technology and the University of Miami to provide a robust modelling tool for assessing the erosion of coastlines from hurricane impacts. Fig. 6.1 shows the main structure of XBeach, which is comparable to that of Reniers et al. (2004).

The model is based on the nonlinear shallow water equations and resolves nearshore hydrodynamics by employing a 2DH description of wave groups and infragravity motions. Wave group forcing is derived from a time varying wave action balance equation, which

subsequently drives the infragravity motions and longshore and cross-shore currents. The Eulerian flow velocities determined by the model governing equations are used to force the sediment transport module.

The sediment transport module uses a depth averaged advection-diffusion equation (Galappatti and Vreugdenhil, 1985) to determine sediment concentration (C_s), using an equilibrium concentration (C_{eq}) as a source term. C_{eq} is determined from, either, the Soulsby-van Rijn formula (Soulsby, 1997) or the van Thiel-van Rijn formulae (van Rijn, 2007a, 2007b; van Thiel de Vries, 2009) with the change in bed level computed from the sediment transport gradients (q_x and q_y) and avalanching mechanism when a critical bed slope is exceeded.

A full description of the governing equations is provided in Appendix B, with the key components relevant to model calibration discussed in more detail within the corresponding sections of this chapter.
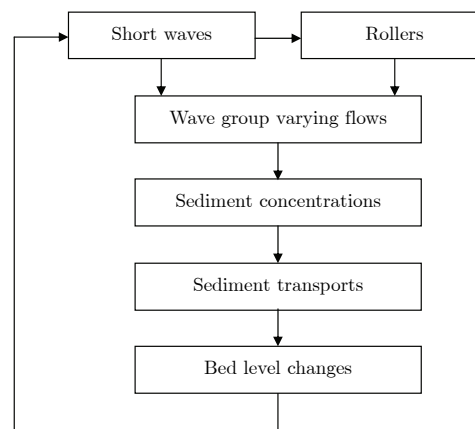
Fig. 6.1 – Simplified description of XBeach model structure

6.1.2 Model domain

The coordinate system in XBeach is such that the computational x-axis is always orientated towards the coast with the y-axis directed alongshore. It is defined relative to world coordinates (x_w, y_w) through the origin (x_{ori}, y_{ori}) and the orientation *alfa*, defined counter-clockwise with relation to the x_w-axis (Fig. 6.2).
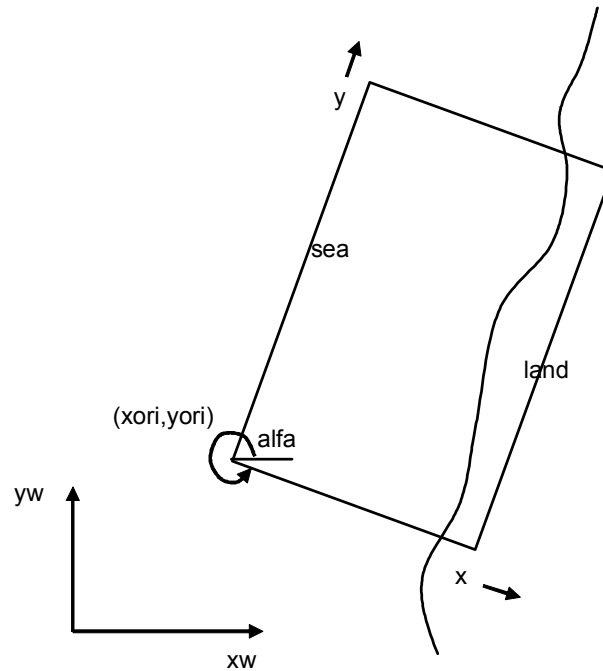
Fig. 6.2 – XBeach model grid (Roelvink et al., 2010)

The grid is a rectilinear, non-equidistant, staggered grid. The bed levels, water levels, water depths and concentrations are defined at cell centres, with the velocities and sediment transport rates determined at the interfaces. In the wave model, wave action, roller energy and radiation stresses are defined in cell centres, with the radiation stress gradients defined at the interfaces.

6.1.3 Model grid

To ensure a computationally efficient model, the grid spacing is varied throughout the domain, with the largest grid size being offshore and decreasing shoreward. It is suggested that the minimum wave period used for the grid sizing be taken as the minimum, mean wave period ($\min(T_m)$) of the wave spectrum. As the storm will be generated using a random JONSWAP spectrum the minimum wave period was set to be 5s, in line with the recommended value. It is also recommended that the grid should be spaced such that there is a maximum decrease of spacing of 15% between each grid point, there are 12 points per longwave and that the onshore spacing is 2m.

6.2   Simulation Accuracy

6.2.1 Brier Skill Score

To validate and assess the accuracy of XBeach, a comparison is made with the measured post-event profiles, with the accuracy being defined using a Brier Skill Score (BSS). The BSS compares the mean square difference between the predicted and measured profiles and the mean square difference between the pre-storm and the measured profile. The use of a BSS to assess morphological model accuracy has become common practice (e.g. van Rijn et al., 2003; Pedrozo-Acuna et al., 2006; de Alegria-Arzaburu et al., 2010). The formulation of the BSS is given in Eq. (6.1).

$$BSS = 1 - \left[\frac{\left\langle \left| x_p - x_m \right|^2 \right\rangle}{\left\langle \left| x_b - x_m \right|^2 \right\rangle} \right]$$

(6.1)

Where x_p is the predicted profile from XBeach; x_m is the measured profile (post-event) and x_b is the initial (pre-event) profile. The classification of BSS provided by van Rijn et al. (2003) gives BSS of < 0 as *"bad"*; $0 - 0.3$ as *"poor"*; $0.3 - 0.6$ as *"reasonable/fair"*; $0.6 - 0.8$ as *"good"*; and $0.8 - 1.0$ as *"excellent"* representations of the measured data.

6.2.2 Volumetric error

In addition to the BSS calculations, the volumetric error between the simulated and measured profiles is determined. As the SPA is to be used in order to assess the erosion of the beach, an accurate representation of the volumetric predictions from XBeach is just as important as an accurate BSS.

6.2.3 Relative Mean Absolute Error

To assess the accuracy in the annual sequence simulation, the relative mean absolute error (RMAE) between the simulated and measured data was determined. The RMAE was determined using Eq. (6.2), in line with van Rijn et al. (2003) and changed into a percentage value for analysis.

$$RMAE = \frac{\langle |x_p - x_m| \rangle}{\langle |x_m| \rangle} \times 100\%$$

(6.2)

Where x_p is the predicted data from XBeach and x_m are the measured data.

6.2.4 Depth of closure

As there are no profile data available further offshore the simulations were further assessed by comparing the morphological limit of the models to the depth of closure (DoC) values at Narrabeen Beach. For the 25-year wave record the annual DoC values were determined using Eq. (6.3) and are provided in Fig. 6.3. These results give mean, maximum and minimum DoC estimates of 6.43m, 7.38m and 5.65m respectively. However, it can be seen that some of the estimates are outwith the limits of the sample mean plus or minus the standard deviation. This highlights the high degree of variability in the wave climate at Narrabeen Beach.

$$h_c = 2.28 H_{s,12} - 68.5 \frac{H_{s,12}^2}{g T_{s,12}^2}$$

<div align="right">(6.3)</div>

Where h_c is the annual DoC and $H_{s,12}$ and $T_{s,12}$ are the significant wave height and period that are exceeded 12 hours per year respectively.
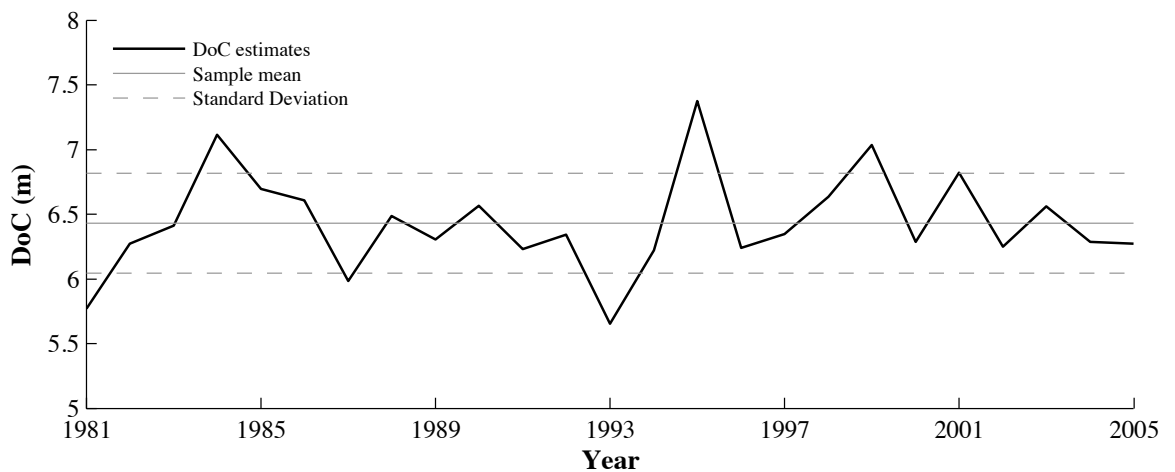
Fig. 6.3 – Estimates of annual DoC values at Narrabeen Beach

6.3   Modelling Storm-induced Erosion

The purpose of the following tests is to calibrate XBeach to effectively simulate storm-induced erosion at Narrabeen Beach. The occurrence of storm events determined from the measured data (Chapter 4) was compared to the profile measurement dates to select suitable profiles for model calibration and validation. As the profiles were measured at approximately monthly intervals, it is common to find more than one storm event occurring between consecutive measurements. For the test results to be as accurate as possible it is important that the chosen profiles have only one storm event between the profile measurement dates and that pre and post event calm periods are as short as possible.

6.3.1 Storm events

To provide a comprehensive calibration of XBeach, four storm events of varying magnitude and duration were modelled. Wave heights and periods for the storm events were taken from measured wave data and analysed for XBeach input. Hourly H_s values along with the energy spectrum were determined, leading to the peak wave height ($H_{s,max}$) and period (T_p) provided in Table 6.1. The storms were input into XBeach in the form of a series of JONSWAP spectra, each one-hour in duration to best encapsulate the actual storm profile. Although the suitability of applying JONSWAP spectra in the Narrabeen region may be in doubt, this is currently the only mechanism for generating spectral wave conditions within XBeach. XBeach has the ability to read SWAN generated spectra as boundary conditions, but this would add an additional component to the methodology that was deemed unnecessary at this early stage of development. Fig. 6.4 shows the variation in H_s during the chosen events with Fig. 6.5 showing the measured pre and post-storm profiles.
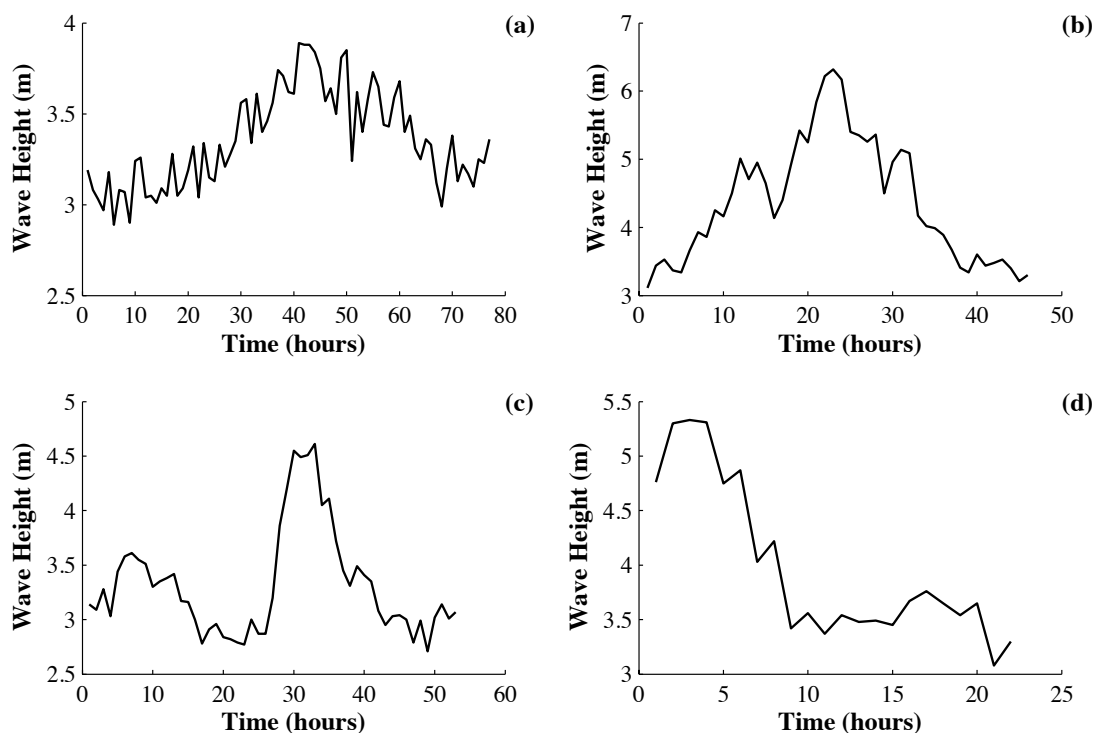
Fig. 6.4 – Wave height measurements for storm events used for calibration of XBeach. (a) storm 1, (b) storm 2, (c) storm 3 and (d) storm 4
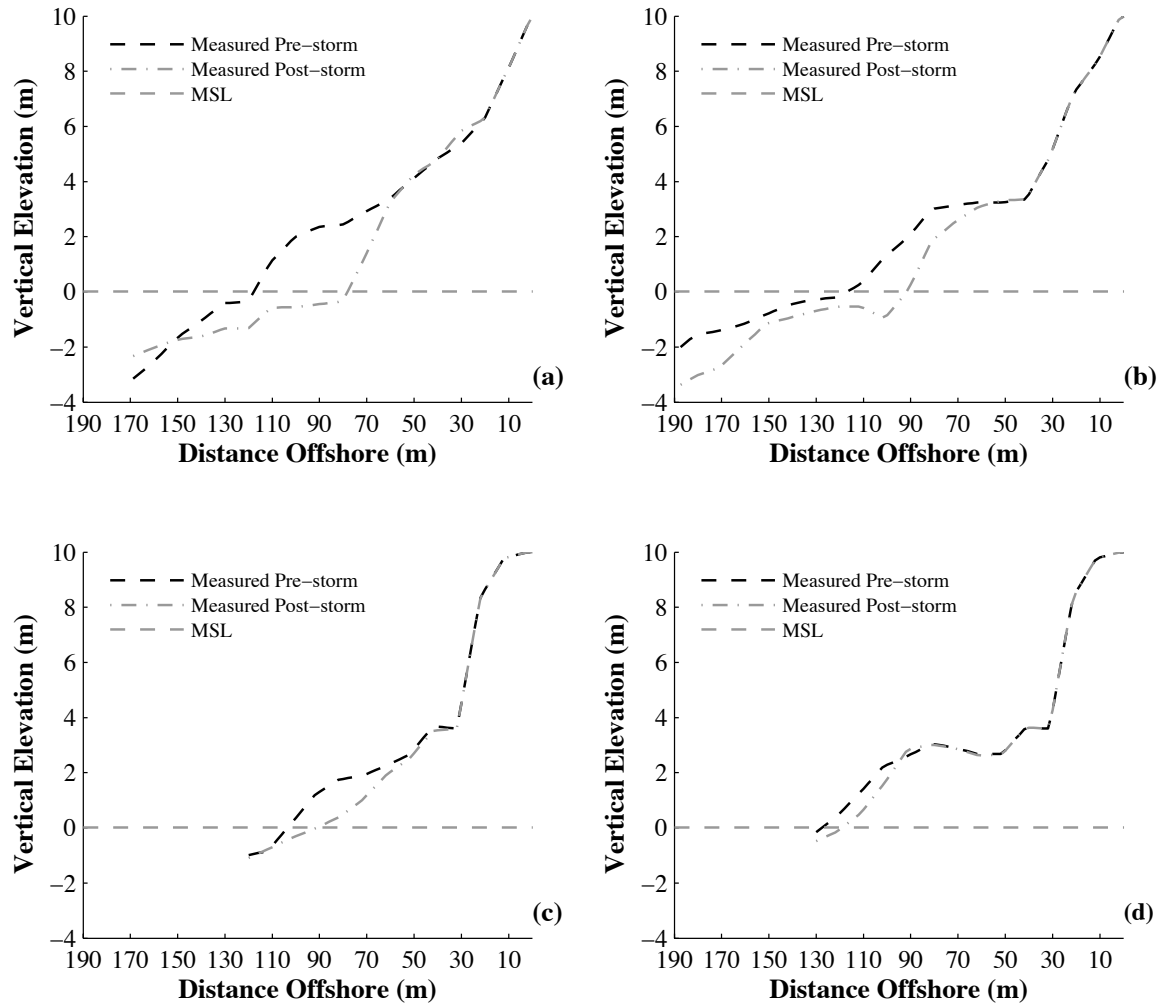
Fig. 6.5 – Measured pre and post-storm profiles for (a) storm 1, (b) storm 2, (c) storm 3 and (d) storm 4

Storm	Profile dates	$H_{s,max}$ (m)	D (hrs)	T_p (s)
1	31/05/83 – 16/06/83	3.89	77	12.4
2	30/10/87 – 27/11/87	6.32	46	9.85
3	19/05/94 – 21/06/94	4.61	53	9.85
4	14/10/94 – 16/11/94	5.33	22	9.85

Table 6.1 – Details of storm events used for erosion model calibration

6.3.2 Measured profiles

Throughout the measurement period the offshore limit of the profiles vary considerably. As there are no measurements significantly beyond the intertidal zone, a constant offshore bed slope of 1:83 (Wright and Short, 1984) has been adopted for extending the profiles offshore. To provide a smooth transition between the measured profile and the offshore region, the bed slope is varied gradually up to 1:83. Although this is not entirely accurate it is the only available information regarding offshore bathymetry at present.

As discussed in Chapter 4 the sediment at Narrabeen Beach vary across the beach and for the purposes of these tests a single average median grain diameter (D_{50}) value has been used. The D_{50} of Narrabeen beach ranges from 0.25 to 0.50 mm (Short, 1985) giving an average diameter of 0.37 mm, which is used in the simulations.

All model runs were made with a constant (initial) water surface level (z_{s0}) that corresponds to the Mean Sea Level (MSL) in the region, provided by Manly Hydraulics Laboratory. This was determined as +0.02m AHD when averaged between 1990 and 2010.

6.3.3 Default simulation

To decide the sensitivity testing that is required for effective calibration, the four storm events were first modelled using the default XBeach parameters. The results, which are provided in Fig. 6.6, show that the default settings of the model significantly over predicts the erosion during all storm events with the BSS values all being less than 0, which is entirely unacceptable.

In order to produce realistic estimates of the storm-induced erosion, key parameters that control erosion were varied in a number of sensitivity tests. These tests include, the implementation of a limiting Shields parameter (θ_{max}) and varying; the Chézy coefficient (C); the permeability coefficient of the beach (k); and the maximum gradient of wet cells before avalanching (*wetslp*).

The Chézy coefficient provides the frictional resistance to the flow, thus affecting the magnitude of the velocity used to drive the sediment transport calculations. Altering the permeability will affect the uprush and return flows, as water will infiltrate into and exfiltrate out of the beach. The use of infiltration and exfiltration requires the groundwater flow module to be implemented (*gwflow* = 1). The accuracy of the simulations will be assessed using a Brier Skill Score (BSS) allowing for the most appropriate parameter values to be determined. At the end of the sensitivity analyses, a suitable set up for modelling storm erosion will be chosen and used throughout the erosion modelling in the SPA. All simulations use the SvR sediment transport regime as this has been extensively validated for simulating sandy beach erosion using XBeach.
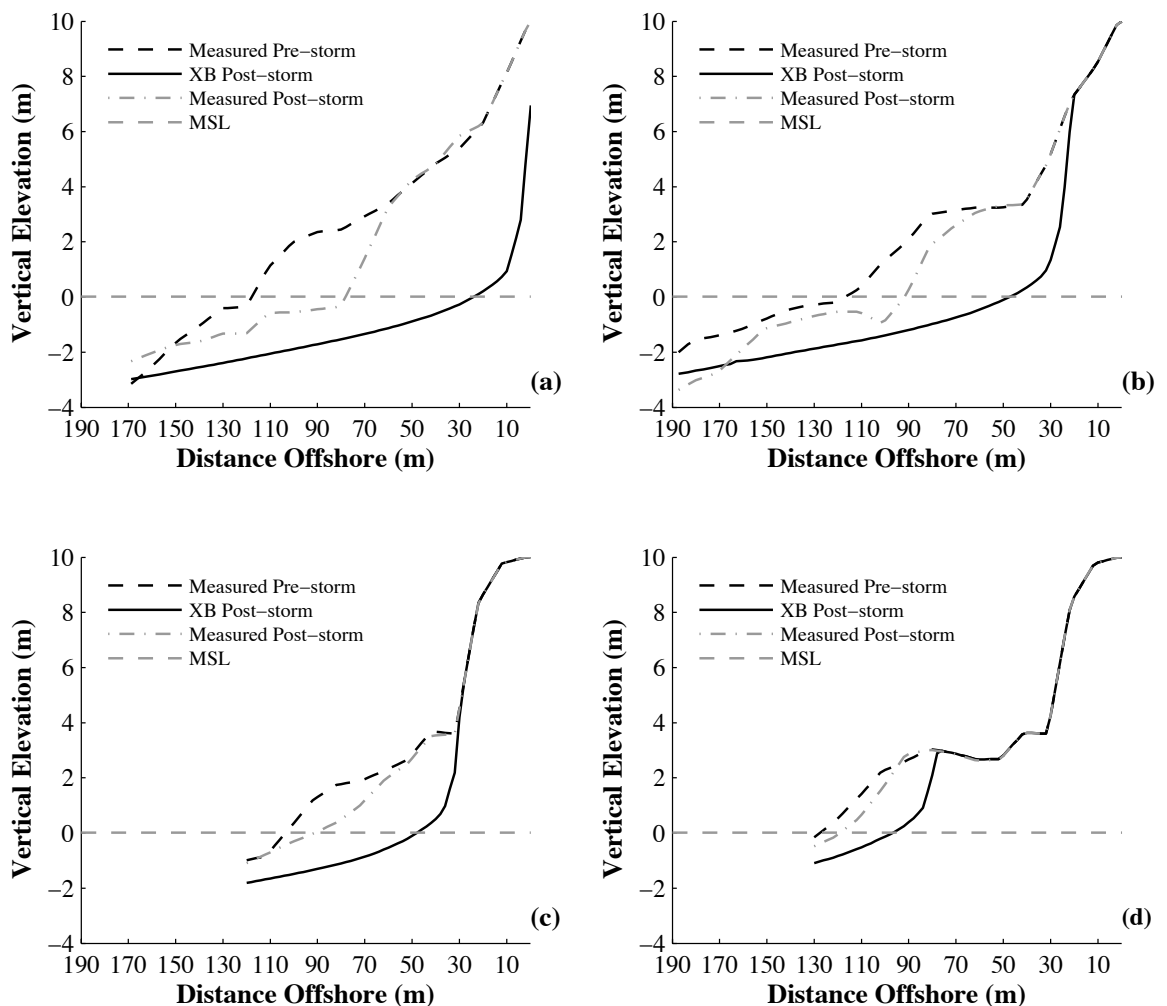
Fig. 6.6 – Results for default XBeach simulations for (a) storm 1, (b) storm 2, (c) storm 3 and (d) storm 4

6.3.4 Limiting Shields parameter

As the SvR formula was developed under bed and suspended load conditions, it is not strictly valid for high velocity sheet flow situations (Soulsby, 1997; McCall et al., 2010). To overcome this, XBeach allows for a threshold velocity condition to be enforced that reduces the stirring velocity ($u^2_{stirring}$) during such situations using Eq. (6.4). Under waves and currents, sheet flow conditions occur when the Shields parameter (θ) is greater than 0.8 (Soulsby, 1997) with the XBeach manual suggesting the limiting value of between 0.8 and 1.0. The $u^2_{stirring}$ limitation is enforced by setting θ_{max} defined by Eq. (6.5). McCall et al. (2010) sets $\theta_{max} = 1.0$ for modelling hurricane impact at Santa Rosa Island, FL, U.S.A. and investigates the effects of a range of θ_{max} (0.8 to 1.2) on the model results. It was found that there was little difference in the model BSS when θ_{max} was varied and the BSS fell below 0 without this limit being applied, as with the default simulations for Narrabeen Beach. As a θ_{max} limit is necessary for using the SvR formula in high velocity situations, it was decided that θ_{max} should be set to 1.0, as it is the middle value of the 0.8 to1.2 range investigated by McCall et al. (2010) and within the range suggested in the XBeach manual.

$$
u^2_{stirring} = \begin{cases} \left|u^E\right|^2 + \dfrac{0.018}{C_D} u_{rms}^{\ 2} & \theta < \theta_{max} \\[2ex] \theta_{max} \dfrac{g D_{50} \Delta}{c_f} & \theta \geq \theta_{max} \end{cases}
$$

(6.4)

$$
\theta_{max} = \frac{c_f u^2_{stirring}}{\Delta g D_{50}}
$$

(6.5)

Where θ is the Shields parameter, θ_{max} is the maximum Shields parameter (start of sheet flow), Δ is the relative density and C_D is the sediment drag coefficient.

A reduction in $u^2_{stirring}$ will reduce C_{eq} and limit the volume of sediment that can be carried by the water column. Limiting C_{eq} lowers the sediment transport rates, and thus reduces the overall erosion of the beach. Implementing θ_{max} has no effect on the flow velocities (u^E)

derived by the model, it solely reduces the value of $u^2_{stirring}$ during sheet flow. Fig. 6.7 is provided for illustrative purposes only to show that u^E is unaffected (a) and total load sediment transport rate is reduced (b) with the implementation of a θ_{max}. These were produced by simulating the conditions of Storm 1 (Table 6.1) with the morphology module of XBeach turned off to make the results comparable.
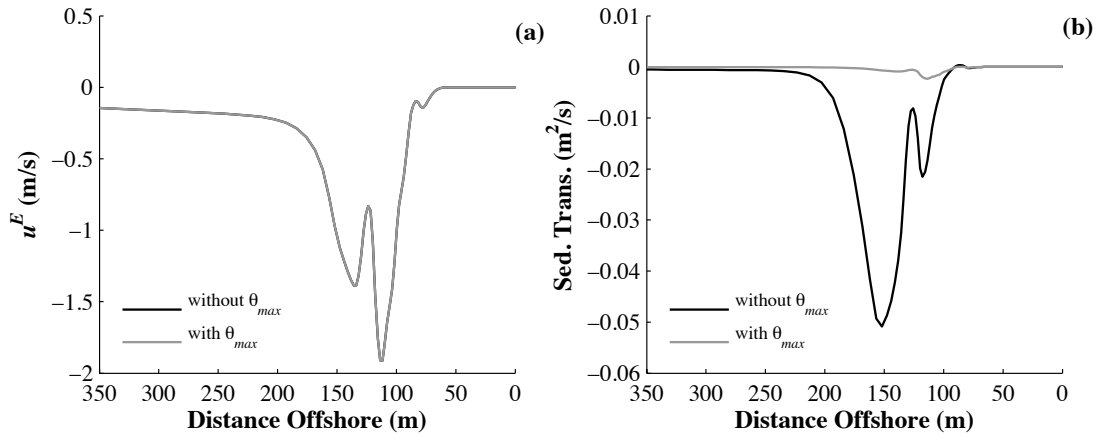
Fig. 6.7 – Effects of inclusion of θ_{max} criterion on (a) u_e and (b) sediment transport rate

6.3.5 Chézy coefficient (C)

Further sensitivity tests were carried out to determine appropriate flow friction coefficient (c_f) and Chézy coefficient (C). The relationship between *cf* and *C* is given in Eq. (6.6), which shows that a reduction in *C* or an increase in c_f would result in a decrease in erosion, by reducing the flow velocities, based on the Chézy flow criterion implemented in XBeach. By default the c_f and *C* values are set as 0.003 and 55 respectively.

$$c_f = \frac{g}{C^2}$$

(6.6)

In addition to the decrease in the flow velocities (u_e), when θ_{max} is implemented, varying *C* will also vary $u^2_{stirring}$ that defines C_{eq}. A reduction in *C* will increase *cf* meaning that

$u^2_{stirring}$ and C_{eq} will also reduce. This further limits the volume of sediment that can be transported in the water column, thus reducing the sediment transport rates and overall erosion. As the sediment data available at Narrabeen Beach indicates a medium to coarse sand, C should be less than the default value. Fig. 6.8 is provided for illustrative purposes only to demonstrate the effects of C on the sediment transport rates and subsequent erosion when the θ_{max} criterion is implemented. This plot was produced using the same conditions as Fig. 6.7. The sensitivity testing was conducted for C ranging from 20 to 55.
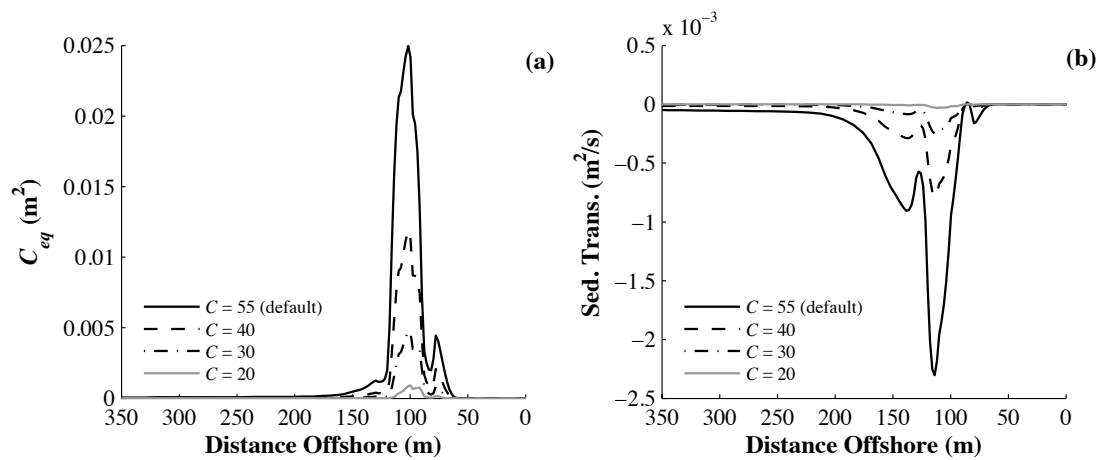
Fig. 6.8 – Effects of reducing C on (a) C_{eq} and (b) sediment transport rate

6.3.6 Coefficient of permeability (k)

The k values (Table 6.2) were determined from Eq. (6.7) and (6.8), using the average D_{50} (0.37mm), a kinematic viscosity at 20ºC and salinity 35 ppt ($\nu = 1.05\text{x}10^{-6}$: average conditions at Narrabeen from Manly Hydraulics Laboratory) and a range of porosities suggested for sandy beaches (Soulsby, 1997). All simulations have no geometric variation in k ($K_I = k_x = k_y = k_z$) and the groundwater level remained constant at MSL.

$$K_p = \frac{\varepsilon^{4.7} d^2}{19.8(1-\varepsilon)}$$

(6.7)

$$K_I = \frac{gK_p}{\nu}$$

Where K_p is the specific permeability; K_I is the coefficient of permeability (k in XBeach); d is the grain diameter and ε is the porosity.

As with the C parameter testing, simulations in which the bed morphology was turned off were carried out to demonstrate the affects of varying k. Fig. 6.9 shows the mean u^E velocities for the k values and indicates that increasing k increases the infiltration into the beach, thus decreasing the return flow and offshore sediment transport rate.

ε	0.30	0.35	0.40 (default)	0.46
K_I	0.0003	0.0007	0.0015	0.0031

Table 6.2 – Permeability values used in erosion model calibration
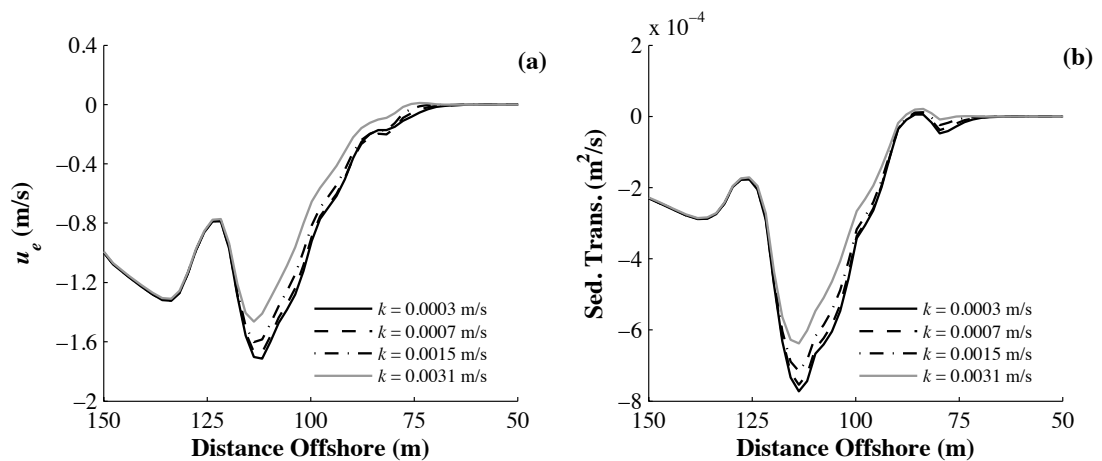
Fig. 6.9 – Effects of varying k on (a) u^E and (b) sediment transport rate

6.3.7 Gradient of wet cells before avalanching

From Fig. 6.5 it can be seen that the post-storm beach face for storms 3 and 4 are considerably shallower than those in storms 1 and 2. When the cells are inundated with water during a storm event the maximum gradient before avalanching occurs can be controlled by using the model parameter *wetslp*. Reducing *wetslp* will reduce the gradient of the beach face and should provide a better representation of the slope evident in the post-storm profiles of storms 3 and 4.

6.3.8 Results

The sensitivity tests were carried out thoroughly and systematically for the range of values of all the parameters discussed previously, and for all storm events. The most accurate model set up was deemed to be the one that gave the highest average BSS and lowest average volumetric error across all four events. The results from the most accurate simulations are provided in Table 6.3 and Fig. 6.10 with Table 6.4 providing details of the calibrated parameter values.

Storm	BSS	Vol. Err.
1	0.91	+6%
2	0.52	+9%
3	0.81	-1%
4	0.78	-1%

Table 6.3 – Results from erosion model calibration
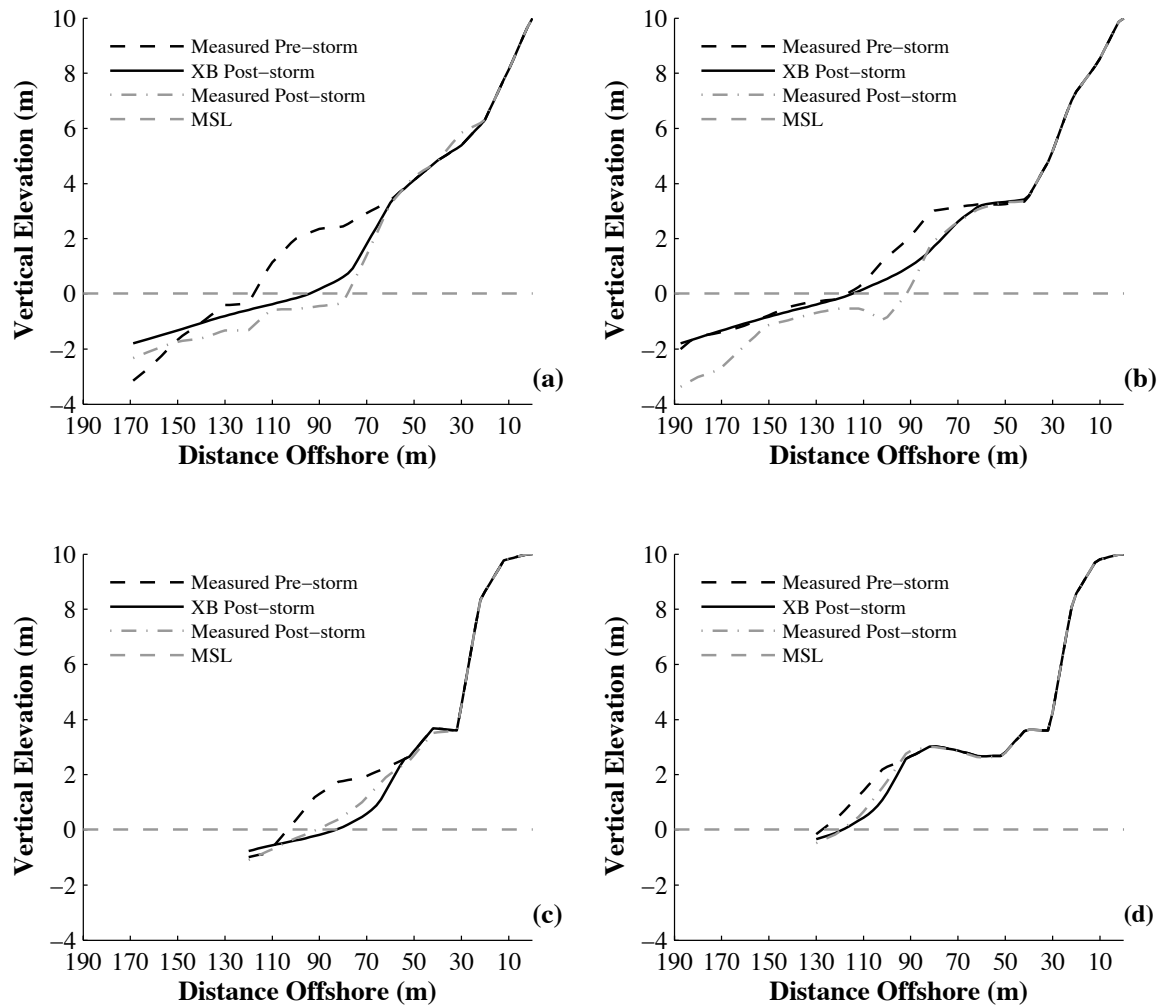
Fig. 6.10 – Results from erosion model calibration for (a) storm 1, (b) storm 2, (c) storm 3 and (d) storm 4

Parameter description	XBeach keyword	Value
Sediment transport regime	*form*	1 (SvR)
Limiting Shields parameter	*smax*	1.0
Chézy coefficient	*C*	45
Permeability	*kx*, *ky* and *kz*	0.0031 m/s
Porosity	*por*	0.46
Max gradient of wet cells	*wetslp*	0.15

Table 6.4 – Calibrated model parameters for erosion model

From Eq. (6.6) a *C* value of 45 gives a c_f value of 0.005 corresponding to a rippled sandy bed (Soulsby, 1997) and can therefore be considered valid for Narrabeen Beach, based on the studies of Short (1984).

The most suitable values of *k* and *ε* are the highest of the range shown in Table 6.2, and are larger than the default values of 0.0031m/s and 0.40. As D_{50} at Narrabeen Beach is larger than the default XBeach value (0.3mm), it is conceivable that *k* and *ε* will also be greater.

The set up provided in Table 6.4 results in an average BSS and volumetric error of 0.76 and +3% respectively. Storm 2 produces the lowest BSS (0.52). However, it can be seen from Fig. 6.10 that the measured post-storm profile after storm 2 contains a nearshore bar, which indicates that the profile has not been measured at the end of the storm but during an intermediate state following the storm event. If the profile measurement was taken closer to the end of the storm event the BSS may be considerably higher as the beach would be exhibiting a dissipative state with a wide planar surf zone as shown in Storm 1. Given that the average BSS for all storms results in a *"good"* BSS rating and an excellent average volumetric error of +3%, it can be stated that XBeach has been accurately calibrated for modelling storm erosion at Narrabeen Beach.

Typical XBeach input file (*params.txt*) and wave boundary condition file (*bcfile*) for modelling storm-induced erosion is provided in Appendix C.1.

6.4   Modelling Post-storm Recovery

The development and current uses of XBeach (discussed in detail in Chapter 3) have shown that the model is primarily used as an erosion model. With this in mind, its use within the SPA for modelling post-storm beach recovery constitutes a novel use of XBeach in itself, as simulation of beach accretion has never been attempted at the timescales or magnitude presented in this thesis. Although XBeach was initially developed and validated as a storm erosion model, it has now been modified to include the physical processes associated with beach accretion.

The purposes of the following tests are to assess and calibrate XBeach for simulating accretion during post-storm recovery periods at Narrabeen Beach. It has been discussed previously, that Narrabeen Beach predominantly exhibits an intermediate beach state with a nearshore bar system present. However, should XBeach be calibrated to simulate this type of profile, a longer-term sequence will result in inadequate protection and continual beach recession. Additionally, due to the limited offshore extents of the measured profiles, the capture of bar formation is relatively rare. It was therefore decided that the recovery model should be calibrated to provide estimations of a reflective beach state. Due to the frequency of the profile measurements it is uncommon to find consecutive profiles where no storm events occurred between them. Additionally, due to the frequency that Narrabeen Beach can change states, and when measurements were made, profiles showing fully reflective states are also uncommon. In order for the SPA to be able to accurately quantify erosion levels in the medium-term it is important that the fully reflective state of Narrabeen Beach can be represented effectively.

As with the storm erosion calibration the accuracy of the simulations was assessed using a BSS and volumetric error allowing for the most appropriate parameter values to be determined. At the end of the sensitivity analyses a suitable set up for modelling post-storm recovery will be chosen for use within the SPA. The processes that govern beach recovery (accretion) are inherently different than those responsible for erosion, leading to a significantly different model set up than that of the erosion model.

6.4.1 Recovery periods

As discussed previously, it is necessary to find profiles that have no storm events between them and exhibit a fully reflective beach state. Along with these requirements, it is also imperative that there be near constant wave data between the profile measurements to ensure the boundary conditions are represented fully. Assessments of the measured wave and profile data lead to two such periods where substantial accretion has taken place, transforming the beach from dissipative to reflective state. Fig. 6.11 shows the measured profiles for these periods. It can be seen that the berm height in each post-recovery profile is at a similar level (approximately +2.5m AHD) but during the recovery period (Fig.

6.11b) there is a small nearshore bar at the offshore limit. This may be due to the shorter recovery duration (20 days rather than 29) where fully reflective state has not quite been reached and the profile is still exhibiting a degree of intermediate morphology.
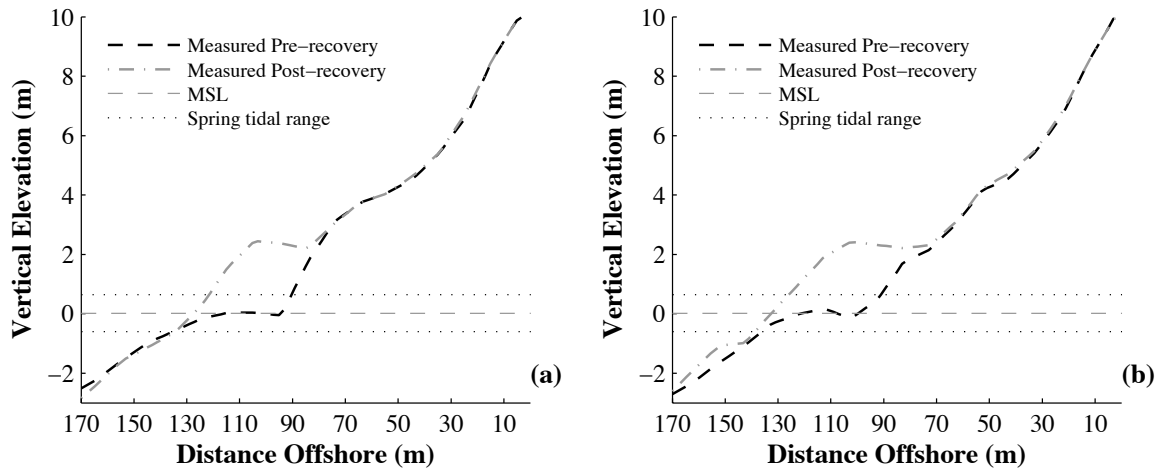
Fig. 6.11 – Measured pre and post-recovery profiles for (a) period 1 and (b) period 2

Analysis of the wave climate during these periods showed that they satisfied the calm wave criteria with all measured wave heights being below the 3.0m storm threshold. Details of the wave conditions are provided in Table 6.5 and Fig. 6.12. As with storm erosion modelling, all beach recovery simulations were forced using JONSWAP spectra that represent the measured wave conditions during the recovery periods. JONSWAP spectra were generated for 24-hour periods using the measured H_s and the overall T_p of the period.

Recovery Period	Profile dates	$H_{s,mean}$ (m)	D (days)	T_p (s)
1	25/08/81 – 23/09/81	1.16	29	9.5
2	25/07/82 – 16/08/82	1.11	20	9.5

Table 6.5 – Details of periods used for recovery model calibration
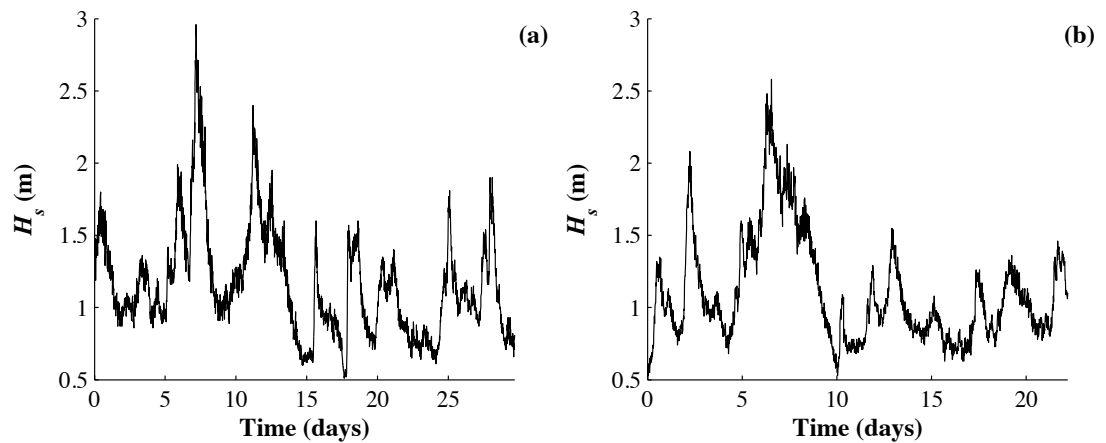
Fig. 6.12 – Measured *H*ₛ during (a) period 1 and (b) period 2

6.4.2 Profiles and grid

The model domains were set up in the same way as the erosion model and described in section 6.3.2.

6.4.3 Default simulations

All recovery simulations invoke the vTvR transport regime as it uses different transport equations for bed and suspended load. During lower velocity recovery simulations, the effects of bed load transport will be greater especially in the swash zone. It is thought that the vTvR regime will better describe bed load transport and result in more accurate prediction of the accreted berm shape.

The default simulations shown in Fig. 6.13 use the vTvR transport regime without invoking the θ_{max} criterion. This shows that under accretionary wave conditions, the default settings mean XBeach is still functioning as an erosion model and considerable beach recession results.
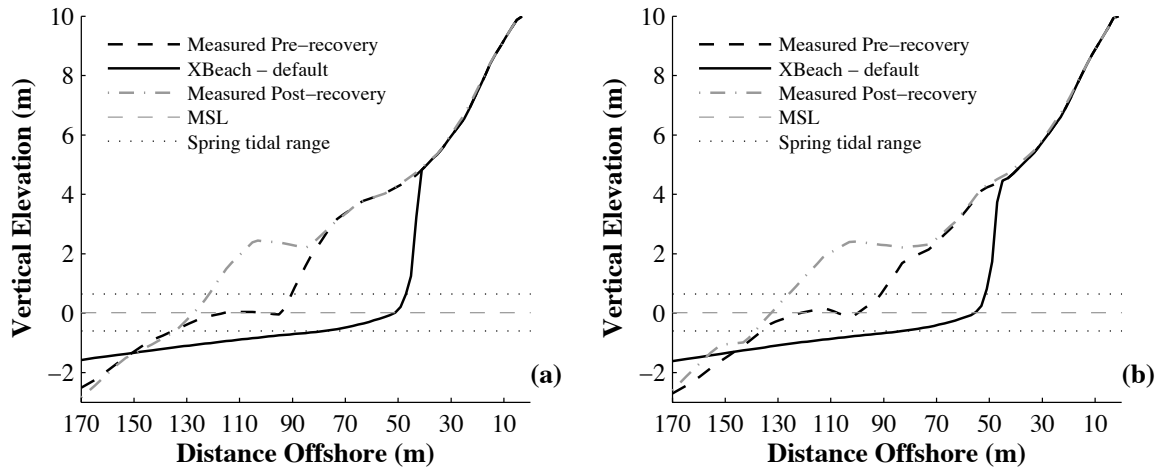
Fig. 6.13 – Results from default XBeach simulations for (a) period 1 and (b) period 2

6.4.4 Onshore transport in XBeach

It has been discussed in Chapter 2 that the predominant mechanisms for the onshore transport of sediment are the skewness and asymmetry of the incident waves.

The sediment transport rate in XBeach is determined using a representative velocity (u_{reps}), the sum of the flow velocity (u^E), and an advection velocity (u^A) from wave skewness and asymmetry. The sediment transport rate in XBeach is determined from Eq. (6.9).

$$q_t = C_s u_{reps} - D_c h \frac{\partial C_s}{\partial x} - 1.6 v_{magu} \frac{\partial z}{\partial x}$$

(6.9)

Where C_s is the sediment concentration, u_{reps} is the representative transport velocity, D_c is the diffusion coefficient, h is the water depth and v_{magu} is a Lagrangian transport velocity. The velocity, u_{reps} is given in Eq. (6.9) and is the representative transport velocity that combines the Eulerian flow velocity (from the NSWE) with the advection velocity from wave skewness and asymmetry, given in Eq. (6.11).

$$u_{reps} = u^E + u^A \tag{6.10}$$

$$u^A = (facSk \times Sk - facAs \times As)u_{rms} \tag{6.11}$$

From Eq. (6.9) to (6.11) it is evident that by varying the factors applied to the skewness (*facSk*) and asymmetry (*facAs*) the magnitude and direction of net sediment transport can be altered. By default *facAs* and *facSk* were calibrated as 0.1 for simulating dune erosion (van Thiel de Vries, 2009).

In XBeach, both *facAs* and *facSk* can be defined separately or together as *facua*. The effect of increasing *facua* on the mean u^A and then, the mean total sediment transport rate is shown in Fig. 6.14 for an example simulation. This is provided for illustrative purposes only and highlights how an increase in *facua* will increase u^A, and eventually results in the shift of the predominant sediment transport gradient from a net offshore to a net onshore direction.
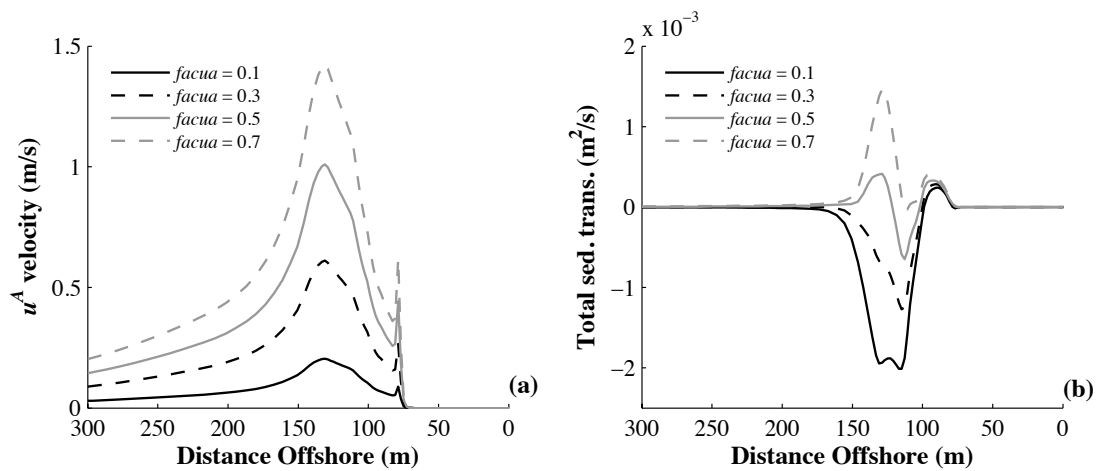
Fig. 6.14 – Effects of increasing *facAs* on (a) u^A and (b) sediment transport rate

The permeability of the beach also plays a significant role in berm formation during the accretion phase (Jensen et al., 2009). For this reason, the groundwater flow module was

activated for all recovery simulations with k taken from the storm erosion tests (0.0031m/s).

6.4.5 Tidal variation

It has been discussed previously (Chapter 2) that the variation in tidal levels plays an important role in berm formation. Inclusion of a tidal variation in the simulations will increase the limits of wave uprush and should allow for a more comprehensive representation of the berm crest to be simulated.

MHL provided data of tidal variation for the Sydney region averaged over 19 years (1990 to 2010), which are shown in Table 6.6. The sensitivity testing was carried out using simplified semi-diurnal mean, spring and high tidal cycles. The high tidal cycle corresponds to a variation between the High Spring Water Solstice and the Indian Low Water Springs.

Tide	Low level (m)	High level (m)
Mean	-0.484	0.524
Spring	-0.607	0.647
High	-0.856	-0.995

Table 6.6 – Details of tidal variations considered for recovery model calibration

The tidal cycles applied to the simulations follow a semi-diurnal sinusoidal function that begins at MSL. An example of 24-hour tidal cycles is shown in Fig. 6.15.
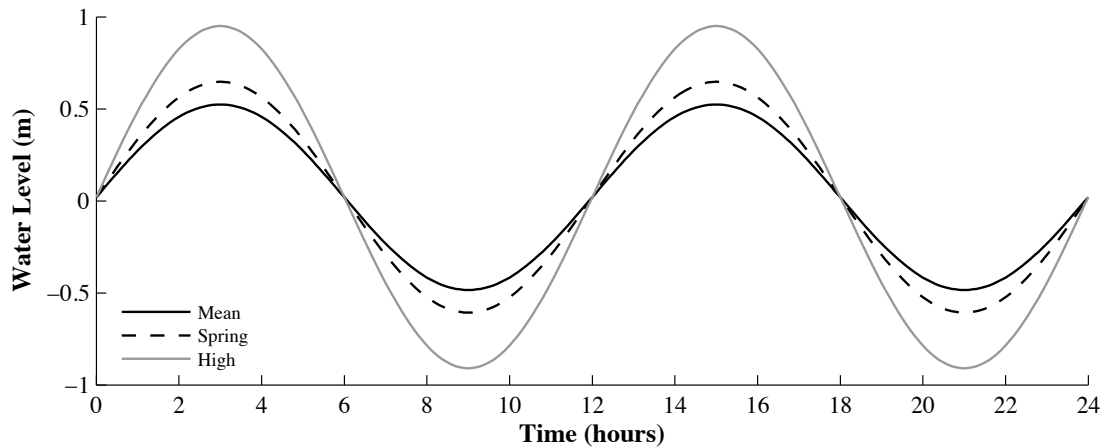
Fig. 6.15 – Example tidal 24-hour tidal cycles based on a sinusoidal function

6.4.6 Morphological acceleration (morfac)

Due to the length of the recovery periods and the requirement for computational efficiency of the SPA, all tests invoked a morphological acceleration factor (*morfac*) of 10. As there is no variation in the tidal limits of each cycle (i.e. spring to neap) the use of *morfac* is deemed appropriate. However, should simulations include varying tidal limits, the suitability of *morfac* would become questionable. The use of *morfac* means that the bed is updated *morfac* times during a hydrodynamic timestep, thus reducing 29 and 20 days simulations to 2.9 and 2.0 days of hydrodynamics. A value of 10 is considered the largest sensible value for these types of morphodynamic simulations (Ranasinghe, Swinkels, et al., 2011). Without the use of *morfac* within the recovery simulations the SPA methodology would not be computationally feasible. For more details of the morfac approach the reader is referred to Roelvink (2006); Roelvink et al. (2010) and Ranasinghe et al. (2011).

6.4.7 Results

The final results of the sensitivity tests for each recovery period are given in Table 6.7 and Fig. **6**.**16**, with Table 6.8 showing the calibrated XBeach parameters.
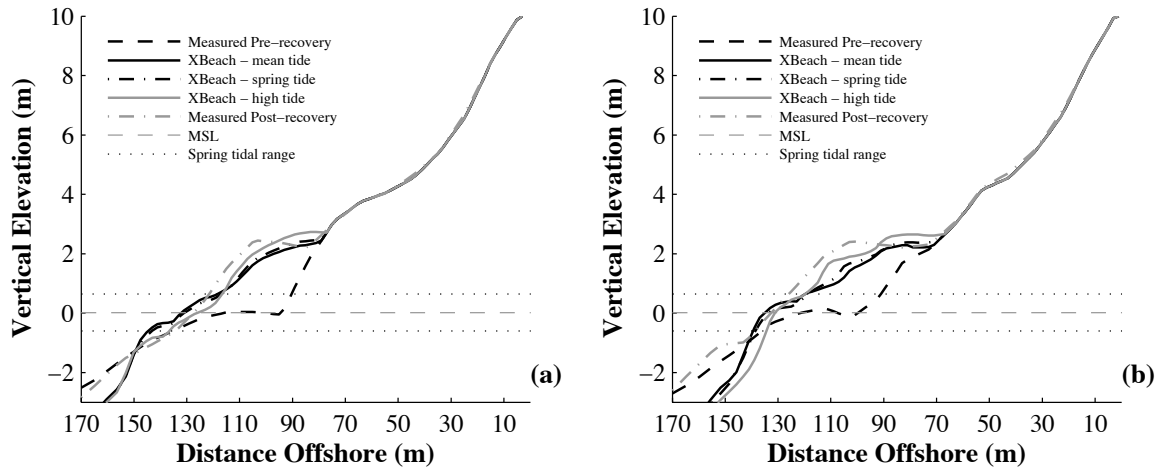
Fig. 6.16 – Results from recovery model calibration for (a) period 1 and (b) period 2

Recovery	Tide	BSS	Vol. Err.
1	mean	0.84	-2%
1	spring	0.86	-2%
1	high	0.89	-2%
2	mean	0.63	-6%
2	spring	0.65	-6%
2	high	0.61	-6%

Table 6.7 – Results from recovery model calibration

Parameter description	XBeach keyword	Value
Sediment transport	*form*	2 (vTvR)
Factor on wave skewness	*facSk*	0.1
Factor on wave asymmetry	*facAs*	1.0
Permeability	*kx*, *ky* and *kz*	0.0031 m/s

Table 6.8 – Calibrated parameters for recovery model

The results presented in Table 6.7 and Fig. **6.16** are extremely encouraging and show that, by considering the hydrodynamic processes necessary for beach accretion and altering the

parameters accordingly, XBeach can be set up such that beach recovery on the weekly to monthly timescale can be successfully modelled. These simulations result in average BSS/volumetric errors of 0.74/-4%, 0.76/-4% and 0.75/-4% for the mean, spring and high tidal cycles respectively. For average values to provide a *"good"* BSS and such a low volumetric error for modelling large-scale beach recovery the calibration process is deemed successful, with an effective set up for modelling the change in Narrabeen beach from dissipative to reflective states achieved. As with the erosion models the results were checked against the DoC values ensuring that XBeach was conserving sediment within this range.

Typical XBeach input file (*params.txt*) and wave boundary condition file (*bcfile*) for modelling storm-induced erosion is provided in Appendix C.2.

6.5   Modelling Annual Beach Change

The SPA methodology presented in this thesis involves the simulation of a sequence of erosion and accretion events to attempt to predict medium-term beach erosion and variability. To assess the accuracy and validity of combining the XBeach storm and recovery model setups in such a sequence, the wave conditions between 25/08/81 and 16/08/82 (*ca.* one year) were divided into erosion and recovery periods, simulated, and compared with the corresponding measured data. Successful implementation of this combination will provide further validation of the individual model calibrations and justify their use within the SPA.

6.5.1 Measured data

The annual period begins and ends with the periods used to calibrate the recovery model. Although this may be considered to introduce a bias to the results, it is important to understand that the use of the two model setups, calibrated previously, allows successful modelling between dissipative and reflective states. It is therefore important to ensure that the time series begins with a fully dissipative profile so as XBeach is able to effectively simulate the initial accretion in the sequence.

Between the first and last profile measurements during this period, 19 storm events had occurred. The full simulation sequence includes 19 storm events and 20 recovery events. These were modelled using three recovery model setups with the different tidal variations considered previously. Fig. 6.17 shows the measured wave conditions and storm events during the period.
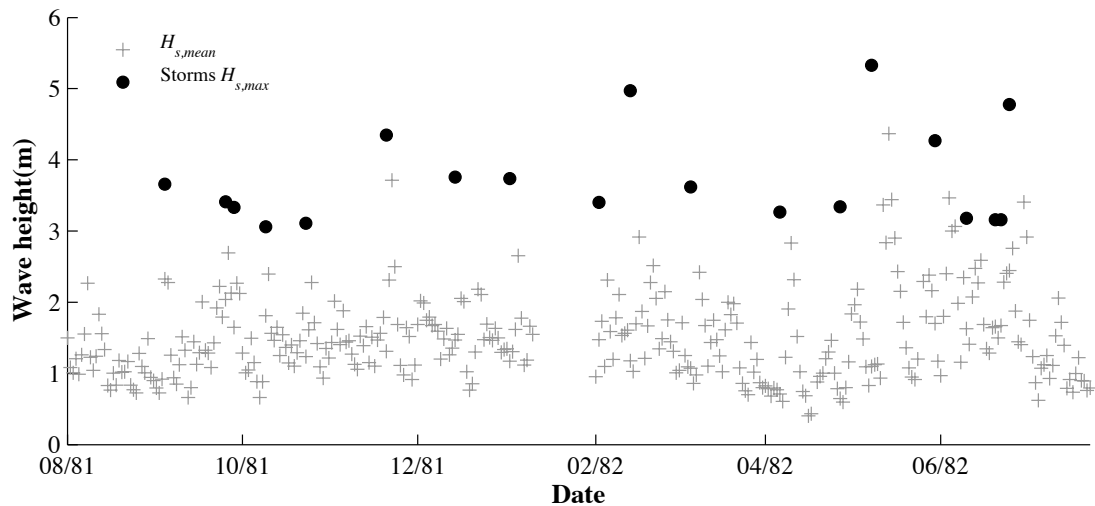
Fig. 6.17 – Measured daily H_s and storm $H_{s,max}$ for the 1981 – 1982 period. Points above the 3.0m threshold not identified as $H_{s,max}$ are a result of events that span multiple days.

For each individual storm event the hourly H_s and overall T_p were used to define the wave boundary conditions for storm erosion simulations, while the average H_s and T_p of the recovery periods defined the boundary conditions for beach recovery simulations.

A comparison of the changes to the subaerial beach volume and positions of the 0m and 2m beach contours, from the measured and simulated profiles, was conducted to assess the accuracy of the simulations.

6.5.2 Modification of XBeach

The simulation of *ca.* one year of beach change using XBeach is an extremely computationally extensive procedure. To make the simulations as efficient as possible the XBeach source code was modified in order to produce outputs in a format that XBeach can read as input bathymetry. This modified XBeach model produces a file that includes the beach profile (z_b) at the end of the simulation. This file is then used as the input bathymetry in the next XBeach model in the sequence (Fig. 6.18). This allows for the sequence of erosion and accretion models to run continuously without the requirement for processing results between simulations.
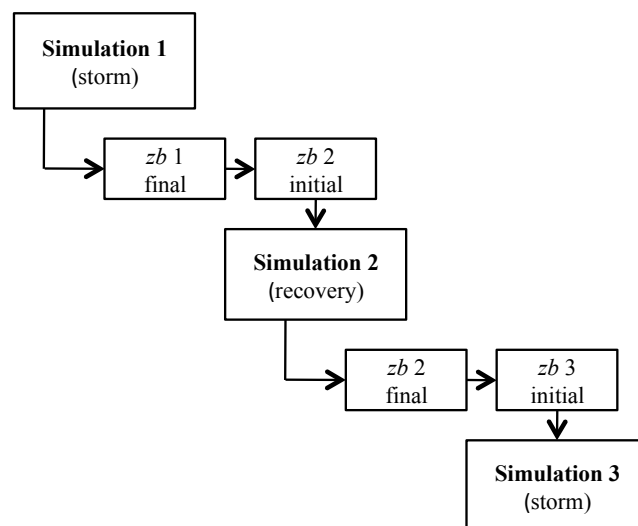
Fig. 6.18 – Simplified description of sequence modelling using XBeach

6.5.3 Results

To provide direct comparison between measured and modelled data, the final profile from XBeach models nearest to the measured profile dates were used for analysis of the results. As the recovery model is only capable of simulating the fully reflective state of the beach, comparing these to measured intermediate states is likely to yield an inaccurate comparison. To quantify the errors in the XBeach sequence RMAE of the subaerial volume change; position of the 0m and 2m beach contours; and the profile envelopes were determined; along with the BSS of the final profile in the sequence. Using the RMAE will

show how effectively the XBeach sequence has followed the trends from the measured data. The contour positions are defined from the distance offshore from the profile benchmark (+10m AHD).

6.5.3.1 Subaerial beach volume and contour positions

The results for subaerial volume change and the contour positions are provided in Table 6.9 and Fig. 6.19 to Fig. 6.21.

Tide	Vol. RMAE	0m Cont. RMAE	2m Cont. RMAE
Mean	6.3%	14.1%	17.2%
Spring	7.3%	12.5%	12.8%
High	10.8%	12.9%	16.4%

Table 6.9 – Errors in subaerial volume and contour positions for 1981-82 simulations
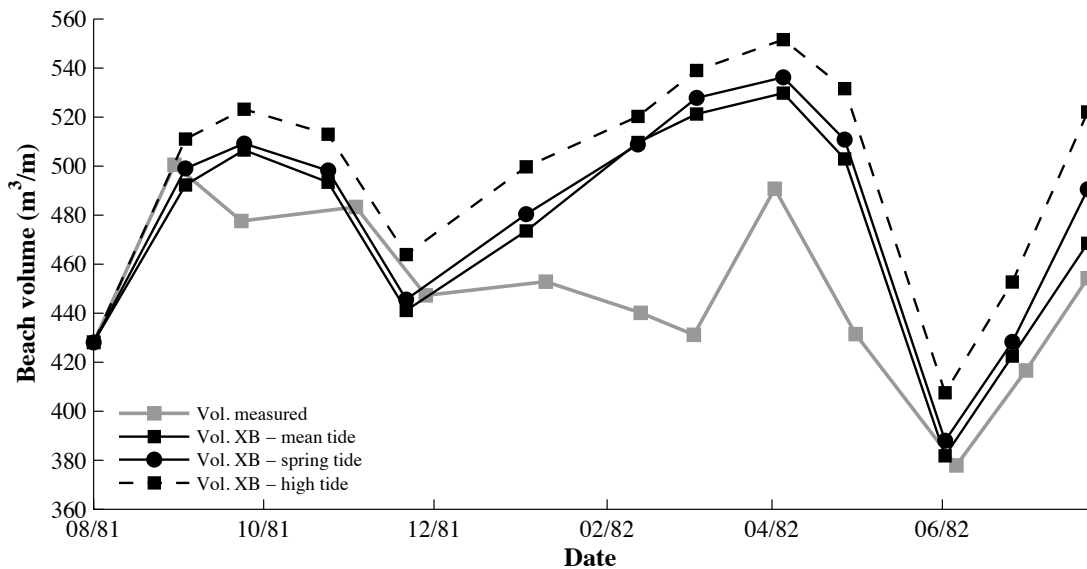
Fig. 6.19 – Comparison of subaerial volume changes for 1981-82 simulations
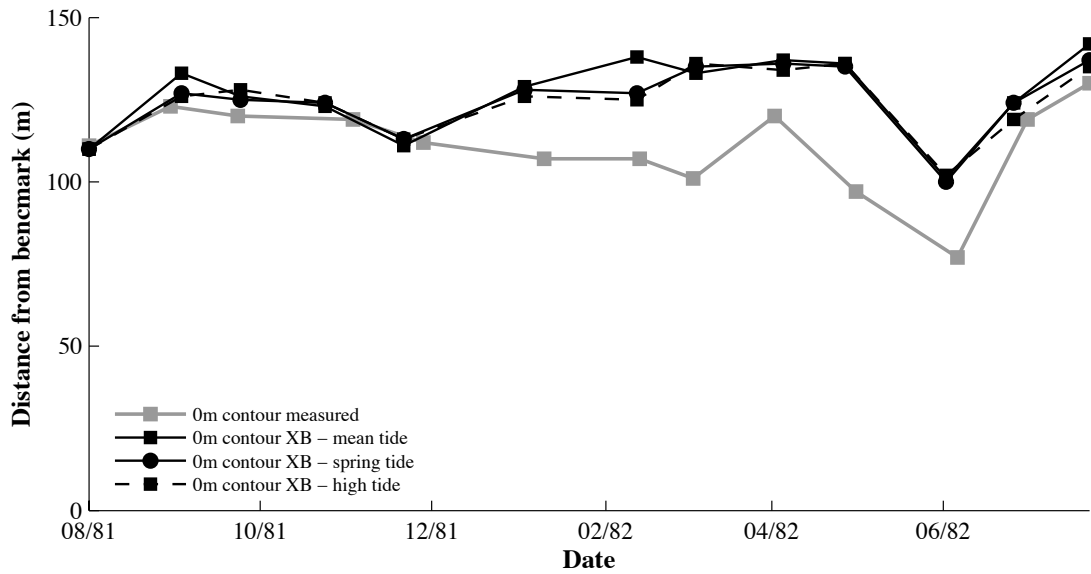
Fig. 6.20 – Comparison of 0m contour positions for 1981-82 simulations
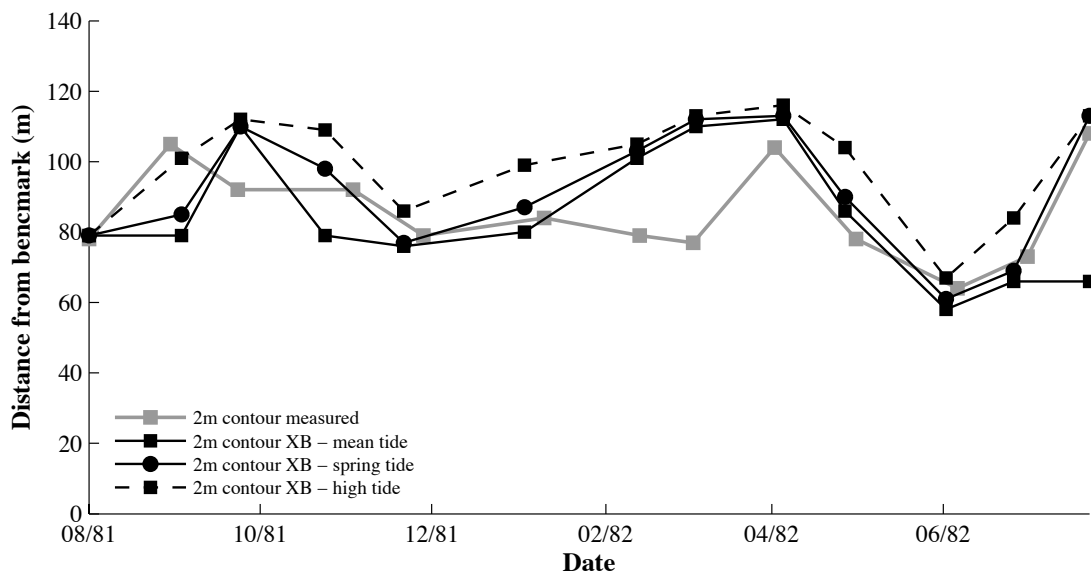
Fig. 6.21 – Comparison of 2m contour positions for 1981-82 simulations

From the results it is clear that the XBeach simulation overestimates the levels of accretion during the period. This results in the overestimations of the beach volume and the RMAE between the measured and simulated data being 6.3%, 7.3% and 10.8% for the mean, spring and high tidal cycles respectively. Better results are provided by the mean and

spring tidal cycles as they produce a lower berm crest and subsequently a lower volume. However, the fact that only the high tidal cycle results in a RMAE of greater than 10% demonstrates the success of the methodology in its ability to model beach volume change at an annual time scale.

Although the position of the 0m and 2m contour result in higher RMAE than the beach volume comparison, the degree to which XBeach can accurately follow the trend in the measured data is extremely satisfying. The most accurate representation of the contour positions is provided by the spring tidal cycle with RMAE of 12.5% and 12.8% for the 0m and 2m contour positions respectively. Considering the complexity of the beach system (Chapter 4) and the simplifications made within the modelling approach, RMAE of this magnitude demonstrates considerable success of the methodology at modelling annual beach variability.

6.5.3.2 Beach profiles

The results for the beach profile envelope and final profile comparisons are provided in Table 6.10 and Fig. 6.22. As the offshore extent of each profile measurement varies, the envelopes have been curtailed at a distance of 130m from the top of the dune, as this is the furthest extent included in all profiles.

Tide	Min RMAE	Mean RMAE	Max RMAE	Av. RMAE	Final BSS
Mean	11.6%	8.8%	4.8%	8.4%	0.71
Spring	10.6%	9.2%	4.9%	8.2%	0.81
High	11.3%	12.4%	6.7%	10%	0.91

Table 6.10 – Errors in beach profile envelopes for 1981-82 simulations
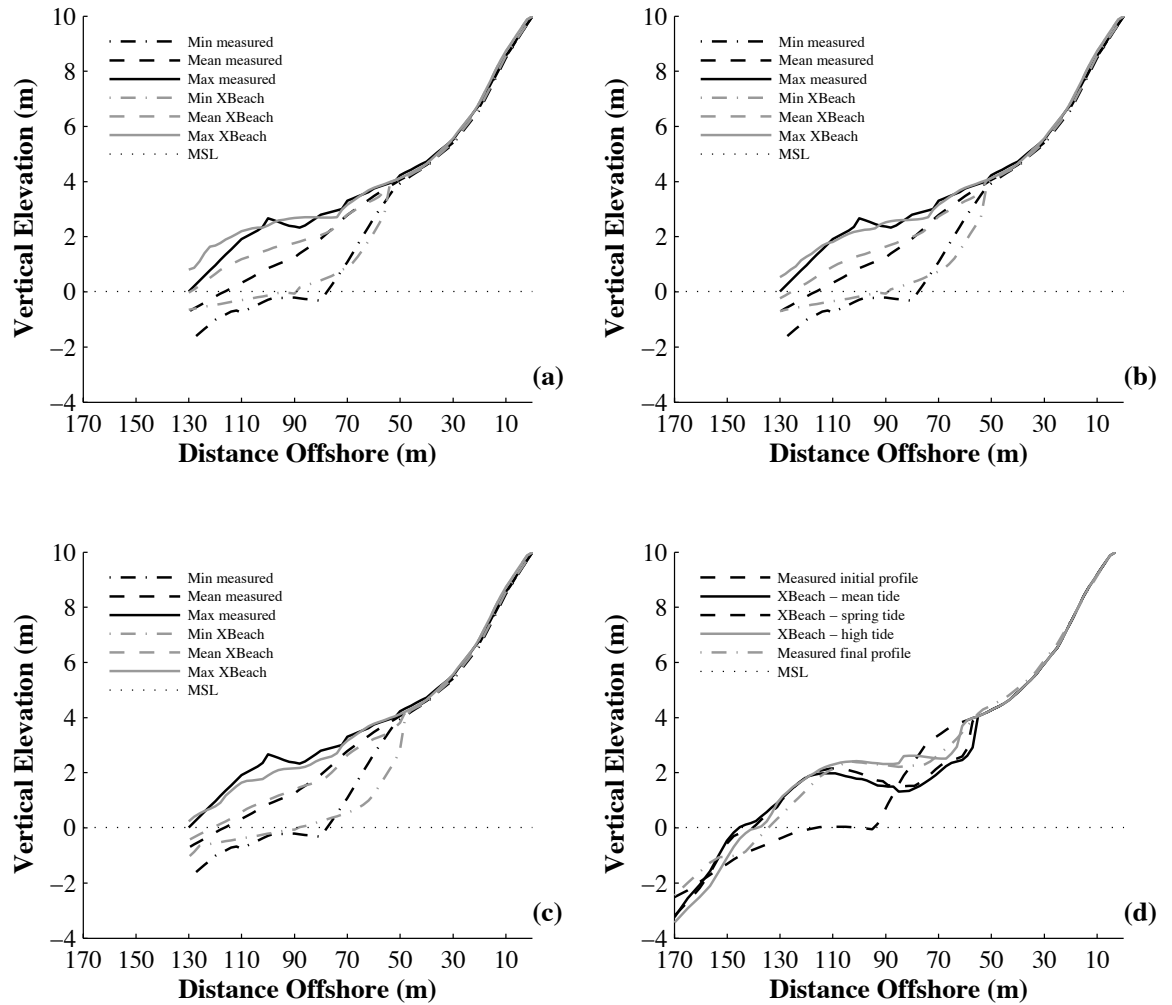
Fig. 6.22 – Comparison of beach profiles for 1981-82 simulations. Envelopes for (a) mean tide , (b) spring tide and (c) high tide. Final profile comparison (d)

The errors for the profile envelope shows that the maximum profile level provides the best correlation to the measured data with an average RAME of 5.5% across all tidal cycles. This can be attributed to the measured profile data containing fully reflective beach states that XBeach has been calibrated to simulate effectively. The RMAEs of the mean and minimum profiles are higher and have average values, across all tidal variations, of 10.1% and 11.2% for the minimum and mean profiles respectively.

The main source of error within all results discussed is due to the simplification of only modelling a fully reflective beach state during calm (recovery) wave periods. It has been

discussed previously in this thesis that Narrabeen Beach predominantly exhibits an intermediate state with a nearshore bar system. To maximise the volumetric stability of longer simulations and due to a lack of accurate profile data, the simulation of an intermediate state during all calm periods is not feasible. It is thought that the lack of berm accretion evident in intermediate states will not provide enough volume to the beach that will be eroded during subsequent storm events. This will lead to constant recession of the beach during longer simulation periods and make this type of modelling unable to produce any sensible results.

The BSS achieved at the end of the simulation period is more than satisfactory, with a high tidal cycle in the recovery simulations able to produce a BSS of greater than 0.70, for all tidal cycles. Although this high BSS can be attributed to the final profile exhibiting a fully reflective state, the fact that this is a result of a culmination of 38 precedent XBeach simulations should not be understated. When reducing such a highly energetic wave climate into simplified erosion and accretion simulations there was a high likelihood that the accumulation of errors within each individual simulation would lead to a large error in the final profile. The fact that such a high BSS can be obtained from this sequence further validates the methodology that will be used to implement the SPA.

6.5.4 Annual time scale calibration

Although the individual event calibrated models have shown to produce a degree of success at modelling an annual time period, it was decided that the recovery model set up should also be calibrated across this period. This will allow for a better representation of the average beach profile during calm periods to be represented; and provide a comparison to the event-calibrated simulations. Calibration was conducted on the same parameters (*facSk* and *facAs*) to determine which combination produced the best representation of the overall annual variability.

The results are provided alongside the individual event calibrations in Table 6.11, , Fig. 6.23, Fig. 6.24, Fig. **6.25** and Fig. 6.26.

Model	Vol. RMAE	0m Cont. RMAE	2m Cont. RMAE
Event	7.3%	12.5%	12.8%
Annual	4.1%	9.0%	12.9%

Table 6.11 – Model calibration comparison of RMAE in subaerial volume and contour positions for 1981-82 simulations.
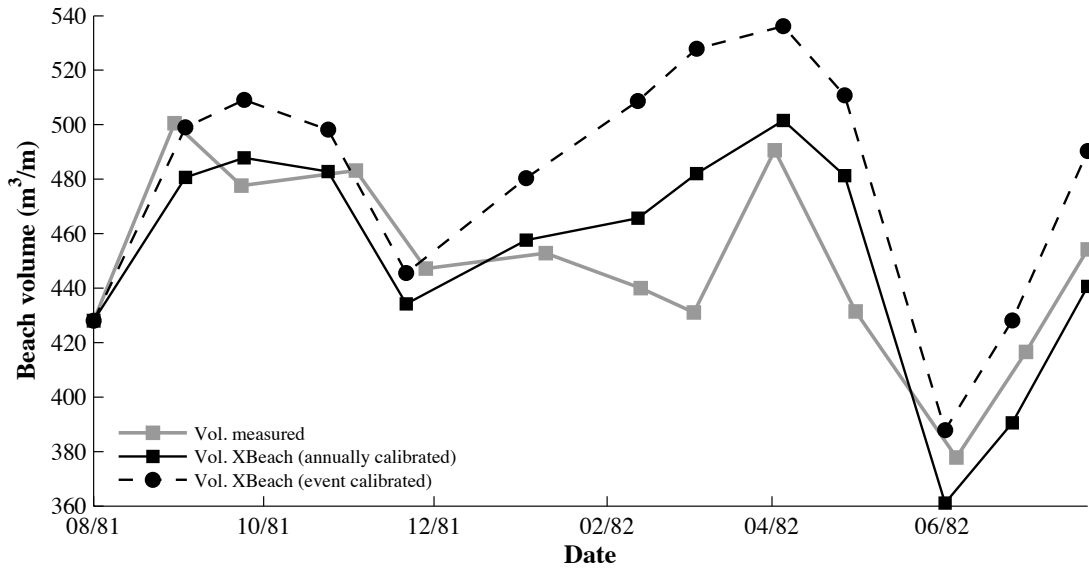
Fig. 6.23 – Model calibration comparison of subaerial volume for 1981-82 simulations
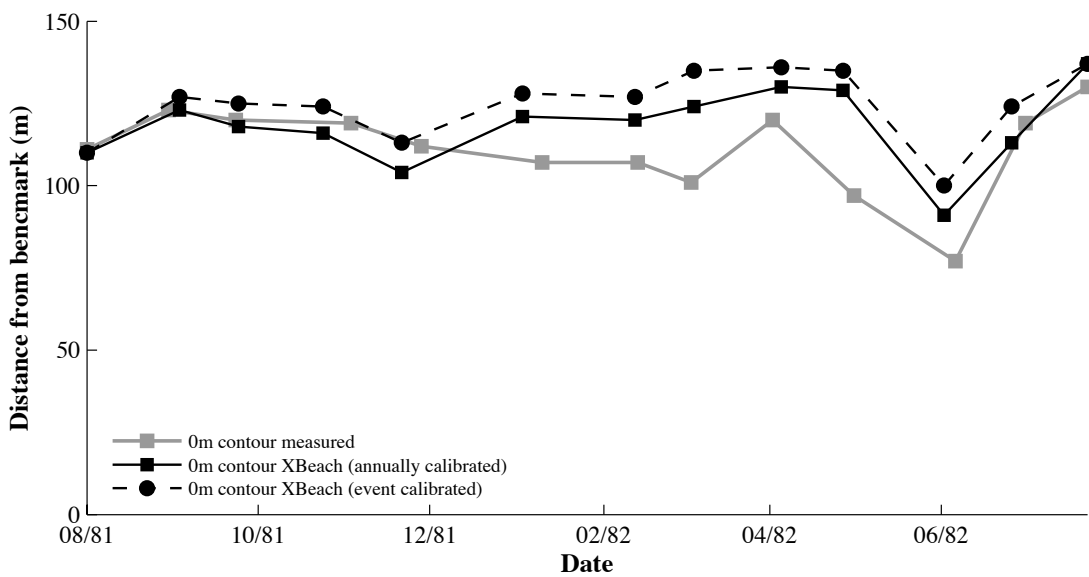
Fig. 6.24 – Model calibration comparison of 0m contour positions for 1981-82 simulations
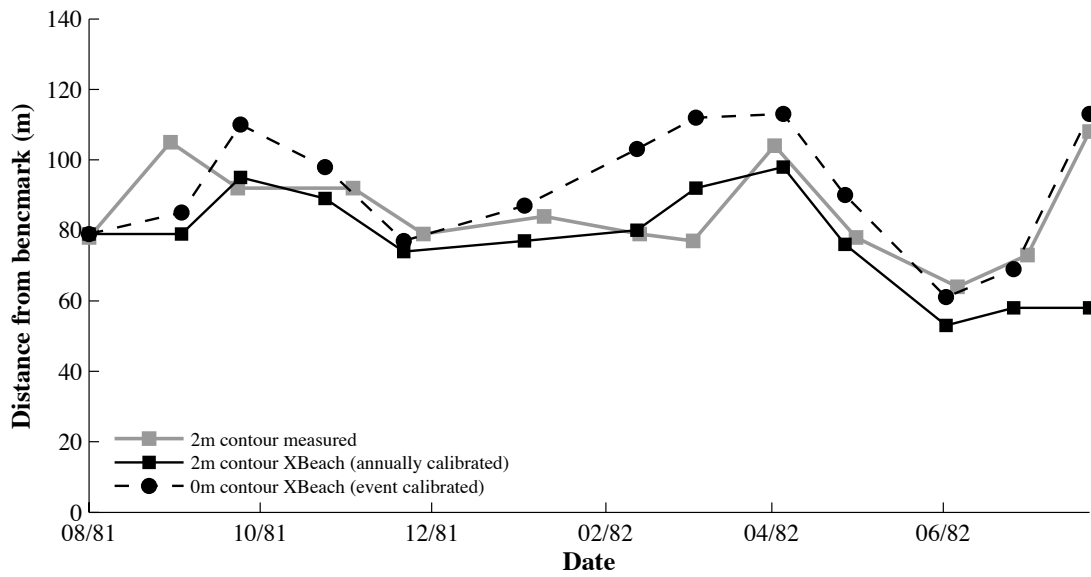
Fig. 6.25 – Model calibration comparison of 2m contour positions for 1981-82 simulations
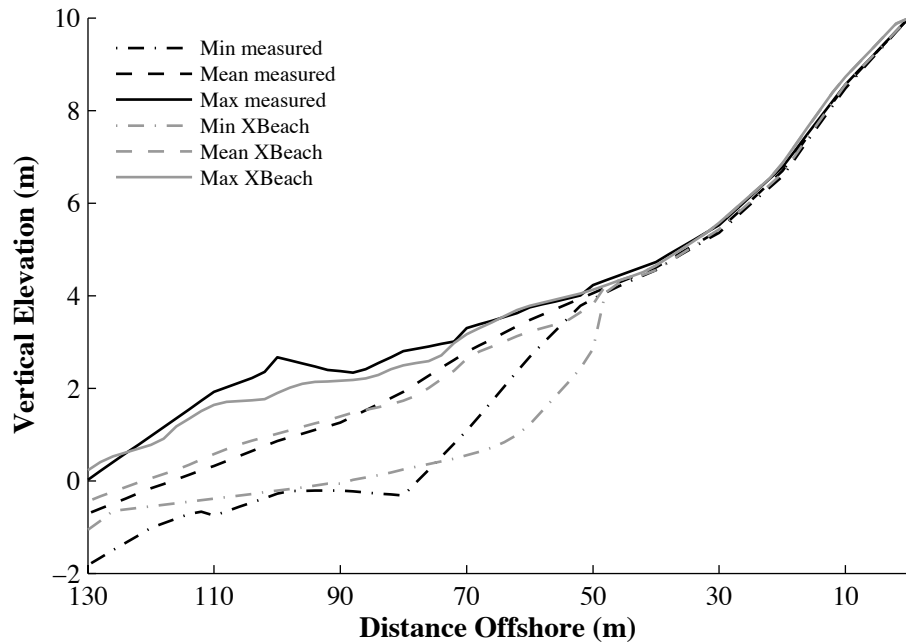
Fig. 6.26 – Comparison of beach profiles for 1981-82 simulations using the annually calibrated recovery model

Model	Min RMAE	Mean RMAE	Max RMAE	Av. RMAE
Event	10.6%	9.2%	4.9%	8.2%
Annual	13.8%	5.1%	4.3%	7.7%

Table 6.12 – Model calibration comparison of RMAE in beach profile envelopes for 1981-82 simulations

From the comparisons of the subaerial volume and beach contour positions, it is evident that the calibration of the recovery model set up over the annual period increases the accuracy of the predictions by reducing the RMAEs. Although there are certain individual RMAEs that increase, this is only slight and does not detract from the overall improvement of the simulation.

Looking at the profile envelope comparisons it is clear that the calibration has had the desired affect as the mean annual profile is now better represented (RMAE of 5.1% compared to 9.2%). That being said, the largest negative impact is evident from these results, as the RMAE of the minimum profile has increased from 10.6% to 13.8%. Although an RMAE of 13.8% can still be considered relatively successful for such a complex beach system, it highlights that longer-term simulations may be more susceptible to recession using this recovery model set up. This is reinforced by Fig. 6.26, which shows the position of the minimum profile has moved closer to the benchmark position at the top of the dune.

The parameter set-up for the annually calibrated recovery model is provided in Table 6.13.

Parameter description	XBeach keyword	Value
Sediment transport	*form*	2 (vTvR)
Factor on wave skewness	*facSk*	0.1
Factor on wave asymmetry	*facAs*	0.8
Permeability	*kx*, *ky* and *kz*	0.0031 m/s

Table 6.13 – Calibrated parameters for the annually calibrated recovery model

Comparing the values in Table 6.13 with the event calibrated parameters it can be seen that *facAs* is lower (0.8 compared to 1.0). This means that less sediment is being transported onshore during the recovery periods and the beach volume is therefore lower after these periods. This accounts for the improved accuracy in the annually calibrated simulations as it allows for a better representation for the average beach profile to be simulated.

6.6   Chapter Summary

The procedure and results demonstrated and presented in this chapter have shown successful calibration of XBeach for modelling, both, storm-induced erosion and post-storm recovery at Narrabeen Beach, NSW, Australia. The erosion model set up has been calibrated using four storm events covering a range of $H_{s,max}$ and D. The calibrated model set up results in an average BSS and volumetric error of 0.76 and +3% respectively, across the four events. The recovery model set up has been calibrated using two periods where the measured H_s was not greater than 3.0m. The two periods chosen showed the transformation of Narrabeen Beach from dissipative to reflective states. The model calibration investigated the effects of three different tidal ranges (Table 6.6). The calibrated model set up results in extremely pleasing average BSS and volumetric errors of 0.74 – 0.76 and -4% across the two periods with the spring cycle. As this calibration of XBeach demonstrates the first use at simulating measured beach recovery the results presented are important in their own right. The ability to accurately represent beach recovery using a process-based model will help to bridge the gap between short and long simulations, the main limitation of process-based morphodynamic modelling at the present time.

The methodology of dividing the wave climate into erosion and accretion periods and simulating them in sequence was validated by the modelling of an annual time period. The results from these simulations show that, with the fully calibrated recovery model, the trends in subaerial beach volume and contour positions are extremely well represented during this annual sequence. Additionally, the simulated profile envelops show high correlation with the measured data. The sequence results a high final BSS of

approximately 0.70, indicating that the shape and stability of the beach has been well represented.

These results showed that the methodology of dividing the wave climate into storm events and recovery periods and modelling them in sequence could successfully represent the annual variability exhibited at Narrabeen Beach. Although there are limitations in only simulating fully reflective beach states during recovery periods, these are overshadowed by the overall success of the methodology. At a region that is frequented by high-energy storm events, and where the beach state is frequently changing, the overall results achieved by these simulations are considered excellent.

To give a comparison between the event calibrated recovery model set up; and to provide a better representation of the average beach profile, the recovery model was calibrated using the annual data. Both of these setups will be used within the SPA to assess the merits of each at estimating medium-term beach erosion.

CHAPTER 7

SPA IMPLEMENTATION

The following chapter discusses the combination of the synthetic 100-year storm climate, presented in Chapter 5, with XBeach to quantify medium-term beach erosion. This combination presents the novel SPA methodology developed by this research.

Prior to the implementation of the procedure, the set up and input conditions are discussed in detail. The results from the SPA are then compared to those measured at Narrabeen Beach to determine the success of the procedure. Upon an analysis of the results, the main limitations of the methodology are discussed in detail.

7.1 SPA Set Up

7.1.1 Computational efficiency

For a methodology that uses a process-based model to make longer-term predictions, such as the SPA, the computational efficiency of the procedure is of the utmost importance. Although the efficiency of the SPA has already been considered by using a *morfac* (Roelvink, 2006; Ranasinghe et al., 2011; Vousdoukas et al., 2012) in the recovery simulations, additional measures are required to make the 100-year simulation more efficient.

To further increase the computational efficiency of the SPA, XBeach was compiled using the Message Passing Interface (MPI) option. This allows for individual simulations to be split across multiple processors on one of the High Performance Computing (HPC) clusters at the University of Glasgow.

7.1.2 Storm event input

The statistical modelling of the storm climate described in Chapter 5 produces random events with representative parameters peak significant wave height ($H_{s,max}$), corresponding significant wave period ($T_{s,max}$) and duration (D). The input of storm events within the SPA is similar to that of the sensitivity tests, in that the storm profile is described as a series of hourly JONSWAP spectra. The storm profile itself can be described as *"idealised"* as it begins with the threshold value of 3.0m, increases linearly to an $H_{s,max}$ peak in the middle, then decreases linearly back to 3.0m at the end.

It has been described previously that $T_{s,max}$ is the wave period that corresponds to $H_{s,max}$. As the JONSWAP spectral input in XBeach requires the T_p of the spectrum $T_{s,max}$ was related to T_p using the empirical relationships of Goda (2010). These relationships are defined in Eq. (7.1), with the assumption that $T_{s,max} = T_{max}$. From these relationships the $T_{s,max}$ values were converted to T_p using $T_p = T_{s,max}/0.92$.

$$T_{1/3}/T_p = 0.93 \Rightarrow T_p = T_{1/3}/0.93$$

$$T_{max}/T_{1/3} = 0.99 \Rightarrow T_p = T_{max}/0.92 \tag{7.1}$$

7.1.3 Recovery period input

Unlike the storm events, the input wave conditions for the recovery models do not vary from simulation to simulation. The recovery simulations use a series of 24-hour JONSWAP spectra that are defined by the average conditions for all measured waves below the storm event threshold (3.0m). From the measured data it was determined that, during non-storm events, the average H_s is 1.50m with the T_p of these waves being 9.5s.

From the results presented in Chapter 6 it was shown that each tidal cycle (mean, spring and high) produced the lowest errors for simulating certain trends in the beach variability.

For the SPA implementation a single tidal cycle was decided upon and applied to every recovery simulation.

As the high tidal cycle was constructed of two extreme water levels, this variation would never occur in reality meaning it was rejected. From the results in Chapter 6, only a small difference can be seen between the simulated beach variability, using mean and spring tidal cycles. However, overall the spring tidal cycle did provide the best results across the majority of the cases considered and analysed. In addition, it produces a better estimation of the berm crest position than the mean tidal cycle due to the higher elevation in water level. This higher water level allows for sediment to be deposited further up the beach and provides a better representation of the berm crest. For these reasons it was decided that a spring tidal cycle should be included in every recovery simulation within the SPA.

7.1.4 Storm event timeseries

As discussed previously, the synthetic storm climate, generated by the statistical model provides the input wave boundary conditions to XBeach. From Hawkes (2000), 2,156 (100 years) of storm events are required to produce an accurate 1 in 10 year return level of erosion. Due to the random aspect of the Monte Carlo simulation, and the inclusion of event spacing, the generation of 2156 storm events lead to a synthetic climate that spans approximately 110 years, rather than the required 100 years. The timeseries of this climate is given in Fig. 7.1.
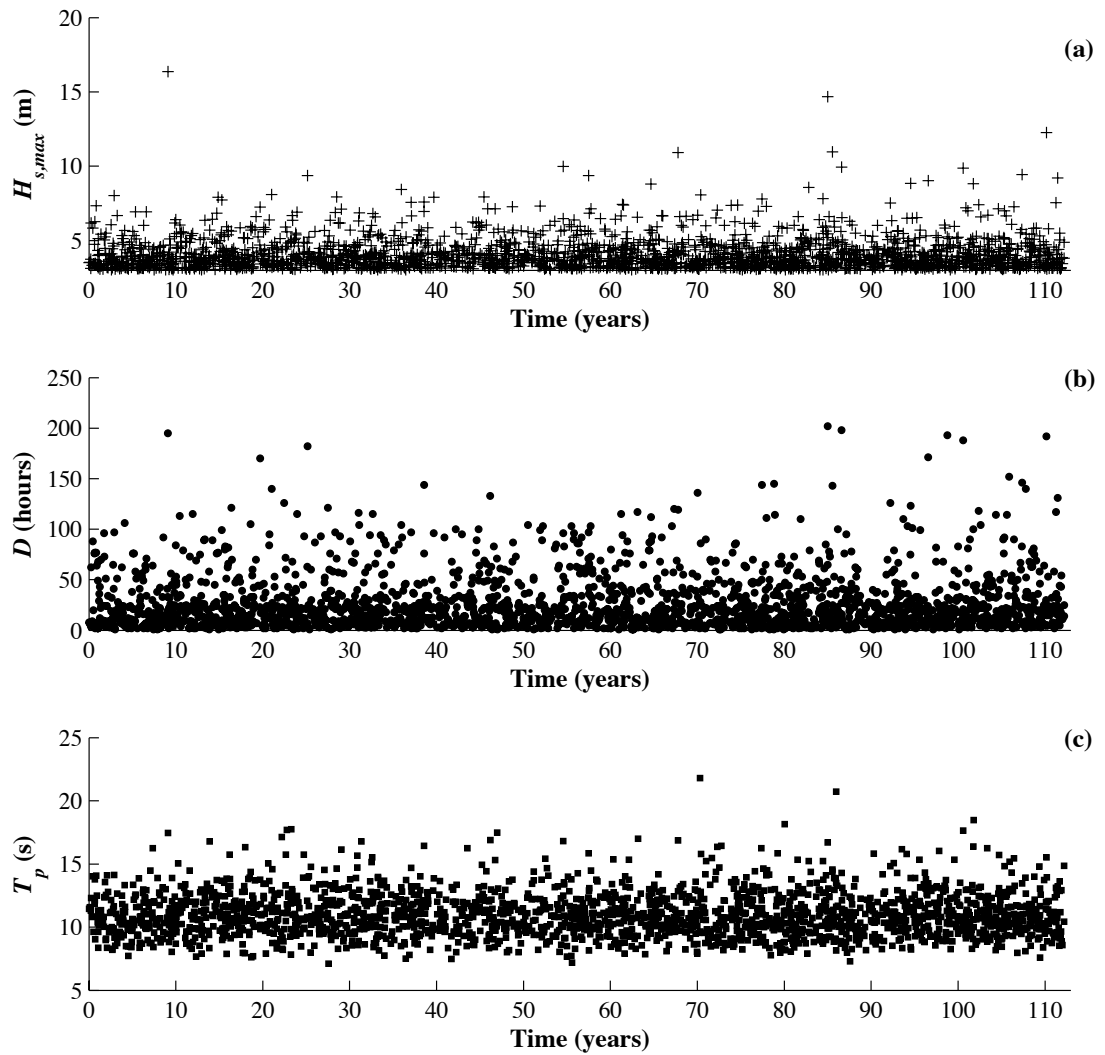
Fig. 7.1 – Random synthetic storm climate used for SPA input. (a) $H_{s,max}$, (b) D and (c) T_p

7.1.5 Inclusion of wave direction

A recent development to the XBeach model has lead to the option for inclusion of oblique wave incidence in 1D simulations. In this case, the variations in wave properties across the computation domain are determined using Snell's law of refraction.

Although the Botany Bay wave data are non-directional, directional storm data, measured at Long Reef point (Fig. 4.1), were obtained from Manly Hydraulics Laboratory. These data contain details of individual storm events (defined by the 3.0m threshold), measured

from 1992 to 2009 and includes the predominant wave direction (θ) for each event. It is these data that are included into the synthetic wave climate.

The study of Callaghan et al. (2008) showed that θ and $H_{s,max}$ are independent of each other, which indicates the fact that each storm event can be assigned a random empirical θ. The same approach has been adopted here with θ being randomly sampled from the empirical data and assigned to each synthetic event. Fig. 7.2 shows the empirical θ vs. $H_{s,max}$ (a) and randomly assigned θ vs. $H_{s,max}$ (b).
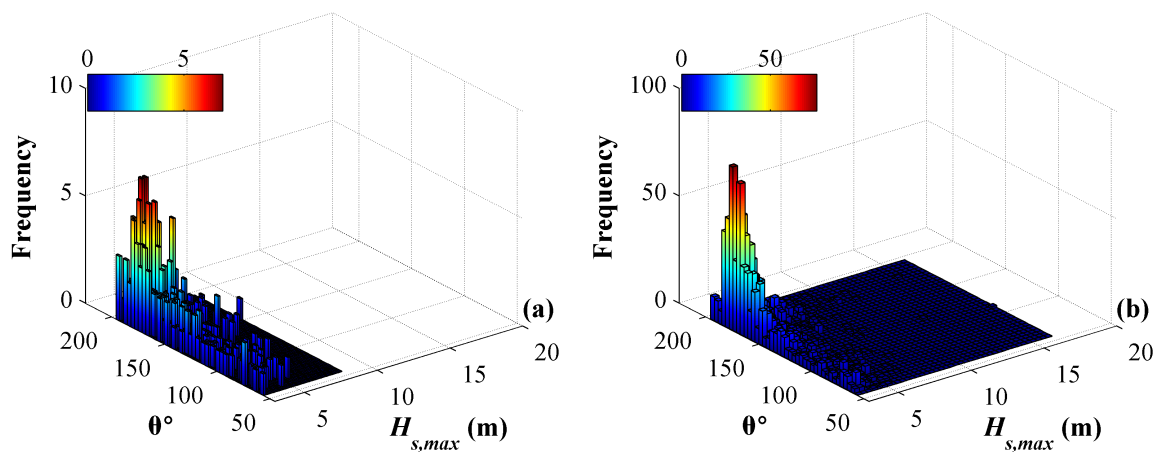
Fig. 7.2 – Storm direction for (a) measured events and (b) synthetic storm climate

From inspection of the empirical data it is evident that the majority of the storm events do not approach perpendicular to the coasts, with the mean wave approach being 158°. This means that the wave energy and subsequent beach erosion should be considerably less than that for an orthogonal 1D approach.

7.2   SPA Implementation and Results

7.2.1 Simulations

As discussed in Chapter 6, two 100-year simulations were conducted with different recovery model setups; event calibrated and annually calibrated models

7.2.2 Results

As with the erosion analysis presented in Chapter 4 (Fig. 4.15); in line with previous studies of erosion at Narrabeen Beach (Hoffman and Hibbert, 1987; Callaghan et al., 2008; Ranasinghe et al., 2011), the erosion levels from the SPA are determined above the 2m beach contour.

7.2.2.1 Empirical erosion levels

To be able to assess the success of the SPA, a comparison with the measured erosion levels at Narrabeen Beach is required. These levels were determined using similar methods to Callaghan et al. (2008) and are described as follows:

- Block averaging procedure – Measured profiles are grouped into blocks of 1.5 month durations and the average volume determined. The erosion is determined by the difference in subsequent block volumes.
- Consecutive volumes with no correction – Erosion is determined from the volumetric difference between consecutive beach profiles.
- Consecutive volumes corrected for the number of storms – The erosion between consecutive profiles is divided by the number of storm events between the measurements.
- Consecutive volumes corrected for the number of effective storms – The erosion between consecutive profiles is divided by the number of *"effective storms"* between the measurements.

The concept of *"effective storms"* is slightly ambiguous and depends on the number of events that were deemed likely to have an erosive impact on Narrabeen Beach (Dr D. Callaghan, personal communication). Due to the lack of information of the storm paths, the analysis conducted in this thesis uses the number of extreme storm events ($H_{s,max} > 4.0$m and $D > 35$ hours) between profile measurements.

Upon determination of the beach erosion volumes using each method, the return periods were determined using Eq. (7.2) for the ith largest event, where T_{RP} is the return period in years, N is the number of events and Y is the erosion period in years. Return periods of the erosion volumes measured at Narrabeen Beach are provided in Fig. 7.3. As the aim of the SPA is to attempt to quantify return levels up to a 10 year return period the empirical erosion levels have been curtailed at 10 years.

$$T_{RP} = \frac{1}{\dfrac{i}{N+1} \times \dfrac{N}{Y}} \approx \frac{Y}{i}$$

(7.2)
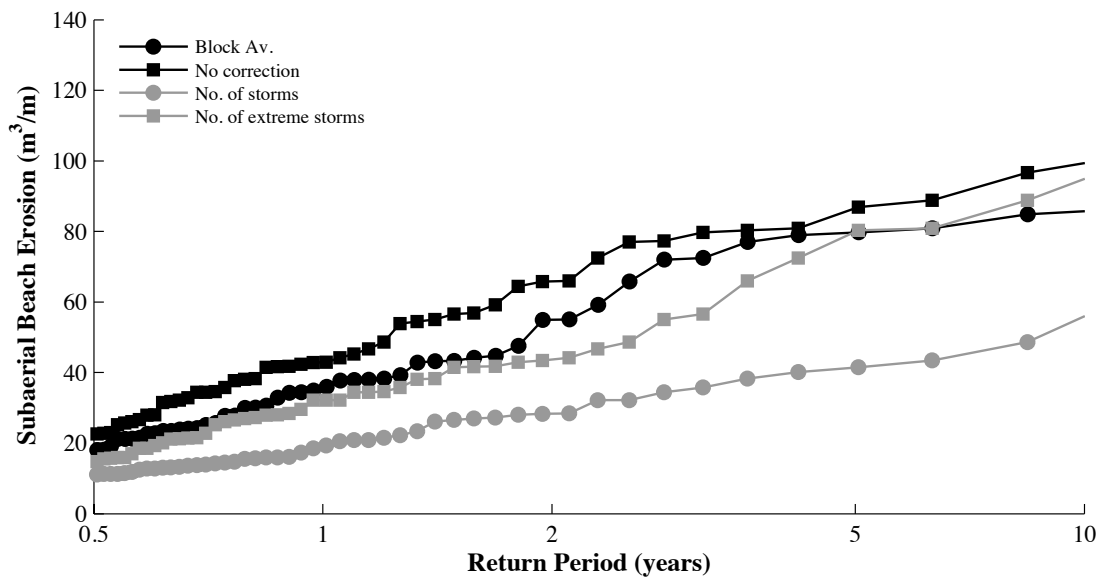
Fig. 7.3 – Empirical beach erosion return levels bounded by the 2m beach contour

7.2.2.2 SPA results

In an attempt to assess the success of the SPA, the return periods of erosion volumes calculated from the continuous simulation of beach change are compared with those obtained from the measured data (Fig. 7.3). The results are shown in Fig. 7.4.
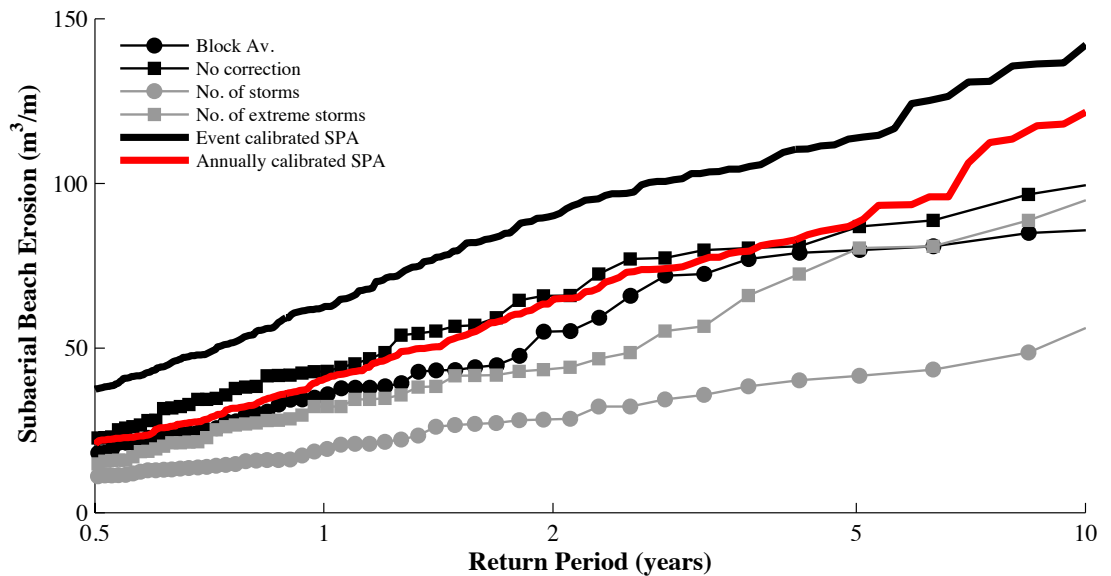
Fig. 7.4 – SPA predicted beach erosion bounded by the 2m beach contour

Fig. 7.4 shows that the event calibrated model consistently overestimates erosion volumes at all return periods. However, the use of the annually calibrated recovery model provides estimates comparable to those measured. This difference can be attributed to the fact that the event calibrated recovery model transforms the profile between dissipative and reflective states thus, focusing on berm creation.

This hypothesis is supported by the study of Harley et al. (2009) who showed that the erosive impact of storm events at Narrabeen Beach depends on the subsequent state of the beach resulting from the precedent calm period. Although the SPA does allow a mechanism for including antecedent beach conditions in the simulations, when using the event calibrated recovery model, this tends to a reflective state. Harley et al. (2009)

showed that greater erosion levels result when the antecedent state is reflective compared to intermediate. This is due to intermediate states having a nearshore bar system that protects the beach from incoming waves by dissipating energy further offshore rather than at the beach itself. In addition, the berm present in the reflective state provides a greater volume of erodible sediment on the beach itself.

The results from the simulation using the annually calibrated recovery model are very encouraging as the erosion estimates closely correspond with the measured data. The best correlation is provided up to the 1-2 year return periods, after which the SPA predictions begin to increase at a greater rate than the measured erosion. It has been regularly mentioned it is expected that a 100-year storm simulation should result in accurate 10-year return levels. This is shown to not be the case as the SPA estimations begin to overestimate measured erosion after a 5-year return period. As the guideline from Hawkes (2000) is only rule-of-thumb, it is conceivable that the divergence at higher return periods is maybe associated with this being inaccurate and better estimation of a 10-year return level would require a longer simulation.

7.3   SPA Limitations

The differences observed between the estimated and measured erosion can be attributed to a number of reasons. These are summarised as follows:

- Misrepresentation of pre and post-storm profiles in measured data.
- Beach rotation at Narrabeen Beach.
- Selection of storm event threshold.
- Bar dynamics at Narrabeen Beach.
- Limitations of the XBeach model.

These limitations are discussed in the following sections, with Chapter 8 providing some recommended future studies deemed necessary to increase the credibility and robustness of the SPA methodology.

7.3.1 *Misrepresentation of erosion in measured profiles*

It should be noted that the beach profiles might not accurately represent exactly those of pre and post-storm due to timing of the surveys. As the post-storm beach recovery at Narrabeen is rapid (Wright and Short, 1984), profiles that are not surveyed within a few days before and after a storm can significantly deviate from the actual pre and post storm-profile. The availability of additional detailed measured erosion levels would provide better actual erosion for a comparison with the estimated erosion.

7.3.2 **Beach rotation**

In addition to the short-term temporal variation in the incident wave climate, the longer-term beach rotation and oscillation due to the El Niño/La Niña phenomena (Short et al., 1995, 2000; Ranasinghe et al., 2004; Short and Trembanis, 2004; Harley et al., 2011b) provides another considerable modelling challenge. It has been shown that these influences result in considerable erosion/accretion cycles at Narrabeen Beach that occurs at approximately 3-5 year intervals (Chapter 4). Although the use of profile 4 attempts to mitigate any significant influence, there could still be an impact of these cycles in the measured data that is not currently accounted for in the SPA.

The influence of longshore transport can also not be neglected. Although the net change in profile 4 during the period considered in this study is minimal, some of the variation could possibly be attributed to longshore transport at the beach.

The simplification of such a complex beach system into 1D does not allow for these influences to be included into the simulations, which may lead to discrepancies between measured and simulated beach erosion.

7.3.3 Sensitivity testing on the storm event threshold

The selection of a 3.0m wave height to define storm events plays an important role in the erosion levels generated by the SPA. Although this value has been selected from detailed analysis of the wave climate in NSW (Lord and Kulmar, 2000; Kulmar et al., 2005) and used in a number of similar studies regarding erosion at Narrabeen Beach (Callaghan et al., 2008; Harley et al., 2009; Ranasinghe et al., 2011) the selection of a different value (e.g. 2.9m or 3.1m) will affect the erosion predictions generated by the SPA. For example, should a threshold of 3.1m be selected, the total number of storm events will reduce (482 compared to 539) and the average duration of these events will also decrease (25 hours compared to 27). As the peak wave heights will remain the same, a reduction in the duration of the storm events will produce less erosion.

Although the selection of a 3.0m storm threshold produced comparable results for Callaghan et al. (2008) and Ranasinghe et al. (2011), their approaches used simple structural functions, based only on $H_{s,max}$, T_p and D, to determine erosion levels. When using a process-based model and inputting the storm events as described in section 7.1.2, this threshold becomes more significant. It may be that, in reality, wave heights around this threshold level actually result in an onshore movement of the bar system, rather than erosion of the beach.

While it is possible for a detailed sensitivity testing of the threshold level to be conducted using the SPA, to fully understand the significance of this value detailed profile and wave measurements during future storm events would be required. Measuring the profile change at Narrabeen during high-energy wave events would provide a better insight into the beach change during storm events and allow for the erosion threshold to be determined in greater detail.

7.3.4 Bar dynamics

Perhaps the most significant contribution to the overestimation of erosion is due to the SPA not effectively modelling the bar dynamics that occur at Narrabeen Beach during calm wave periods. It has been discussed previously that Narrabeen Beach exhibits the full range (dissipative, reflective and reflective) of beach states (Short and Wright, 1981; Wright and Short, 1984; Wright et al., 1985). As the event calibrated recovery model only simulates the change between dissipative and reflective states, it favours berm creation rather than bar morphology and provides no means for simulating the predominant intermediate state of Narrabeen Beach.

Calibrating the recovery model over an annual time period, to better represent the average beach profile, reduced the overestimation. However, this modification results in more of a compromise between an intermediate and average state and still does not allow for the modelling of the full range of beach states. Being able to simulate the full range of beach states will provide the basis to model the gradual recovery of the beach and provide a more realistic estimation of the morphodynamics and erosion of the beach.

7.3.5 XBeach limitations

The limitations of XBeach also play a role in the inability to model the actual bar dynamics that occur at Narrabeen Beach. It has already been discussed that different parameter setups are necessary in order to simulate erosion and accretion using XBeach. As the model was developed and calibrated for simulating erosion, the ability to simulate bar dynamics has not been thoroughly tested. In order to use XBeach more effectively for simulating the gradual recovery and associated bar movements, extensive model development may be required.

7.4 Chapter Summary

This chapter has presented the implementation of the SPA methodology for modelling medium-term beach variability. Two simulations were conducted using the event calibrated and annually calibrated recovery model setups, from Chapter 6.

The results show that the event calibrated simulations give a poor estimation of beach erosion where the model consistently overestimated erosion volumes. Calibration of the recovery model for an annual storm time series significantly improved the results. This difference can be attributed to the event calibrated model focusing on berm accretion and providing a larger volume of erodible sediment on the beach.

A number of potential reasons that may contribute the discrepancies between measured and SPA simulated erosion volumes were proposed and discussed.

CHAPTER 8

CONCLUSIONS AND RECOMMENDATIONS

This chapter provides the conclusions drawn from the research conducted and presented in the previous chapters of this thesis. It summarises the results of the XBeach model calibration and the implementation of the SPA methodology. The limitations of the SPA methodology, discussed in Chapter 7, are then used to propose future studies and recommendations to improve and expand on the method developed by this research.

8.1 Conclusions

This thesis has presented the first attempt of establishing a methodology to allow a process-based model to be used for forecasting medium term beach profile erosion and variability. The work carried out by Callaghan et al. (2008) on modelling long-term beach erosion showed that, although there may be possible improvements to the statistical approach they used, the main limitation is the use of an empirical structural function to simulate beach erosion and post-storm beach recovery. The use of the semi-empirical dune impact model by Ranasinghe et al. (2011) partially overcame this limitation, however they still adopt the same crude approach to determine beach recovery used by Callaghan et al. (2008). The SPA methodology presented here expands on these approaches by using a fully process-based coastal morphodynamic model to simulate, both, storm-induced beach erosion and post-storm recovery. This allows for the inclusion of antecedent beach profiles into the methodology, thus providing a more detailed simulation of beach variability, which is not possible from the previous methods.

The calibration and validation of the coastal morphodynamic model, XBeach, at Narrabeen Beach gives very encouraging results. It was demonstrated that, when calibrated against a

range of storm events, with varying degree of intensity and duration, on average, XBeach can reproduce storm-induced profile change with a *"good"* BSS. Additionally, the ability of XBeach to reproduce accretion during post-storm calm periods was also highlighted by *"good"* average BSS, along with very good estimations of volumetric change in the beach. This representation of beach recovery at a time scale of weeks is one of the most encouraging results presented. Although Jamal et al. (2010) investigate the accretion of gravel beaches using their XBeach variant, their work is limited to a timescale of a number of waves. The recovery simulations presented and discussed in this thesis therefore provide the first attempt at modelling the accretion of a sandy beach at a timescale of days to weeks. The high BSS achieved in these simulations are therefore not only useful in terms of developing the SPA, but also for process-based morphodynamic modelling as a whole. Accurate representation of beach recovery using this type of model will help to bridge the gap between short and long-term simulations of beach change, the main limitation of this type of modelling at the present time.

Upon successful calibration of XBeach for individual storm and recovery events, the two model setups were run in sequence to assess the suitability of switching between erosion and accretion. The simulation was implemented over an annual time period, with the results being compared to the measured data to assess the suitability of the approach for modelling longer-term sequences. It was shown that the event calibrated setups can reproduce the behaviour of Narrabeen Beach at an annual time scale with a reasonable degree of accuracy. The trends in the subaerial beach volume and position of beach contours were successfully followed during this annual period, with the procedure also providing a good representation of the beach profile shape. However, due to the recovery model being calibrated for simulating the transition between dissipative and reflective beach states, this resulted in an overestimation of the beach volume and contour positions. To provide a better estimation of the average profile that occurred during the period, an additional calibration of the recovery model set up was conducted. This calibration was made using the entire annual time series to allow for the best representation of the variability of the beach to be captured. The success provided by these calibrations gave the validation necessary to attempt to use XBeach within the longer-term SPA methodology.

To assess the capabilities of the SPA, a random 100-year storm timeseries was simulated. From these simulations the erosion return levels were determined and compared to those observed from the measured profiles of Narrabeen Beach. These comparisons allowed for the success of the SPA to be determined. It was shown that, to achieve comparable results, the annually calibrated recovery model is more suitable as the event calibrated model consistently overestimates erosion. It was discussed that this is due to the sensitivity that the antecedent beach state has on erosion (Harley et al., 2009). However, considering the complexity of the Narrabeen Beach system and the incoming wave field, these comparable results should not be understated. Additionally, as a first attempt at using XBeach for simulations of this time-scale, the results are very encouraging.

The primary limitation of the SPA methodology is in its inability to simulate gradual beach recovery through the full range of beach states. The omission of the most common intermediate beach state during recovery phases is hypothesised as the main reason for the overestimation of return levels from the event calibrated simulations.

Although the presented SPA methodology has its limitations, it does provide valuable insight into process-based coastal morphodynamic modelling at medium-term timescales. The methodology and results presented in this thesis go a long way to demonstrate the longer-term modelling capabilities of one of the most robust morphodynamic models currently available. It is thought that, with some more studies that attempt to mitigate the highlighted limitations of the methodology, this type of modelling framework may become a usable decision making tool in future coastal management plans.

8.2   Future Recommendations

The novel research discussed and presented in this thesis has given rise to a number of potential future studies that can be recommended in order to expand and improve the SPA methodology. These developments will help to validate the procedure and potentially develop the SPA as a decision making tool for future coastal management projects.

8.2.1 The intermediate beach state

The inability to model the full range of beach states using the presented approach is a major limitation. It has been discussed in detail that the antecedent beach states partially control the level of erosion that occurs during subsequent storm events; and that greater erosion levels result when the antecedent state is reflective (Harley et al., 2009). This issue was partly overcome by using the annually calibrated recovery model as it provides a better estimation of the average beach profile. However, this approach still does not allow for the simulation of the intermediate and reflective states. Including a mechanism that enabled the SPA to account for the full range of beach states would go a long way in improving the credibility and robustness of the approach.

In order to achieve this a detailed analysis of the transformation between beach states, during clam periods, at Narrabeen Beach is required. This type of study would require measurements of the wave climate and profile changes that occur during these periods. Implementing this will provide the required data to attempt to calibrate XBeach for the modelling of the intermediate beach state.

To include this within the SPA, the calm post-storm periods would have to be subdivided to account for the different states that can occur during these periods. In its simplest form the duration of recovery periods could be used to determine whether an intermediate or reflective state will occur. For example, the 400 hour threshold for full beach recovery defined by Callaghan et al. (2008) could be used to model an intermediate/reflective state if the duration of the recovery period is less/more than this threshold.

It is felt that this is the key limitation that has to be overcome in order to progress the SPA methodology presented in this thesis. However, for this to be implemented a detailed study of the transformation of the beach profile during the intermediate states is required for model calibration and validation purposes.

8.2.2 Storm event threshold selection

The requirement for a threshold selection to be made to distinguish between periods of erosion (storm events) and accretion is also one of the major limiting factors in the methodology. The choice of a 3.0m threshold level is not without precedent and has been used successfully in previous studies (Callaghan et al., 2008; Harley et al., 2009; Ranasinghe, Callaghan, et al., 2011); as well as being used for collection of storm data in the region (Kulmar et al., 2005). Although it would be possible for a sensitivity test on this threshold to be conducted using the approach presented here, it is felt that this would have no real benefit as XBeach has to be calibrated to individual events. As there has been extensive studies into this threshold; and it is commonly agreed that 3.0m best divides erosion and accretion at Narrabeen Beach, it is thought that such a test will not give any additional benefit the methodology.

What would be more appropriate is an investigation into other methods that can be used to distinguish between erosion and accretion periods in the wave climate. Recently, this issue was tackled in a more detailed approach by Davidson et al. (2013) who used a disequilibrium technique to define periods of erosion and accretion at Narrabeen Beach. The basis of this approach uses a time varying dimensionless fall velocity (Gourlay, 1968; Wright et al., 1985) to distinguish between erosion and accretion, depending on its relationship to the equilibrium state. Inclusion of this within their simplified model yielded a good estimation of the variability in the shoreline position at Narrabeen Beach over a six-year period.

It is thought that, once the modelling of an intermediate state with XBeach can be achieved, a similar technique to this could be employed to determine which beach state is likely to occur during the calm periods between storm events. Although this may provide a more detailed method for dividing the wave climate into erosion and accretion periods, it is still limited in the requirement to switch between different XBeach setups to perform the simulations.

8.2.3 Single XBeach set up

Even if the inclusion of an intermediate state and division of the wave climate had been overcome, the approach would still have the limitation of requiring different XBeach calibrations to model the different morphological states. This is a limitation with the XBeach model itself as it has originally been developed and calibrated to simulate erosion. The ability for the model to adapt to varying hydrodynamic conditions would be necessary to overcome this limitation.

Some exploratory tests were conducted to determine whether the recovery model set up would allow for erosion during higher wave events. However, with the higher waves come higher velocities, meaning that increasing *facSk* and *facAs* during storm events leads to accretion rather than erosion. For this reason a single model set up is currently unachievable.

What may be more appropriate is achieving one model calibration that can simulate the gradual recovery through the intermediate to the reflective state including bar dynamics. This would overcome the limitation of having to divide the wave climate into the three different states and allow for the modelling of the intermediate and reflective states to be dependent on the duration of the accretion periods.

8.2.4 1D simplification

Simplifying the beach into 1D omits the ability to include the temporal variation of the El Niño/La Niña phenomena. Although it was shown that profile 4 acts as a fulcrum during beach rotation; and is least influenced by longshore transport (Ranasinghe et al., 2004; Harley et al., 2011b), regular changes in beach width during these periods were still evident. Although this may occur solely from cross-shore sediment transport, a detailed study of the longshore transport rates during these periods should be conducted and included in the 1D simplification. To include this within the methodology an extensive

study into the wave climate and beach morphology during these periods would be required and will therefore not be feasible in the short-term due to the length of these cycles.

8.2.5 Application at additional sites

Should the additional studies proposed result in successful validation of the SPA at Narrabeen Beach; the methodology should be applied to other field sites. If this type of methodology were to be used as a future decision making tool for coastal management, it will require validation at a number of sites to demonstrate its applicability. This is therefore limited to regions that have an extensive wave climate and beach profile measurements and where the longshore transport effects are minimal so as the simulations can be carried out in 1D.

8.3   Closing Statement

This thesis has demonstrated a novel approach for modelling medium-term beach variability and erosion. The SPA methodology presented provides the first attempt of using a process-based morphodynamic model to provide longer-term statistical predictions of beach erosion. This is achieved through the combination of a detailed statistical model of the incident storm climate and XBeach. It has been shown that, when accounting for the dominant physical processes, XBeach can be successfully calibrated to simulate, both, storm-induced erosion and post-storm accretion. These simulations provide the first instance that XBeach has been used to simulate post-storm beach recovery. The *"good"* BSS obtained after calibration provide a valuable insight into the capabilities of one of the most widely used morphodynamic models. Successful calibration of XBeach at an individual event scale led to the combination of the setups for modelling annual beach change. Although the wave climate during this period has been simplified into erosion and accretion periods, the combination of these setups produced a good comparison of the volumetric change and beach contour positions at this timescale. This successful application of the two model setups over an annual time period justified its use within the longer-term SPA methodology. The results from a 100-year simulation using the SPA

resulted in comparable erosion levels to those measured at Narrabeen Beach. Considering the complexity of the incident wave climate and the simplified approach used to breakdown it into erosive and accretive events, the results obtained are very encouraging. Although the proposed SPA is not without limitations, this research has provided a valuable starting point for progressing the use of process-based models into longer-term, morphodynamic simulations.

REFERENCES

de Alegria-Arzaburu, A.R., Williams, J.J., Masselink, G., 2010. Application of XBeach to Model Storm Response on a Macrotidal Gravel Barrier, in: *Proceedings of 32nd International Conference on Coastal Engineering*. Shanghai, China.

Baldock, T.E., Holmes, P., Horn, D.P., 1997. Low frequency swash motions induced by wave grouping. *Coastal Engineering* 32, pp. 197–222.

Baldock, T.E., Huntley, D.A., Bird, P.A.D., O'Hare, T.O., Bullock, G.N., 2000. Breakpoint generated surf beat induced by bichromatic wave groups. *Coastal Engineering* 39, pp. 213–242.

Baldock, T.E., Manoonvoravong, P., Pham, K.S., 2010. Sediment transport and beach morphodynamics induced by free long waves, bound long waves and wave groups. *Coastal Engineering* 57, pp. 898–916.

Battjes, J.A., 1974. Surf Similarity, in: *Proceedings of 14th International Conference on Coastal Engineering*. Copenhagen, Denmark, pp. 466–480.

Bolle, A., Mercelis, P., Roelvink, D., Haerens, P., Trouw, K., 2010. Application and Validation of XBeach for Three Different Field Sites, in: *Proceedings of 32nd International Conference on Coastal Engineering*. Shanghai, China.

Box, G.E.P., Muller, M.E., 1958. A Note on the Generation of Random Normal Deviates. T*he Annals of Mathematical Statistics* 29, pp. 610–611.

Bruun, P., 1954. Coastal Erosion and the Development of Beach Profiles. *Technical Memorandum No.44, Beach Erosion*.

Bruun, P., 1962. Sea-level rise as a cause of shore erosion. *Journal of Waterways and Harbours Division*, ASCE 88, pp. 117–130.

Bruun, P., 1988. The Bruun Rule of Erosion by Sea-Level Rise: A Discussion on Large-Scale Two- and Three- Dimensional Usages. *Journal of Coastal Research* 4, pp. 627–648.

Butler, A., Heffernan, J.E., Tawn, J.A., Flather, R.A., Horsburgh, K.J., 2007. Extreme value analysis of decadal variations in storm surge elevations. *Journal of Marine Systems* 67, pp. 189–200.

Butt, T., Russell, P., 1999. Suspended sediment transport mechanisms in high-energy swash. *Marine Geology* 161, pp. 361–375.

Calitz, F., 1973. Maximum likelihood estimation of the parameters of the three-parameter lognormal distribution - A reconsideration. *Australian Journal of Statistics* 15, pp. 185–190.

Callaghan, D., Nielsen, P., Short, A., Ranasinghe, R., 2008. Statistical simulation of wave climate and extreme beach erosion. *Coastal Engineering* 55, pp. 375–390.

Cañellas, B., Orfila, A., Méndez, F.J., Menéndez, M., Tintoré, J., 2007. Application of a POT model to estimate the extreme significant wave height levels around the Balearic Sea (Western Mediterranean). *Journal of Coastal Research* 2007, pp. 329–333.

Coelho, C., Veloso-Gomes, F., 2004. Crosshore Beach Profile Models – Application to Aveiro Coast. *Journal of Coastal Research* 39.

Cohen, A.C., 2011. Censored Sampling in the Progressively Distribution Three Parameter Log-Normal Distribution. *Technometrics* 18, pp. 99–103.

Cohen, A.C., Whitten, B.J., 1980. Estimation - Parameter in the Three Lognormal Distribution. *Journal of the American Statistical Association* 75, pp. 399– 404.

Coles, S., 2001. *An Introduction to Statistical Modelling of Extreme Values*, 1st ed. Springer.

Coles, S., Heffernan, J., Tawn, J., 1999. Dependence Measures for Extreme Value Analyses. *Extremes* 2:4, pp. 339–365.

Coles, S.G., Tawn, J.A., 1991. Modelling Extreme Multivariate Events. *Journal of the Royal Statistical Society: Series B (Methodological)* 53, pp. 377–392.

Cooper, J.A.G., Pilkey, O.H., 2004. Sea-level rise and shoreline retreat: time to abandon the Bruun Rule. *Global and Planetary Change* 43, pp. 157–171.

Cowell, P.J., Roy, P.S., Jones, R.A., 1995. Simulation of large-scale coastal change using a morphological behaviour model. *Marine Geology* 126, pp. 45–61.

Davidson, M.A., Splinter, K.D., Turner, I.L., 2013. A simple equilibrium model for predicting shoreline change. *Coastal Engineering* 73, pp. 191–202.

Davidson-Arnott, R., 2010. *Introduction to Coastal Processes and Geomorphology*, 1st ed. Cambridge University Press.

Dean, R.G., 1973. Heuristic Models of Sand Transport in the Surf Zone, in: *First Australian Conference on Coastal Engineering, 1973: Engineering Dynamics of the Coastal Zone*. Sydney, Australia.

Dean, R.G., 1977. *Equilibrium Beach Profiles: US Atlantic and Gulf Coasts*. Ocean Engineering Report No. 12. University of Delaware.

Dean, R.G., 1987. Coastal sediment processes: toward engineering solutions, in: *Coastal Sediments*. New Orleans, USA, pp. 1–24.

Dean, R.G., 1991. Equilibrium Beach Profiles: Characteristics and Applications. *Journal of Coastal Research* 7, pp. 53–84.

Dean, R.G., Healy, T., Dommerholt, A., 1993. A "blind-folded" test of equilibrium beach profile concepts with New Zealand data. *Marine Geology* 109, pp. 253–266.

Deigaard, R., 1993. A note on the three dimensional shear stress distribution in a surf zone. *Coastal Engineering* 20, pp. 157–171.

Dennis, J.E., Schnabel, R.B., 1983. *Numerical Methods for Unconstarined Optimization and Nonlinear Equations*. Prentice-Hall, Englewood Cliffs, NJ.

Dolan, R., Davis, R.E., 1994. Coastal Storm Hazrads. *Journal of Coastal Research Special Issue*, pp. 103–114.

Dupuis, D.J., 1998. Exceedances over High Thresholds: A Guide to Threshold Selection. *Extremes* 1, pp. 251–261.

Fisher, J.S., Overton, M.F., 1984. Numerical model for dune erosion due to wave uprush, in: *Proceedings of 19th International Conference on Coastal Engineering*. Houston, TX, USA, pp. 1553–1558.

Fredsøe, J., Deigaard, R., 1992. *Mechanics of Coastal Sediment Transport*, 1st ed. World Scientific.

Galappatti, G., Vreugdenhil, C.B., 1985. A depth-integrated model for suspended sediment transport. *Journal of Hydraulic Research* 23, pp. 359–377.

Galvin, C.J., 1968. Breaker Type Classification on Three Laboratory Beaches. J*ournal of Geophysical Research* 73, pp. 3651–3659.

Garrity, N.J., 2006. Evaluation of event and response approaches to estimate the 100-year coastal flood for pacific coast sheltered waters, in: *Proceeedings of 30th International Conference on Coastal Engineering*. San Diego, CA, pp. 1651–1663.

Van Geer, P., De Vries, B., Van Dongeren, A., Van Thiel de Vries, J., 2012. Dune erosion ner sea walls: model-data comparison, in: *Proceedings of 33rd International Conference on Coastal Engineering*. Santander, Spain.

Geman, S., Geman, D., 1984. Stochastic Relaxation, Gibbs Distributions, and the Bayesian Restoration of Images, in: *IEEE Transactions on Pattern Analysis and Machine Intelligence*. pp. 721–741.

Goda, Y., 2010. *Random seas and design of maritime structures*, 3rd ed. World Scientific.

van Goor, M., Zitman, T.J., Wang, Z.B., Stive, M.J.F., 2003. Impact of sea-level rise on the morphological equilibrium state of tidal inlets. *Marine Geology* 202, pp. 211–227.

Gourlay, M.R., 1968. *Beach and Dune Erosion*. Delft Hydraulics Laboratory, Report M935/M936.

Grasso, F., Michallet, H., Barthélemy, E., 2011. Sediment transport associated with morphological beach changes forced by irregular asymmetric, skewed waves. J*ournal of Geophysical Research* 116, pp. 1–12.

Hallermeier, R.J., 1981. A Profile Zonation for Seasonal Sand Beaches from Wave Climate. *Coastal Engineering* 4, pp. 253–277.

Hanson, H., Aarninkhof, M., Capobianco, M., Jiménez, J.A., Larson, M., Nicholls, R.J., Plant, N.G., Southgate, H.N., Steetzel, H.J., Stive, M.J.F., de Vriend, H.J., 2003. Modelling of coastal evolution on yearly to decadal time scales. *Journal of Coastal Research* 19, pp. 790–811.

Harley, M.D., Turner, I.L., Short, A., Ranasinghe, R., 2009. An empirical model of beach response to storms - SE Australia, in: *Proceedings of 19th Australasian Conference on Coastal and Ocean Engineering*. Wellington, New Zealand.

Harley, M.D., Turner, I.L., Short, A.D., Ranasinghe, R., 2010. Interannual variability and controls of the Sydney wave climate. *International Journal of Climatology* 30, pp. 1322–1335.

Harley, M.D., Turner, I.L., Short, A.D., Ranasinghe, R., 2011a. Assessment and integration of conventional, RTK-GPS and image-derived beach survey methods for daily to decadal coastal monitoring. *Coastal Engineering* 58, pp. 194–205.

Harley, M.D., Turner, I.L., Short, A.D., Ranasinghe, R., 2011b. A re-evaluation of coastal embayment rotation: The dominance of cross-shore versus alongshore sediment transport processes, Collaroy-Narrabeen Beach, southeast Australia. *Journal of Geophysical Research* 116.

Hasselman, K., Barnett, T.P., Bouws, E., Carlsen, H., Cartwright, D.E., Enkee, K., Ewing, J.A., Gienapp, H., Hasselman, D.E., Kruseman, P., Meerburg, A., Muller, P., Olber, D.J., Richter, K., Sell, W., Walden, H., 1973. Measurements of wind-wave growth and swell decay during the joint North Sea wave project (JONSWAP). *Deutches Hydrographisches* 8.

Hawkes, P.J., 2000. *The Joint Probability of Waves and Water Levels: JOIN-SEA: a rigorous but practical new approach*. HR Wallingford. Report TR 71.

Hawkes, P.J., Gouldby, B.P., Tawn, J.A., Owen, M.W., 2002. The joint probability of waves and water levels in coastal engineering design. *Journal of Hydraulic Research* 40, pp. 241–251.

Hill, B.M., 1963. The Three-Parameter Lognormal Distribution and Bayesian Analysis of a Point-Source Epidemic. *Journal of the American Statistical Association* 58, pp. 72–84.

Hirose, H., 1997. Maximum likelihood parameter estimation in the three-parameter lognormal distribution using the continuation method. *Computational Statistics & Data Analysis* 24, pp. 139–152.

Hoffman, J., Hibbert, K., 1987. Public Works Department, Coastal Branch, N.S.W., PWD Report No. 87040. Sydney, Australia.

Holthuijsen, L.H., Booij, N., Herbers, T.H.C., 1989. A Prediction Model for Stationary, Short-crested Waves in Shallow Water with Ambient Currents. *Coastal Engineering* 13, pp. 23–54.

Horn, D.P., 2002. Beach groundwater dynamics. *Geomorphology* 48, pp. 121–146.

Horn, D.P., 2006. Measurements and modelling of beach groundwater flow in the swash-zone: a review. *Continental Shelf Research* 26, pp. 622–652.

Horn, D.P., Mason, T., 1994. Swash zone sediment transport modes. *Marine Geology* 120, pp. 309–325.

Jamal, M.H., Simmonds, D.J., Magar, V., 2012. Gravel beach profile evolution in wave and tidal environments, in: *Proceedings of 33rd International Conference on Coastal Engineering.* Santander, Spain.

Jamal, M.H., Simmonds, D.J., Magar, V., Pan, S., 2010. Modelling infiltration on gravel beaches with an XBeach Variant, in: *Proceedings of 32nd International Conference on Coastal Engineering.* Shanghai, China.

Jensen, S.G., Aagaard, T., Baldock, T.E., Kroon, A., Hughes, M., 2009. Berm formation and dynamics on a gently sloping beach; the effect of water level and swash overtopping. *Earth Surface Processes and Landforms* 1546, pp. 1533–1546.

Karunarathna, H., Chadwick, A.J., 2007. On low frequency waves in the surf and swash. *Ocean Engineering* 34, pp. 2115–2123.

Kriebel, D.L., 1986. Verification study of a dune erosion model. *Shore and Beach* 54, pp. 13–21.

Kriebel, D.L., Dean, R.G., 1985. Numerical simulation of time-dependent beach and dune erosion. *Coastal Engineering* 9, pp. 221–245.

Kriebel, D.L., Dean, R.G., 1993. Convolution Method for Time-Dependent Beach-Profile Response. *Journal of Waterway, Port, Coastal and Ocean Engineering* 119, pp. 204–226.

Kriebel, D.L., Kraus, N.C., Larson, M., 1991. Engineering methods for predicting beach profile response, in: *Proceedings of Coastal Sediments*. Seattle, WA, pp. 557–571.

Kulmar, M., Lord, D., Sanderson, B., 2005. Future Directions for Wave Data Collection in New South Wales, in: *Proceedings of Coasts and Ports: Coastal Living - Living Coast.* Australasian Conference.

Larson, M., Erikson, L., Hason, H., 2004. An analytical model to predict dune erosion due to wave impact. *Coastal Engineering* 51, pp. 675–696.

Larson, M., Kraus, N., 1989. *SBEACH: numerical model for simulating storm induced beach change*. Report 1, Empirical Foundation and Model Development, Tech Rept. Vicksburg, MS.

Larson, M., Kraus, N.C., Wise, R.A., 1999. Equilibrium beach profiles under breaking and non-breaking waves. *Coastal Engineering* 36, pp. 59–85.

Larson, M., Kubota, S., Erikson, L., 2004. Swash-zone sediment transport and foreshore evolution: field experiments and mathematical modeling. *Marine Geology* 212, pp. 61–79.

Lesser, G.R., Roelvink, J.A., van Kester, J.A.T.M., Stelling, G.S., 2004. Development and validation of a three-dimensional morphological model. *Coastal Engineering* 51, pp. 883–915.

Lindemer, C.A., Plant, N.G., Puleo, J. a., Thompson, D.M., Wamsley, T.V., 2010. Numerical simulation of a low-lying barrier island's morphological response to Hurricane Katrina. *Coastal Engineering* 57, pp. 985–995.

Liu, J.C., Lence, B.J., Isaacson, M., 2010. Direct Joint Probability for Estimating Extreme Sea Levels. *Journal of Waterway, Port, Coastal and Ocean Engineering* 136, pp. 66–76.

Longuet-Higgins, M.S., 1970. Longshore current generated by obliquely incident sea waves, 1&2. *Journal of Geophysical Research* 75, pp. 6778–6801.

Lord, D., Kulmar, M., 2000. The 1974 Storms Revisited: 25 Years Experience in Ocean Wave Measurement Along the South-East Australian Coast. in: *Proceedings 27th International Conference on Coastal Engineering.* Sydney, Australia, pp. 559–572.

Lu, Y., Garrido, J., 2005. Doubly periodic non-homogeneous Poisson models for hurricane data. *Statistical Methodology* 2, pp. 17–35.

Luceño, A., Menéndez, M., Méndez, F.J., 2006. The effect of temporal dependence on the estimation of the frequency of extreme ocean climate events. *Proceedings of the Royal Society A: Mathematical, Physical and Engineering Sciences* 462, pp. 1683–1697.

Marsaglia, G., Bray, T.A., 1964. A Convenient Method for Generating Normal Variables. *SIAM Review* 6, pp. 260–264.

Masselink, G., Hughes, M., 2003. I*ntroduction to Coastal Processes and Geomophology*, 1st ed. Hodder Arnold, London.

Masselink, G., Li, L., 2001. The role of swash infiltration in determining the beachface gradient: a numerical study. *Marine Geology* 176, pp. 139–156.

Mathiesen, M., Goda, Y., Hawkes, P.J., Mansard, E., Martin, M.J., Peltier, E., Thompson, E.F., van Vledder, G., 1994. Recommended Practice for Extreme Wave Analysis. *Journal of Hydraulic Research* 32, pp. 803–814.

McCall, R.T., Masselink, G., Roelvink, D., Russell, P., Davidson, M., Poate, T., 2012. Modelling overwash and infiltration on gravel barriers, in: *Proceedings of 33rd International Conference on Coastal Engineering*. Santander, Spain.

McCall, R.T., Van Thiel de Vries, J.S.M., Plant, N.G., Van Dongeren, A.R., Roelvink, J.A., Thompson, D.M., Reniers, A.J.H.M., 2010. Two-dimensional time dependent hurricane overwash and erosion modeling at Santa Rosa Island. *Coastal Engineering* 57, pp. 668–683.

Moore, B.D., 1982. *Beach Profile Evolution in Response to Changes in Water Level and Wave Height*, PhD Thesis, University of Delaware.

Muir, L., El-Shaarawi, A., 1986. On the calculation of extreme wave heights: A review. *Ocean Engineering* 13, pp. 93–118.

Nairn, R.B., Southgate, H.N., 1993. Deterministic profile modelling of nearshore processes. Part 2. Sediment transport and beach profile development. *Coastal Engineering* 19, pp. 57–96.

Nash, J.C., 2012. R Package "optimx". *http://cran.ma.imperial.ac.uk/*

Nishi, R., Kraus, N.C., 1996. Mechanism for calculation of sand dune erosion by storms, in: *Proceedings of 25th International Conference on Coastal Engineering*. Orlando, FL, USA, pp. 3034–3047.

O'Connor, B.A., Nicholson, J., 1999. Modelling short-term beach profile changes, in: *Proc.of 5th Int. Conf. on Coastal and Port Engineering in Developing Countries*. Cape Town, pp. 277–287.

O'Connor, B.A., Pan, S., Nicholson, J., MacDonald, N., Huntley, D.A., 1998. A 2D model of waves and undertow in the surf zone, in: *Proceedings of 26th International Conference on Coastal Engineering*. Copenhagen, Denmark, pp. 286–296.

Parisi, F., Lund, R., 2000. Seasonality and Return Periods of Landfalling Atlantic Basin Hurricanes. *Australian and New Zealand Journal of Statistics* 42, pp. 271–282.

Pedrozo-Acuna, A., Simmonds, D.J., Otta, A.K., Chadwick, A.J., 2006. On the cross-shore profile change of gravel beaches. *Coastal Engineering* 53, pp. 335–347.

Pilkey, O.H., Cooper, J.A.G., 2004. Society and sea-level rise. *Science* 303, pp. 1781–1782.

Pilkey, O.H., Young, R.S., Riggs, S.R., Smith, A.W.S., Wu, H., Pilkey, W.D., 1993. The Concept of Shoreface Profile of Equilibrium: A Critical Review. J*ournal of Coastal Research* 9, pp. 255–278.

Powell, K.A., 1990. *Predicting short term profile response for shingle beaches*, HR Wallingford Report SR 219.

Pritchard, D., Hogg, A.J., 2005. On the transport of suspended sediment by a swash event on a plane beach. *Coastal Engineering* 52, pp. 1–23.

Ranasinghe, R., Callaghan, D., Stive, M.J.F., 2011. Estimating coastal recession due to sea level rise: beyond the Bruun rule. *Climatic Change* 110, pp. 561–574.

Ranasinghe, R., McLoughlin, R., Short, A., Symonds, G., 2004. The Southern Oscillation Index, wave climate, and beach rotation. *Marine Geology* 204, pp. 273–287.

Ranasinghe, R., Stive, M.J.F., 2009. Rising seas and retreating coastlines. *Climatic Change* 97, pp. 65–468.

Ranasinghe, R., Swinkels, C., Luijendijk, A., Roelvink, D., Bosboom, J., Stive, M., Walstra, D., 2011. Morphodynamic upscaling with the MORFAC approach: Dependencies and sensitivities. *Coastal Engineering* 58, pp. 806–811.

Reddy, M.P., 2001. *Descriptive Physical Oceanography*, 1st ed. A. A. Balkema Publishers.

Reeve, D., Chadwick, A., Fleming, C., 2004. *Coastal Engineering: Processes, Theory and Design Practice*, 1st ed. Spon Press.

Reniers, A.J.H.M., Roelvink, J.A., Thornton, E.B., 2004. Morphodynamic modeling of an embayed beach under wave group forcing. *Journal of Geophysical Research* 109.

Reniers, A.J.H.M., Roelvink, J.A., Walstra, D.J.R., 1995. *Validation study of UNIBEST-TC model*. Report H2130. Delft, The Netherlands.

Restrepo-Posada, P.J., Eagleson, P.S., 1982. Identification of independent rainstorms. *Journal of Hydrology* 55, pp. 303–319.

van Rijn, L.C., 2007a. Unified View of Sediment Transport by Currents and Waves. I: Initiation of Motion, Bed Roughness, and Bed-Load Transport. *Journal of Hydraulic Engineering* 133, pp. 649–667.

van Rijn, L.C., 2007b. Unified view of sediment transport by currents and waves. II: Suspended transport. *Journal of Hydraulic Engineering* 133, pp. 668–689.

van Rijn, L.C., 2009. Prediction of dune erosion due to storms. *Coastal Engineering* 56, pp. 441–457.

van Rijn, L.C., Tonnon, P.K., Walstra, D.J.R., 2011. Numerical modelling of erosion and accretion of plane sloping beaches at different scales. *Coastal Engineering* 58, pp. 637–655.

van Rijn, L.C., Walstra, D.J.R., Grasmeijer, B., Sutherland, J., Pan, S., Sierra, J.P., 2003. The predictability of cross-shore bed evolution of sandy beaches at the time scale of storms and seasons using process-based Profile models. *Coastal Engineering* 47, pp. 295 – 327.

van Rijn, L.C., Wijnberg, K.M., 1996. One-dimensional modelling of individual waves and wave-induced longshore currents in the surf zone. *Coastal Engineering* 28, pp. 121–145.

Roelvink, D., Stelling, G., Hoonhout, B., Risandi, J., Jacobs, W., Merli, D., 2012. Developemetn and feild validation of a 2DH curvlinear storm impact model, in: *Proceedings of 33rd International Conference on Coastal Engineering*. Santander, Spain.

Roelvink, J.A., 1993. Dissipation in random wave groups incident on a beach. *Coastal Engineering* 19, pp. 127–150.

Roelvink, J.A., 2006. Coastal morphodynamic evolution techniques. *Coastal Engineering* 53, pp. 277–287.

Roelvink, J.A., Broker, I., 1993. Cross-shore profile models. *Coastal Engineering* 21, pp. 163–191.

Roelvink, J.A., Reniers, A., van Dongeren, A., van Thiel De Vries, J., Lescinski, J., McCall, R., 2010. *XBeach Model Description and Manual*. Deltares, Delft, The Netherlands.

Roelvink, J.A., Reniers, A., van Dongeren, A., van Thiel De Vries, J., McCall, R., Lescinski, J., 2009. Modelling storm impacts on beaches, dunes and barrier islands. *Coastal Engineering* 56, pp. 1133–1152.

Roelvink, J.A., Stive, M.J.F., 1989. Bar-generating cross-shore flow mechanisms on a beach.pdf. *Journal of Geophysical Research* 94, pp. 4785–4800.

Sallenger, A.H., 2000. Storm Impact Scale for Barrier Islands. *Journal of Coastal Research* 16, pp. 890–895.

Sallenger, A.H., Howd, P., Stockdon, H., Guy, K., Morgan, K.L.M., 2003. On predicting storm-induced coastal change, in: *Coastal Sediments*. Clearwater Beach, Florida, pp. 1–9.

Sangal, B.P., Biswas, A.K., 1970. The 3-ParameterLognormal Distribution Applications in Hydrology. *Water Resources Research* 6, pp. 505–515.

Schnabel, R.B., Koontz, J.E., Weiss, B.E., 1985. A modular sustem of algorithms for unconstrained minimization. *ACM Transactions on Mathematical Software* 11, pp. 419–440.

Shand, R.D., Bailey, D.G., Shepherd, M.J., 1999. An Inter-Site Comparison of Net Offshore Bar Migration Characteristics and Environmental Conditions. *Journal of Coastal Research* 15, pp. 750–765.

Short, A., Trembanis, A., 2004. Decadal scale patterns in beach oscillation and rotation Narrabeen beach, Australia: time series , PCA and wavelet analysis. *Journal of Coastal Research* 20, pp. 523–532.

Short, A.D., 1979. A three-dimensional beach stage model. *Journal of Geology* 87, pp. 553–571.

Short, A.D., 1984. Beaches and Nearshore Facies: Southeast Australia. *Marine Geology* 60, pp. 261–282.

Short, A.D., 1985. Rip-Current Type, Spacing and Persistance, Narrabeen Beach, Australia. *Marine Geology* 65.

Short, A.D., 1992. Beach systems of the central Netherlands coast: Processes, morphology and structural impacts in a storm driven multi-bar system. *Marine Geology* 107, pp. 103–137.

Short, A.D., 1999. *Handbook of Beach and Shoreface Morphodynamics*. John Wiley & Sons.

Short, A.D., 2006. Australian Beach Systems—Nature and Distribution. *Journal of Coastal Research* 221, pp. 11–27.

Short, A.D., Cowell, P.J., Cadee, M., Hall, W., van Dijke, B., 1995. Beach rotation and possible relation to the Southern Oscillation, in: *Proceedings of Ocean and Atmospheric Pacific International Conference*. Adelaide, Australia.

Short, A.D., Trembanis, A., Turner, I.L., 2000. Beach oscillation, rotation and the Southern Oscialltion, Narrabeen Beach, Australia, in: *Proceedings of 27th International Conference on Coastal Engineering*. Sydney, Australia.

Short, A.D., Trenaman, N.L., 1992. Wave climate of the Sydney region, an energetic and highly variable ocean wave regime. *Australian Journal of Marine and Freshwater Research* 43, pp. 765-791.

Short, A.D., Wright, L.D., 1981. Beach systems of the Sydney region. *Australian Geographer* 15, pp. 8–16.

Sierra, J.P., 1999. *CIIRC-LIM runs for Egmond Pilot Experiment*, Report RR-CIIRC/AHC-99-1.

Sierra, J.P., Azuz, I., Rivero, F.J., Sánchez-Acrilla, A., Rodríguez, A., 1997. Morphodynamic modelling in the nearshore area, in: *International Conference on Computer Modelling of Seas and Coastal Regions*. La Coruña, pp. 433–422.

Soulsby, R.L., 1997. *Dynamics of Marine Sands*, 1st ed. Thomas Telford, London.

Southgate, H.N., Nairn, R.B., 1993. Deterministic profile modelling of nearshore processes. Part 1. Waves and currents. *Coastal Engineering* 19, pp. 27–56.

Splinter, K.D., Holman, R.A., Plant, N.G., 2011. A behavior-oriented dynamic model for sandbar migration and 2DH evolution. *Journal of Geophysical Research* 116, pp. 1–21.

Stephensen, A., Ferro, C., 2008. R Package "evd". *http://cran.ma.imperial.ac.uk/*

Stive, M.J., de Vriend, H.J., 1995. Modelling shoreface profile evolution. *Marine Geology* 126, pp. 235–248.

Stive, M.J.F., Ranasinghe, R., Cowell, P.J., 2009. *Sea level rise and coastal erosion, in: Handbook of Coastal and Ocean Engineering*. World Scientific, pp. 1023–1038.

Svendsen, 1984. Wave heights and set-up in a surf zone. *Coastal Engineering* 8, pp. 303–329.

Svendsen, I.A., 2006. *Introduction to nearshore hydrodynamics*, 1st ed. World Scientific.

Tancredi, A., Anderson, C., O'Hagan, A., 2006. Accounting for threshold uncertainty in extreme value estimation. *Extremes* 9, pp. 87–106.

Tawn, J.A., 1988. An extreme-value theory model for dependent observations. *Journal of Hydrology* 101, pp. 227–250.

Tawn, J.A., 1990. Modelling multivariate extreme value distributions. *Biometrika* 77, pp. 245–253.

Tawn, J.A., 1992. Estimating Probabilities of Extreme Sea-Levels. *Applied Statistics* 41, pp. 77-93 .

van Thiel de Vries, J., 2012. Dune erosion above revements, in: P*roceedings of 33rd International Conference on Coastal Engineering*. Santander, Spain.

van Thiel de Vries, J.S.M., 2009. *Dune erosion during storm surges*, PhD Thesis, Delft University of Technology.

Thom, B.G., Hall, W., 1991. Behaviour of beach profiles during accretion and erosion dominated periods. *Earth Surface Processes and Landforms* 16, pp. 113–127.

Thompson, P., Cai, Y., Reeve, D., Stander, J., 2009. Automated threshold selection methods for extreme wave analysis. *Coastal Engineering* 56, pp. 1013–1021.

Turner, I.L., Masselink, G., 1998. Swash infiltration-exfiltration and sediment transport. *Journal of Geophysical Research* 103, pp. 813–824.

Turner, I.L., Nielsen, P., 1997. Rapid water table fluctuations within the beach face: Implications for swash zone sediment mobility? *Coastal Engineering* 32, pp. 45–59.

Vellinga, P., 1986. *Beach and Dune Erosion Storm Surges*. PhD Thesis, Delft University of Technology.

Vousdoukas, M.I., Ferreira, Ó., Almeida, L.P., Pacheco, A., 2012. Toward reliable storm-hazard forecasts: XBeach calibration and its potential application in an operational early-warning system. *Ocean Dynamics* 62, pp. 1001–1015.

de Vriend, H.J., Capobianco, M., Chesher, T., de Swart, H.E., Latteux, B., Stive, M.J.F., 1993. Approaches to long-term modelling of coastal morphology: a review. *Coastal Engineering* 21, pp. 225–269.

de Vriend, H.J., Zyserman, J., Nicholson, J., Roelvink, J.A., Pechon, P., Southgate, H.N., 1993. Medium-term 2DH coastal area modelling. *Coastal Engineering* 21, pp. 193–224.

Walstra, D.J.R., Reniers, A.J.H.M., Ranasinghe, R., Roelvink, J.A., Ruessink, B.G., 2012. On bar growth and decay during interannual net offshore migration. *Coastal Engineering* 60, pp. 190–200.

Watanabe, A., Dibajnia, M., 1988. Numerical modelling of nearshore waves, cross-shore sediment transport and beach profile change, in: *IAHR Symposium on Mathematical Modelling of Sediment Transport in the Coastal Zone*. Copenhagen, pp. 166–174.

Wijnberg, K.M., 1996. On the systematic offshore decay of breaker bars, in: *Proceeding of 25th International Conference on Coastal Engineering*. Orlando, FL, USA, pp. 3600–3613.

Williams, J.J., de Alegría-Arzaburu, A.R., McCall, R.T., van Dongeren, A., 2012. Modelling gravel barrier profile response to combined waves and tides using XBeach: Laboratory and field results. *Coastal Engineering* 63, pp. 62–80.

Wright, L.D., Short, A.D., 1984. Morphodynamic Variability of Surf Zones and Beaches: A Synthesis. *Marine Geology* 56, pp. 93–118.

Wright, L.D., Short, A.D., Green, M.O., 1985. Short-term Changes in the Morphodynamic States of Beaches and Surf Zones: An Empirical Predictive Model. *Marine Geology* 62, pp. 339–364.

APPENDIX A

Fit extreme value and dependency distributions to $H_{s,max}$ and D

Generalised Pareto Distribution

The GPD is a threshold distribution used for modelling threshold excesses with the probability distribution and cumulative distribution function (cdf) defined by Eq. (A.1) and Eq. (A.2) respectively. Where u is the threshold level, σ is the scale parameter and ξ is the shape parameter.

$$\Pr\{X > x \mid X > u\} = \left[1 + \xi \left[1 + \left(\frac{x - u}{\sigma} \right) \right] \right]^{\frac{-1}{\xi}}$$

(A.1)

$$\Pr\{X < x \mid X > u\} = 1 - \left[1 + \xi \left[1 + \left(\frac{x - u}{\sigma} \right) \right] \right]^{\frac{-1}{\xi}} = F(x)$$

(A.2)

From this, if u has been exceeded then these become:

$$\Pr\{X > x\} = \zeta_u \left[1 + \xi \left[1 + \left(\frac{x - u}{\sigma} \right) \right] \right]^{\frac{-1}{\xi}}$$

(A.3)

$$\Pr\{X < x\} = 1 - \zeta_u \left[1 + \xi \left[1 + \left(\frac{x - u}{\sigma} \right) \right] \right]^{\frac{-1}{\xi}} = F(x)$$

(A.4)

where $\zeta_u = \Pr\{X > u\}$.

The GPD is fitted to the storm data by estimating σ and ξ using a maximum likelihood estimation (MLE) approach (Eq.(A.5)).

$$\prod_{i=1}^{N} \Pr\{X_i = x_i \mid X_i > u\}$$ (A.5)

$$\prod_{i=1}^{N} f(x_i)$$

Where $f(x)$ is the pdf of the GPD, and for any distribution can be defined as Eq. (A.6). From this relationship the pdf of the GPD can be determined and is given in Eq. (A.7).

$$f(x) = \frac{dF(x)}{dx} = \frac{d}{dx}\left[1 - \Pr\{X > x \mid X > u\}\right]$$ (A.6)

$$f(x) = \Pr\{X = x\} = \frac{1}{\sigma}\left(1 + \frac{\xi(x-u)}{\sigma}\right)^{\left(\frac{-1}{\xi} - 1\right)}$$ (A.7)

It is common practice when carrying out MLE to maximise the log of the likelihood function, as it is more convenient. The log-likelihood can therefore be defined as.

$$\ell(x \mid \sigma, \xi) = \sum_{i=1}^{N} \ln f(x_i)$$ (A.8)

Dependency distribution

The probability distribution and cdf of the model are given in Eq. (A.9) and Eq. (A.10) respectively. The logistics model is used to model pairs of Fréchet variates, where the standard Fréchet distribution is that in Eq. (A.11).

$$\Pr\{X \ge x, Y \ge y\} = 1 - e^{-x^{-1}} - e^{-y^{-1}} + e^{-(xy)^{-1}\left(x^{-\alpha^{-1}} + y^{-\alpha^{-1}}\right)^{\alpha}}$$

(A.9)

$$\Pr\{X \le x, Y \le y\} = 1 - e^{-\left[x^{-\alpha^{-1}} + y^{-\alpha^{-1}}\right]^{\alpha}} = F(x,y)$$

(A.10)

$$\Pr\{Z \le z\} = F(z) = e^{\frac{-1}{z}}, \quad z > 0$$

(A.11)

The dependency (α) is estimated using a MLE approach with pairs of Fréchet variates (x and y). In this case the physical values of $H_{s,max}$ and D are scaled to Fréchet variates using the marginal GPD distributions and the standard Fréchet distribution. If Eq. (A.10) is rearranged in terms of the physical value (x) it becomes:

$$x = u + \left[\frac{\sigma}{\xi}\left(\frac{1 - F(x)}{\zeta_u}\right)^{-\xi} - 1\right]$$

(A.12)

In order that x can be transformed to a standard Fréchet variate Eq. (A.12) becomes Eq.(A.13) by substituting Eq. (A.11).

$$x = u + \left[\frac{\sigma}{\xi}\left(\frac{1 - e^{\frac{-1}{z}}}{\zeta_u}\right)^{-\xi} - 1\right]$$

(A.13)

where x is the physical value and z is a standard Fréchet variate. The transform of physical values to Fréchet variates can then be obtained from Eq. (A.14).

$$z = \begin{cases} -\ln\left\{\left[\left[1 - \zeta_u\left[1 + \xi\left(\dfrac{x-u}{\sigma}\right)\right]^{\frac{-1}{\xi}}\right]\right]^{-1}\right\}, & \xi \neq 0 \\[4em] -\ln\left\{\left[\left[1 - \zeta_u \, exp\left(-\dfrac{x-u}{\sigma}\right)\right]\right]^{-1}\right\}, & \xi = 0 \end{cases}$$

(A.14)

where x is either $H_{s,max}$ or D; σ, ξ and ζ_u are the corresponding parameter estimates and z is the standard Fréchet variate.

Fitting a conditional distribution to wave period to $T_{s,max}$

Modelling $T_{s,max}$ uses a 3-parameter lognormal distribution and follows the same procedure outlined by Callaghan et al. (2008). The pdf for the 3-parmeter log-normal distribution is given in Eq. (A.15) with, κ being a threshold parameter used to ensure exceedance over a certain limiting value.

$$\Pr\{T_{s,max} = x\} = \left\{(x - \kappa)\sigma\sqrt{2\pi}\right\}^{-1} e^{-\frac{1}{2}\left(\frac{\ln(x-\kappa)-\mu}{\sigma}\right)^2}$$

(A.15)

Callaghan et al. (2008) showed that the minimum T_s for a given H_s at Narrabeen Beach is represented by, $T_{s,min} \approx 3.9 H_s^{0.5}$. Using the $T_{s,min}$ value the corresponding wavelength (L_s) can be determined from solving the dispersion equation, shown in Eq. (A.16), at the water depth of interest. This in turn can be used to determine wave steepness (S) from $S = H_s/L_s$. The relationship between $T_{s,min}$ and $H_{s,max}$ at Botany Bay represents a maximum practical storm wave steepness of approximately 0.04 (Callaghan et al., 2008).

$$L = \frac{gT^2}{2\pi} \tanh\left(\frac{2\pi h}{L}\right)$$

(A.16)

To ensure that most random realisations exceed this limit, the parameters (σ, μ and κ) are related to the wave height ($H_{s,max}$). The expectation of the 3-parameter log-normal distribution is given by Eq. (A.17), leading to the parameters, relating to $H_{s,max}$, being defined as those in Eq. (A.18), resulting in the modified expectation shown in Eq. (A.19).

$$E(T_S) = \kappa + e^{\mu + \frac{\sigma^2}{2}}$$

(A.17)

$$(\kappa, \mu, \sigma) = \left(aH_{s,max}^{b}, \ln cH_{s,max}^{d}, \sqrt{\ln fH_{s,max}^{g}}\right)$$

(A.18)

$$E(T_S) = aH_{s,max}^{b} + cfH_{s,max}^{d+g}$$

(A.19)

This newly defined expectation means that the parameters (a, b, c, d, f and g) were estimated from MLE by maximising the log-likelihood function given in Eq. (A.20).

$$\ell(x \,|\, a,b,c,d,f,g) = \sum_{i=1}^{N} \ln \Pr\{T_{S,max} = x\}$$

(A.20)

Fit non-homogeneous Poisson process to storm spacing

Callaghan et al. (2008) use a modified technique that fits the Poisson process to the spaces between events. It is defined using the following notation: the initial event occurs at time $t_{0,s}$ and ends at $t_{0,e}$, with subsequent events have starting times of: $t_{1,s}$, $t_{2,s}$ ....,$t_{n,s}$. The gaps between the events are then $G_i = (t_{i,s}-t_{i-1,e} \geq 0)$. If the occurrence intensity of the events is defined as $\lambda(t|\boldsymbol{\theta})$ then the probability of exceedance is that in Eq. (A.21).

$$F(t_{i,s} \mid t_{i-1,e}) = F(t_{i-1,e} + G_i \mid t_{i-1,e}) = 1 - e^{-\int_{t_{i-1,e}}^{t_{i-1,e}+G_i} \lambda(t|\theta)\, dt} \tag{A.21}$$

$\boldsymbol{\theta}$ is a vector of parameters depending on the particular seasonal occurrence intensity model being fitted to the data. The data were fitted to three annual intensity models, for constant, annual and twice annual occurrences. These models are described below.

$$\lambda(t \mid \theta) = \theta_0, \quad \text{constant}$$

$$\lambda(t \mid \theta) = \theta_0 + \theta_1 \sin(wt) + \theta_2 \cos(wt), \quad \text{annual} \tag{A.22}$$

$$\lambda(t \mid \theta) = \theta_0 + \theta_1 \sin(wt) + \theta_2 \cos(wt)\theta_3 \sin(2wt) + \theta_4 \cos(2wt), \quad \text{twice annual}$$

Again a MLE approach is followed with Eq. (A.23) and Eq. (A.24) showing the likelihood function and log-likelihood functions respectively.

$$L(t \mid \theta) = \prod_{i=1}^{N} \Big[1 - F(t_{i-1,e} + G_i \mid t_{i-1,e}) \Big] \lambda\big(t_{i-1,e} + G_i \mid \theta \big) \tag{A.23}$$

$$\ell(t \mid \theta) = -\sum_{i=1}^{N} \int_{t_{i-1,e}}^{t_{i-1,e}+G_i} \lambda(t \mid \theta)\, dt + \sum_{i=1}^{N} ln\big(\lambda(t_{i-1,e} + G_i) \mid \theta \big)\, dt \tag{A.24}$$

Monte Carlo simulation of synthetic storm climate

Generate pairs of $H_{s,max}$ and D using Gibbs sampling

The generation of random pairs of $H_{s,max}$ and D using the fitted distributions are carried out using a Gibbs sampling technique (Geman and Geman, 1984) which transforms a random number ($A \sim U(0,1)$) to the target distribution ($F(x)$) by solving $F(x) = \Pr\{X < x\} = A$ for x. The Gibbs sampling technique generates random pairs of dependent Fréchet variates (x and y), which can be transformed into their physical values using the GPD. The procedure is as follows:

1. Generate y_0 using $A \sim U(0,1)$ and $y_0 = (-\ln(A))^{-1}$.

2. For the *i*th storm

   a. Generate $(A$ and $B) \sim U(0,1)$

   b. Transform A to the Fréchet scale with dependency α, by solving

   $$A = \Pr\{X \le x_i \mid Y = y_{i-1}\}$$

   (A.25)

   $$= \left(x_i^{-\alpha^{-1}} + y_{i-1}^{-\alpha^{-1}}\right)^{\alpha-1} y_{i-1}^{\frac{\alpha-1}{\alpha}} e^{-\left(x_i^{-\alpha^{-1}} + y_{i-1}^{-\alpha^{-1}}\right)^{\alpha} + y_{i-1}^{-1}}$$

   c. Transform B to the Fréchet scale with dependency α, by solving

   $$B = \Pr\{Y \le y_i \mid X = x_i\}$$

   (A.26)

   $$= \left(x_i^{-\alpha^{-1}} + y_i^{-\alpha^{-1}}\right)^{\alpha-1} x_i^{\frac{\alpha-1}{\alpha}} e^{-\left(x_i^{-\alpha^{-1}} + y_i^{-\alpha^{-1}}\right)^{\alpha} + x_i^{-1}}$$

   d. Transform the random Fréchet pair (x_i and y_i) to the physical values ($H_{s,max}$ and D) by solving

   $$Tr\{z\} = \begin{cases} u + \left[\dfrac{\sigma}{\xi}\left(\left(\dfrac{1-e^{\frac{-1}{z}}}{\zeta_u}\right)^{-\xi} - 1\right)\right] & \xi \ne 0 \\[2em] u - \sigma ln\left\{\dfrac{1-e^{\frac{-1}{z}}}{\zeta_u}\right\} & \xi = 0 \\[2em] \text{empirical distribution} \end{cases} \quad \begin{matrix} e^{\frac{-1}{z}} \ge 1 - \zeta_u \\[3em] \\[3em] e^{\frac{-1}{z}} < 1 - \zeta_u \end{matrix}$$

   (A.27)

Generate random Ts,max corresponding to random Hs,max

A modification of the Box-Muller method (Box and Muller, 1958), known as the polar-Marsaglia approximation (Marsaglia and Bray, 1964), is implemented to generate a random $T_{s,max}$ associated with the random $H_{s,max}$ generated previously. This produces a random normal deviate that is scaled and transformed using the 3-parameter log-normal distribution using the following steps, where the parameters (σ, ξ and κ) are determined from Eq., using the previously determined random $H_{s,max}$ and the estimated *a ,b, c, d, f* and *g*:

1. Scale standard normal deviate (w) using: $w' = \mu + \sigma w$ κ;

2. Transform w' to the 3-parameter log-normal distribution using:

$$\text{Tr}\{w'\} = \kappa + e^{w'}.$$

Generate time to the next storm event

The time to the next storm event is generated in the same way as described for the other variables. The procedure begins with $t_{i-1,e}$ being equal to the duration of the event from the random $H_{s,max}$ and D pair. An example using the annual occurrence intensity is as follows:

1. Generate a uniform random deviate $A \sim U(0,1)$

2. Solve the integrations of Eq. giving

$$F(G_i) = 1 - e^{-\left\{\dfrac{\theta_0 w G_i + \theta_1\left(\cos(wt_{i-1,e}) - \cos(w(t_{i-1,e}+G_i))\right) - \theta_2\left(\sin(wt_{i-1,e}) - \cos(w(t_{i-1,e}+G_i))\right)}{w}\right\}} \quad \text{(A.28)}$$

3. Solve Eq. for G_i using $F(G_i) = A$.

APPENDIX B – XBEACH MODEL

This Appendix provides a summary of the governing equations behind the hydrodynamics within XBeach and how they are formulated. Although XBeach has the ability to compute wave current interaction (wci) this has not been rigorously tested and is therefore not implemented in this thesis or included in the following equations. The model description provided here has been condensed from Roelvink et al. (2009, 2010) and van Thiel de Vries (2009). For further details regarding XBeach see these references and those within.

The model uses an explicit numerical scheme (upwind or Lax-Wendroff) with the timestep being controlled by the Courant-Friedrichs-Lewy (CFL) condition given in Eq. (B.1). A larger CFL number increases the numerical timestep and allows for higher flow velocities before the simulation becomes unstable.

$$CFL \geq \frac{u \Delta t}{\Delta x}$$

(B.1

Hydrodynamics

Short waves

Wave group forcing is derived from a time varying wave action (A_w) balance equation, which then drives the infragravity motions and longshore and cross-shore currents. The model implemented is similar to that of the HISWA model (Holthuijsen et al., 1989) and accounts for the directional distribution of the incident waves with the frequency being represented by a single frequency. This is provided in Eq. (B.2) to (B.4).

$$\frac{\partial A}{\partial t} + \frac{\partial c_x A}{\partial x} + \frac{\partial c_y A}{\partial y} + \frac{\partial c_\theta A}{\partial \theta} = -\frac{D_w}{\sigma}$$

(B.2)

$$A = \frac{S_w}{\sigma}$$

(B.3)

$$\sigma = \sqrt{gk_w \tanh k_w h}$$

(B.4)

Where S_w is the wave energy in each directional bin, σ is the intrinsic wave frequency, D_w is wave energy dissipation due to breaking, θ is angle of wave incidence with respect to x-axis and h is water depth. The wave celerity (c) and wave number (k_w) are determined from linear wave theory. The celerity in the x and y directions and the θ space are given by Eq. (B.5) to Eq. (B.7). Where u^L and v^L are cross-shore and longshore, depth-averaged Lagrangian velocities; and c_g is the wave group velocity, obtained from linear wave theory.

$$c_x = c_g \cos(\theta)$$

(B.5)

$$c_y = c_g \sin(\theta)$$

(B.6)

$$c_\theta = \frac{\omega}{\sinh 2k_w h}\left(\frac{\partial h}{\partial x}\sin\theta - \frac{\partial h}{\partial y}\cos\theta\right)$$

(B.7)

The total dissipation of wave energy due to breaking ($\overline{D}_w$) is modelled based on the formula proposed by Roelvink (1993) and is provided in Eq. (B.8).

$$\overline{D}_w = 2\frac{\alpha}{T_{rep}}Q_b E_w \frac{H_{rms}}{h}$$

(B.8)

$$Q_b = 1 - exp\left(-\left(\frac{H_{rms}}{H_{max}}\right)^n\right), \; H_{rms} = \sqrt{\frac{8Ew}{\rho g}}, \; H_{max} = \frac{\gamma \tanh kh}{k} \qquad \text{(B.9)}$$

$$E_w = \int_0^{2\pi} S_w d\theta \qquad \text{(B.10)}$$

Where α is a calibration factor of $O(1)$; ρ_w is the water density; f_m is the mean intrinsic frequency; h is the water depth; H_{rms} is the wave height computed from the short wave energy (E_w) by Eq. (B.10); and P_b is the fraction of breaking waves.

From this, the total wave energy dissipation ($\overline{D}_w$) is distributed across all wave directions as shown by Eq. (B.11).

$$D_w = \frac{S_w}{E_w} \overline{D}_w \qquad \text{(B.11)}$$

The dissipation of energy due to bed friction (D_f) is determined from Eq. (B.12).

$$D_f = \frac{2}{3} \rho \pi f_w \left(\frac{\pi H}{T_{rep}\sinh kh}\right)^3 \qquad \text{(B.12)}$$

From the equations discussed for the wave action balance and energy, the radiation stresses are then evaluated using linear wave theory. This is provided in Eq. (B.13) to (B.15).

$$S_{xx} = \int\left(\frac{c_g}{c_w}\left(1 + \cos^2\theta\right) - \frac{1}{2}\right) S_w d\theta \qquad \text{(B.13)}$$

$$S_{xy} = S_{yx} = \int \sin\theta \cos\theta \left(\frac{c_g}{c_w} S_w \right) d\theta \qquad \text{(B.14)}$$

$$S_{yy} = \int \left(\frac{c_g}{c_w} \left(1 + \sin^2\theta \right) - \frac{1}{2} \right) S_w d\theta \qquad \text{(B.15)}$$

The roller energy balance is then coupled to the wave action/energy balance with the dissipation of energy within the short waves (D_w) serving as a source term in the roller energy balance given by Eq. (B.16) The directional distribution and frequency of the roller energy are accounted for in the same way as the wave action/energy.

$$\frac{\partial S_r}{\partial t} + \frac{\partial c_x S_r}{\partial x} + \frac{\partial c_y S_r}{\partial y} + \frac{\partial c_\theta S_r}{\partial \theta} = -D_r + D_w \qquad \text{(B.16)}$$

Where S_r is the roller energy in each directional bin, D_r is the roller energy dissipation and $c_{x/y}$ is the roller speed in the x and y direction, with c being the short wave celerity obtained from linear wave theory and provided by Eq. (B.17) to (B.19).

$$c_x = c\cos(\theta) \qquad \text{(B.17)}$$

$$c_y = c\sin(\theta) \qquad \text{(B.18)}$$

$$c = \frac{\sigma}{k} \qquad \text{(B.19)}$$

The roller energy dissipation is based that of Reniers et al. (2004) and combines the formulae outlined by Deigaard (1993) and Svendsen (1984). This formula is given in Eq. (B.20).

$$\overline{D}_r = \frac{2g\beta_r E_r}{c}$$

(B.20)

$$E_r = \frac{1}{2}\frac{\rho A_r c^2}{L} \text{ where } E_r = \int_0^{2\pi} S_r d\theta$$

(B.21)

Where β_r is the slope of the roller, L is the wavelength, c is the wave celerity and A_r is the roller area. As with the dissipation of wave energy, $\overline{D}_r$ is distributed proportionally over the wave directions as shown by Eq. (B.22).

$$D_r = \frac{S_r}{E_r}\overline{D}_r$$

(B.22)

From this, the roller contribution to the radiation stresses is determined from Eq. (B.23) to (B.25) and added to that of the short waves. This finally allows for the formation of the total radiation stress tensor, which determines the wave forcing (F), given by Eq. (B.26) and (B.27).

$$S_{xx,r} = \int\cos^2\theta S_r d\theta$$

(B.23)

$$S_{xy,r} = S_{yx,r} = \int\sin\theta\cos\theta S_r d\theta$$

(B.24)

$$S_{yy,r} = \int\sin^2\theta S_r d\theta$$

(B.25)

$$F_x = -\left(\frac{\partial S_{xx,w} + S_{xx,r}}{dx} + \frac{\partial S_{xy,w} S_{xy,r}}{dy}\right)$$

(B.26)

$$F_y = -\left(\frac{\partial S_{xy,w} + S_{xy,r}}{dx} + \frac{\partial S_{yy,w} S_{yy,r}}{dy}\right)$$

(B.27)

To determine the infragravity and mean flows, the Non-linear Shallow Water Equations (NSWE) are used. The onshore wave-induced mass flux and subsequent return flows are determined using the depth averaged Generalised Lagrangian Mean (GLM) formulation shown in Eq. (B.28). The Eulerian shallow water velocities u^E and v^E are replaced by the equivalent Lagrangian velocities (u^L and v^L) using the Stokes drift (u^s and v^s) given by Eq. (B.30) to (B.32).

$$\frac{\partial u^L}{\partial t} + u^L \frac{\partial u^L}{\partial x} + v^L \frac{\partial u^L}{\partial y} - fv^L - v_h\left(\frac{\partial^2 u^L}{\partial x^2} + \frac{\partial^2 u^L}{\partial y^2}\right) = \frac{\tau_{sx}}{\rho h} - \frac{\tau_{bx}^E}{\rho h} - g\frac{\partial \eta}{\partial h} + \frac{F_x}{\rho h}$$

(B.28)

$$\frac{\partial v^L}{\partial t} + u^L \frac{\partial v^L}{\partial x} + v^L \frac{\partial v^L}{\partial y} - fv^L - v_h\left(\frac{\partial^2 v^L}{\partial x^2} + \frac{\partial^2 v^L}{\partial y^2}\right) = \frac{\tau_{sy}}{\rho h} - \frac{\tau_{by}^E}{\rho h} - g\frac{\partial \eta}{\partial h} + \frac{F_y}{\rho h}$$

(B.29)

$$\frac{\partial \eta}{\partial t} + \frac{\partial hu^L}{\partial x} + \frac{\partial hv^L}{\partial y} = 0$$

(B.30)

$$u^E = u^L - u^S \text{ and } v^E = v^L - v^S$$

(B.31)

$$u^S = \frac{E_w \cos\theta}{\rho hc} \text{ and } v^S = \frac{E_w \sin\theta}{\rho hc}$$

(B.32)

where: τ is the bed shear stress; η is the water level; F is the wave forcing from the radiation stresses, v_h is the horizontal viscosity; and f is the Coriolis coefficient.

The mass flux carried shorewards within the wave groups and rollers returns offshore as a return flow or a rip current during the swash and collision regimes. Transporting sediment from the dune face offshore continues the process of erosion.

Sediment transport

Advection–diffusion equation

The sediment transport module uses a depth averaged advection-diffusion equation (Galappatti and Vreugdenhil, 1985) for determining the sediment concentration (C_s), using an equilibrium concentration (C_{eq}) as a source term, as shown in Eq. (B.33). The advection-diffusion equation is forced using Eulerian flow velocities (u^E and v^E)

$$\frac{\partial h C_s}{\partial t} + \frac{\partial h C_s u^E}{\partial x} + \frac{\partial h C_s v^E}{\partial y} + \frac{\partial}{\partial x}\left[D_c h \frac{\partial C_s}{\partial x}\right] + \frac{\partial}{\partial y}\left[D_c h \frac{\partial C_s}{\partial y}\right] = \frac{h C_{eq} - h C_s}{T_s} \qquad \text{(B.33)}$$

The sediment concentration adapts to changing hydraulic conditions using an adaptive time scale (T_s) for entrainment. This is given by Eq. (B.34), which is a simple relationship based on the local water depth, h, and the sediment fall velocity w_s.

$$T_s = \max\left(0.05\frac{h}{w_s}, T_{s,min}\right) \qquad \text{(B.34)}$$

$T_{s,min}$ is a user-specified minimum (1s by default). In shallow water ($T_s \approx T_{s,min}$) the sediment concentration responds almost instantaneously to changing hydrodynamic conditions. The volume of sediment entrained is determined between the miss-match of C_s and C_{eq}, here C_{eq} represents the maximum allowable concentration in the water column.

Soulsby – van Rijn transport regime

The original XBeach model only allowed for the Soulsby–van Rijn (SvR) transport formulation (Soulsby, 1997) to be used as the source term in the advection diffusion equation. The SvR transport regime was derived for total load transport driven by waves and currents on a planar or sloping bed. The total load transport rate can be calculated using Eq. (B.35).

$$q_t = A_s \overline{U} \left[\left(\overline{U}^2 + \frac{0.018}{C_D} U^2_{rms} \right)^{\frac{1}{2}} - \overline{U}_{cr} \right]^{2.4} \left(1 - 1.6 \tan\beta \right) \tag{B.35}$$

$$A_s = A_{sb} + A_{ss} \tag{B.36}$$

$$A_{sb} = \frac{0.005 h (d_{50} / h)^{1.2}}{\left[(s-1) g d_{50} \right]^{1.2}} \tag{B.37}$$

$$A_{ss} = \frac{0.012 d_{50} D_*^{-0.6}}{\left[(s-1) g d_{50} \right]^{1.2}} \tag{B.38}$$

$\overline{U}$ = depth averaged current velocity

U_{rms} = root - mean - square wave orbital velocity

$C_D = \left[\dfrac{0.40}{\ln(h/z_0) - 1} \right]^2$ = drag coefficient due to the current

$\overline{U}_{cr}$ = threshold current velocity

β = slope of bed in streamwise direction

h = water depth

d_{50} = median grain diameter

z_0 = bed roughness length

s = relative density of sediment

g = acceleration due to gravity

v = kinematic viscosity of water

$D_* = \left[\dfrac{g(s-1)}{v^2} \right]^{\frac{1}{3}} d_{50}$

van Thiel – van Rijn transport regime

More recently XBeach, has been modified to include a second sediment transport regime (van Thiel de Vries, 2009). The equations are those presented by van Rijn (2007a, 2007b) and this is therefore known as the van Thiel–van Rijn (vTvR) regime. The bedload and suspended load transport rates, along with the associated coefficients are provided in Eq. (B.39) to (B.42).

$$q_b = 0.015\rho_s uh(d_{50}/h)^{1.2} M_e^{1.5} \tag{B.39}$$

$$q_s = 0.012\rho_s u d_{50} M_e^{2.4}\left(D_*\right)^{-0.6} \tag{B.40}$$

q_b and q_s = bedload and suspended load transport rates

$$M_e = \frac{(u_e - u_{cr})}{[(s-1)gd_{50}]^{0.5}} = \text{mobility parameter}$$

$u_e = u + \gamma u_w$ = effective velocity

u = depth averaged velocity

$\gamma = 0.4$ for regular waves and 0.8 for irregular waves

u_w = peak orbital velocity

$u_{cr} = \beta u_{cr,c} + (1-\beta) u_{cr,w}$ = critical velocity

$u_{cr,c}$ = critical velocity for currents

$u_{cr,w}$ = critical velocity for waves

$$A_{sb} = \frac{0.015h(d_{50}/h)^{1.2}}{[(s-1)gd_{50}]^{0.75}} \tag{B.41}$$

$$A_{ss} = \frac{0.012d_{50}D_*^{-0.6}}{[(s-1)gd_{50}]^{1.2}} \tag{B.42}$$

Implementation of sediment transport in XBeach

In order to determine the sediment transport rates in XBeach, C_{eq} is determined using either the SvR or vTvR regime. C_{eq} is the maximum allowable concentration and is given by Eq. (B.43) and (B.44) for the SvR and vTvR respectively. The near bed orbital velocity (u_{rms}) is obtained from linear wave theory and modified ($u_{rms,2}$) to include the effects of breaker induced turbulence (k_b). These are presented in Eq. (B.45) and (B.46).

$$C_{eq} = \frac{A_s}{h}\left(\sqrt{\left|u^E\right|^2 + \frac{0.018}{C_D}u^2_{rms,2}} - u_{cr}\right)^{2.4}(1-1.6\tan\beta) \tag{B.43}$$

$$C_{eq} = \frac{A_{sb}}{h}\left(\sqrt{\left|u^E\right|^2 + 0.64u^2{}_{rms,2}} - u_{cr}\right)^{1.5} + \frac{A_{ss}}{h}\left(\sqrt{\left|u^E\right|^2 + 0.64u^2{}_{rms,2}} - u_{cr}\right)^{2.4} \tag{B.44}$$

$$u_{rms} = \frac{\pi H_{rms}}{\sqrt{2}T_m \sinh(k_w h)} \tag{B.45}$$

$$u_{rms,2} = \sqrt{u^2{}_{rms} + 1.45k_b} \tag{B.46}$$

There are two main differences between the SvR and vTvR transport regimes. Firstly the stirring velocity ($u_{stirring}$) differs. This is defined as the difference between the velocity imparted on the bed and the critical velocity (u_{cr}). $u_{stirring}$ for the SvR and vTvR are given by Eq. (B.47) and (B.48) respectively.

$$u_{stirring} = \sqrt{\left(u^E\right)^2 + \frac{0.018}{C_D}u^2{}_{rms,2}} - u_{cr} \tag{B.47}$$

$$u_{stirring} = \sqrt{\left(u^E\right)^2 + 0.64u^2{}_{rms,2}} - u_{cr} \tag{B.48}$$

It can be seen that the factor applied to the wave orbital velocity (u_{rms}) for each regime differs, with the SvR formula being related to drag coefficient (C_D) whereas the vTvR is not. Additionally, both methods employ the same suspended load equation but different bedload equations. This difference is evident by comparing the bedload coefficients (A_{sb}) for each method. These differences between the transport regimes mean that the vTvR regime results in lower transport rates than the SvR regime for the default XBeach parameters.

Bed updating and avalanching

The sediment transport gradients are used to update the bed levels in the wet areas with the updating defined by Eq. (B.49). This procedure can include use of a morphological acceleration factor (*morfac*) to perform longer simulations with computational efficiency. More information of the *morfac* approach discussed in Roelvink (2006) and Ranasinghe et al. (2011).

$$\frac{\partial z_b}{\partial t} = \frac{1}{(1-p)}\left(\frac{\partial q_x}{\partial x} + \frac{\partial q_y}{\partial y}\right)morfac \qquad \text{(B.49)}$$

The sediment transport rates (q_x and q_y) are determined from Eq. (B.50) and (B.51).

$$q_x = hC_s(u^E + u^A\sin\theta_m) + \frac{\partial}{\partial x}\left(D_c h \frac{\partial C_s}{\partial x}\right) \qquad \text{(B.50)}$$

$$q_y = hC_s(v^E + v^A\cos\theta_m) + \frac{\partial}{\partial y}\left(D_c h \frac{\partial C_s}{\partial y}\right) \qquad \text{(B.51)}$$

Where u^A and v^A are advection velocities resulting from wave skewness and asymmetry and D_c is the diffusion coefficient.

During dune erosion the bed material slumps prior to being transported offshore. This slumping of bed material is accounted for in XBeach using the avalanching function shown in Eq. (B.52). Inundated regions are more susceptible to slumping, meaning that wet and dry cells have separate critical slopes (m_{cr}) of 1.0 and 0.3 respectively.

Avalanching typically occurs when part of the dune front becomes inundated. When the bed levels of wet cells decrease during erosion this leads to the subsequent dry cell

exceeding its critical slope. When this occurs, the dry sand in the dune slumps into the wet region and is transported offshore in the undertow and infragravity wave backwash.

$$\left|\frac{\partial z_b}{\partial x}\right| > m_{cr} \tag{B.52}$$

Groundwater flow

Recent developments to XBeach have included the implementation of a basic groundwater module that is capable of simulating infiltration/exfiltration to/from the beach. The groundwater flow module utilises the principle of Darcy flow and includes vertical interaction between surface water and groundwater. The infiltration and exfiltration to and from the beach is defined by a flow velocity (w) and is positive from the surface water to the groundwater. The vertical velocity (w) can be calculated using Eq. (B.53). Exfiltration takes place when the ground water level (η_{gw}) is greater than the bed level (z_b). The infiltration of surface water into the beach takes place when the groundwater level is less than the bed level (η_{gw} - z_b). This can be determined using a variation of the Darcy flow relationship provided by Eq. (B.54).

$$w_{i,j}^n = \left(\frac{[\eta]_{i,j}^{n-1} - [z_b]_{i,j}^{n-1}}{\Delta t}\right)por \tag{B.53}$$

$$w = -k_z\left(\frac{dp}{dz} + 1\right) \tag{B.54}$$

Boundary conditions

Offshore flow boundary

The offshore flow boundary is an artificial boundary at which the wave and flow conditions are specified. This boundary is defined as being weakly reflective so there is minimal reflection of any waves or currents, from within the domain, that pass through the boundary. The boundary conditions need to satisfy the following two conditions:

1) The motion within the domain can be influenced through the incident long waves and currents along the boundaries.
2) The long waves that propagate out of the domain can propagate though the boundary with minimal reflection.

Bay-side flow boundary

The boundary conditions on the shore-side of the domain can either be set to represent a 1D or 2D absorbing boundary, or a no flux (wall) boundary.

Lateral flow boundaries

Along the lateral flow boundaries the longshore water level gradients are prescribed as the difference in water levels at the offshore corners divided by the longshore length of the model domain. These boundaries can be defined as either a Neumann boundary or a no flux wall. The Neumann boundary conditions have been shown to provide good representation in situations where the coast can be considered uniform out with the model domain (Roelvink et al., 2009). Wall boundary conditions are preferred in 1D (cross-shore) simulations. However, for applying an incident wave direction to 1D simulations, Neumann lateral boundaries are required.

Wave boundary conditions

The input wave conditions for XBeach simulations can be applied as, either, spectral or non-spectral inputs.

The non-spectral inputs are defined as either stationary waves or non-stationary bichromatic wave groups. For stationary inputs the short wave height, representative wave period and wave direction are specified. For bichromatic wave groups, the long wave/wave group periods is also specified.

Spectral wave conditions are defined within XBeach as JONSWAP spectrum or as a SWAN spectrum generated out with XBeach. The simulations discussed in this thesis are forced using JONSWAP spectra and therefore the use of SWAN spectra will not be discussed. JONSWAP spectra can be defined as, either, a single spectrum or a series of varying spectra. Specifying the significant wave height; peak frequency; directional spreading; peak enhancement factor; direction; maximum frequency allowed; and the frequency step size define the spectra.

Model outputs

There are a number of different types of output available from XBeach simulations. Only the ones used within this thesis are described below. Details of all output options are given in Roelvink et al. (2010).

Regular spatial output

This type of output provides information on numerous variables across the model domain at specified points in time. The user defines which variables are required and at what times during the simulation. Should the output time be equal to that of the simulation time, the final parameter values are the only output. This is how the final bed levels are abstracted from XBeach for simulations shown within this thesis.

Time-averaged spatial output

This output determines the time-averaged values of variables across the entire model domain. The user defines the variables and time over which to average their values. These types of outputs are used for the example simulations presented in Sections 6.3 and 6.4.

APPENDIX C – XBEACH INPUT FILES

C.1 - XBeach input for calibrated storm-induced erosion model

Example input file - params.txt

```
--------------------------------------------------------------------------------------------------------
General constants
--------------------------------------------------------------------------------------------------------
rho = 1025              density of sea water
g = 9.81                gravitational constant


--------------------------------------------------------------------------------------------------------
Grid input
--------------------------------------------------------------------------------------------------------
nx = 617                number of cross-shore grid points
ny = 0                  number of longshore grid points
xori = 0                x-origin world coordinates
yori = 0                y-origin world coordinates
alfa = 0                angle of grid
depfile = z1D.grd       bathymetry file
posdwn = 0
vardx = 1               variable grid spacing
xfile = x1D.grd         X coordinates of bathymetry file
thetamin = -90          lower directional limit
thetamax = 90           upper directional limit
dtheta = 180            directional resolution (one directional bin)
thetanaut = 0           option to use nautical convention


--------------------------------------------------------------------------------------------------------
Simulation Timings
--------------------------------------------------------------------------------------------------------
tstart = 0              simulation start time
tstop = 25200           simulation end time


--------------------------------------------------------------------------------------------------------
Numerics input
--------------------------------------------------------------------------------------------------------
CFL = 0.9               Courant Friedrichs Law number
scheme = upwind_2       numerical scheme
thetanum = 1            sediment transport numerical scheme (upwind)
```

Wave Boundary Conditions

----

instat = 41   *wave boundary condition type (series of JONSWAP spectra)*
bcfile = storm.txt   *details of JONSWAP spectra*

Flow Boundary Conditions

----

front = 0   *seaward boundary condition (absorbing-generating boundary in 1D)*
back = 1   *bayside boundary condition (absorbing-generating boundary in 1D)*
left = 1   *no flux wall*
right = 1   *no flux wall*

Tide Boundary Conditions

----

tideloc = 0   *number of tidal timeseries*
zs0 = 0.02   *water level*

Wave Parameters

----

break = 3   *wave breaking model*

Groundwater Parameters

----

gwflow = 1   *groundwater flow module*
kx = 0.0031   *Darcy permeability coefficient in x-direction*
ky = 0.0031   *Darcy permeability coefficient in y-direction*
kz = 0.0031   *Darcy permeability coefficient in z-direction*
por = 0.46   *porosity of sediment*
gw0 = 0.02   *initial groundwater head*

Bed Composition

D50 = 0.00037   *uniform D_{50} sediment diameter*
D90 = 0.00055   *uniform D_{90} sediment diameter*
rhos = 2650   *density of sediment*

Sediment Transport Parameters

----

form = 1   *sediment transport regimen (Soulsby-van Rijn)*
bulk = 1.0   *determine total load sediment transport*
smax = 1.0   *maximum Shields parameter to limit sheet flow*
C = 45   *Chézy coefficient*

Morphology Parameters

----

morfacopt = 0   *morphological acceleration option*
morfac = 1   *morphological acceleration factor*
wetslp = 0.15   *critical slope before avalanching under water*

Outputs

----

nglobalvar = 1   *number of global output variables*
zb   *global output variable (bed level)*

tintg = 25200   *interval for global output variables*

Example bcfile – storm.txt

Boundary condition files are in the form: H_s, T_p, dir0, peak enhancement, s, duration, dt.

```
3.00   9.82   270   3.30   10.00   3600   0.50
3.20   9.82   270   3.30   10.00   3600   0.50
3.40   9.82   270   3.30   10.00   3600   0.50
3.60   9.82   270   3.30   10.00   3600   0.50
3.40   9.82   270   3.30   10.00   3600   0.50
3.20   9.82   270   3.30   10.00   3600   0.50
3.00   9.82   270   3.30   10.00   3600   0.50
```

C.2 – XBeach input for calibrated post-storm recovery model

Example input file - params.txt

```
-------------------------------------------------------------------------------------------------------
General constants
-------------------------------------------------------------------------------------------------------
rho = 1025              density of sea water
g = 9.81                gravitational constant


-------------------------------------------------------------------------------------------------------
Grid input
-------------------------------------------------------------------------------------------------------
nx = 617                number of cross-shore grid points
ny = 0                  number of longshore grid points
xori = 0                x-origin world coordinates
yori = 0                y-origin world coordinates
alfa = 0                angle of grid
depfile = z1D.grd       bathymetry file
posdwn = 0
vardx = 1               variable grid spacing
xfile = x1D.grd         X coordinates of bathymetry file
thetamin = -90          lower directional limit
thetamax = 90           upper directional limit
dtheta = 180            directional resolution (one directional bin)
thetanaut = 0           option to use nautical convention


-------------------------------------------------------------------------------------------------------
Simulation Timings
-------------------------------------------------------------------------------------------------------
tstart = 0              simulation start time
tstop = 60480           simulation end time


-------------------------------------------------------------------------------------------------------
Numerics input
-------------------------------------------------------------------------------------------------------
CFL = 0.9               Courant Friedrichs Law number
scheme = upwind_2       numerical scheme
thetanum = 1            sediment transport numerical scheme (upwind)


-------------------------------------------------------------------------------------------------------
Wave Boundary Conditions
-------------------------------------------------------------------------------------------------------
instat = 41             wave boundary condition type (series of JONSWAP spectra)
bcfile = waves.txt       details of JONSWAP spectra
```

Flow Boundary Conditions

----

front = 0	seaward boundary condition (absorbing-generating boundary in 1D)
back = 1	bayside boundary condition (absorbing-generating boundary in 1D)
left = 1	no flux wall
right = 1	no flux wall

Tide Boundary Conditions

----

tideloc = 1	number of tidal timeseries
zs0file = tide.txt	tidal variation throughout simulation

Wave Parameters

----

break = 3	wave breaking model
facSk = 0.5	factor applied to wave skewness
facAs = 0.8	factor applied to wave asymmetry

Groundwater Parameters

----

gwflow = 1	groundwater flow module
kx = 0.0031	Darcy permeability coefficient in x-direction
ky = 0.0031	Darcy permeability coefficient in y-direction
kz = 0.0031	Darcy permeability coefficient in z-direction
por = 0.46	porosity of sediment
gw0 = 0.02	initial groundwater head

Bed Composition

D50 = 0.00037	uniform D_{50} sediment diameter
D90 = 0.00055	uniform D_{90} sediment diameter
rhos = 2650	density of sediment

Sediment Transport Parameters

----

form = 2	sediment transport regimen (van Thiel-van Rijn)
bulk = 0	determine bed and suspended load sediment transport separately

----

Morphology Parameters

----

morfacopt = 0	morphological acceleration option
morfac = 10	morphological acceleration factor

Outputs
----
nglobalvar = 1   *number of global output variables*
zb   *global output variable (bed level)*
tintg = 60480   *interval for global output variables*

Example bcfile – waves.txt

Boundary condition files are in the form: H_s, T_p, dir0, peak enhancement, s, duration, dt.

1.5   9.5   270   3.30   10   8640   0.50
1.5   9.5   270   3.30   10   8640   0.50
1.5   9.5   270   3.30   10   8640   0.50
1.5   9.5   270   3.30   10   8640   0.50
1.5   9.5   270   3.30   10   8640   0.50
1.5   9.5   270   3.30   10   8640   0.50
1.5   9.5   270   3.30   10   8640   0.50